5-2011

Kinematic evolution of the Homestake and Slide Lake shear zones, central Colorado: Implications for mid-crustal deformation during the Mesoproterozoic

Patricia Elizabeth Lee
plee9@utk.edu

To the Graduate Council:

I am submitting herewith a thesis written by Patricia Elizabeth Lee entitled "Kinematic evolution of the Homestake and Slide Lake shear zones, central Colorado: Implications for mid-crustal deformation during the Mesoproterozoic." I have examined the final electronic copy of this thesis for form and content and recommend that it be accepted in partial fulfillment of the requirements for the degree of Master of Science, with a major in Geology.

Micah J. Jessup, Major Professor

We have read this thesis and recommend its acceptance:

Robert D. Hatcher, Jr., William M. Dunne

Accepted for the Council:
Carolyn R. Hodges

Vice Provost and Dean of the Graduate School

(Original signatures are on file with official student records.)

To the Graduate Council:

I am submitting herewith a thesis written by Patricia Elizabeth Lee entitled "Kinematic evolution of the Homestake and Slide Lake shear zones, central Colorado: Implications for mid-crustal deformation during the Mesoproterozoic." I have examined the final electronic copy of this thesis for form and content and recommend that it be accepted in partial fulfillment of the requirements for the degree of Master of Science, with a major in Geology.

Micah J. Jessup
Major Professor

We have read this thesis
and recommend its acceptance:

Robert D. Hatcher, Jr.

William M. Dunne

Accepted for the Council:

Carolyn R. Hodges

Vice Provost and
Dean of the Graduate School

Original signatures are on file with official student records

KINEMATIC EVOLUTION OF THE HOMESTAKE AND SLIDE LAKE SHEAR ZONES, CENTRAL COLORADO: IMPLICATIONS FOR MID-CRUSTAL DEFORMATION DURING THE MESOPROTEROZOIC

A thesis presented for the
Master of Science
Degree
The University of Tennessee, Knoxville

Patricia Elizabeth Lee
May 2011

ACKNOWLEDGEMENTS

The generous efforts of many faculty members, organizations, and several of my peers supported this project. I would like to thank The Department of Earth and Planetary Sciences at the University of Tennessee for two and a half years of funding through a Graduate Teaching Assistantship as well as funding from a Geological Society of America student research grant. Thanks also to ExxonMobil Exploration Company for providing me with a summer internship and industry experience. I thank my advisor, Micah Jessup, for his patience and insight both in the classroom and through two field seasons in the Sawatch and Indian Himalaya. I would also like to thank my committee members, Bob Hatcher and Bill Dunne, for providing critical feedback and revisions. I also thank Colin Shaw and Joe Allen for a guided tour of the Homestake shear zone during the 2008 field season. Thanks also to Colin Shaw at Montana State University for running my EBSD samples. Many thanks to Donnie Hicks for being an excellent field assistant and helping with initial structure models of the SLSZ. Thanks to Jackie Langille for her help with microstructural kinematic analyses in the lab and for an amazing field season in India. In addition, I like to thank my fellow graduate students for their support through the last 2.5 years of my time here at UT, specifically Aubrey Modi, Melissa Hage, Eric Hogan, Heather Byars, Caitlyn Williams, and Megan Carr.

ABSTRACT

Kinematic analysis and field mapping of the Homestake shear zone (HSZ) and Slide Lake shear zone (SLSZ) in central Colorado provide new evidence for strain partitioning in the mid-crust at ~1.4 Ga. The northeast-striking, steeply dipping HSZ comprises a ~10-km-wide set of anastomosing ductile shear zones and pseudotachylyte-bearing faults. Approximately 3-km south of the HSZ, the north-northeast-striking, shallowly dipping mylonites of the SLSZ form three 1-10-m-thick shear zone splays. Both top-up-to-the-northwest and top-down-to-the-southeast shear sense are recorded in the SLSZ and HSZ. Oblique stretching lineations in both shear zones show vertical (top-down-to-the-southeast and top-up-to-the-northwest) and dextral movement occurred during mylonite development. Quartz and feldspar deformation mechanisms and quartz [c] axis lattice preferred orientation (LPO) patterns are consistent with deformation temperatures ranging from ~280-500°C in the HSZ to ~280-600°C in the SLSZ. Mean kinematic vorticity and quartz [c] axis LPOs for parts of each shear zone suggest plane and non-plane strain general shear with contributions of 47-69% pure shear and 31-53% simple shear. Based on micro- and mesoscale kinematics along with mean kinematic vorticity values and deformation temperature estimates, we propose that HSZ and SLSZ formed during strain localization and partitioning within a mid-crustal transpressional shear zone system that involved subvertical shuffling at ~1.4 Ga.

TABLE OF CONTENTS

LIST OF TABLES

LIST OF FIGURES

LIST OF ATTACHMENTS

CHAPTER 1

INTRODUCTION

Continental tectonics can involve shortening and transpression during oblique convergence (e.g. Harland, 1971; Sanderson and Marchini, 1984; Tikoff and Teyssier, 1994), as well as crustal extension (e.g., Wernicke and Axen, 1988; Wheeler and Butler, 1994). Subvertical shear zones with steeply plunging stretching lineations are commonly associated with oblique convergence (Tikoff and Greene, 1997). Low-angle normal faults occur in active and exhumed convergent tectonic settings in the western U.S. (Lister and Davis, 1989), the Himalaya (Burchfiel et al., 1992; Murphy et al., 2002), the eastern Alps (Selverstone, 1988), and the Scandinavian Caledonides (Anderson et al., 1991). Systems of oblique convergence can be associated with wide orogenic zones with strike-slip shear zones (e.g. White Mountain shear zone, western Idaho shear zone in the North American Cordillera) that partition transpression into transtensional and transpressional structures (Teyssier et al., 1995; Tikoff and Greene, 1997; Giorgis et al., 2004; Sullivan and Law, 2007). This contribution focuses on the kinematic partitioning of transpressional strain into low-angle and steep shear zones at mid-crustal levels during intracontinental deformation of juvenile continental lithosphere. The work is relevant to strain partitioning in crust that contains inherited anisotropy related to continental assembly.

Proterozoic rocks throughout central Colorado record an early high-temperature foliation that was steepened into northeast-southwest trending upright folds during the Paleoproterozoic and was further steepened and reactivated a series of prominent subvertical shear zones in the Mesoproterozoic (Tweto and Sims, 1963; Karlstrom and Humphreys, 1998; Karlstrom and

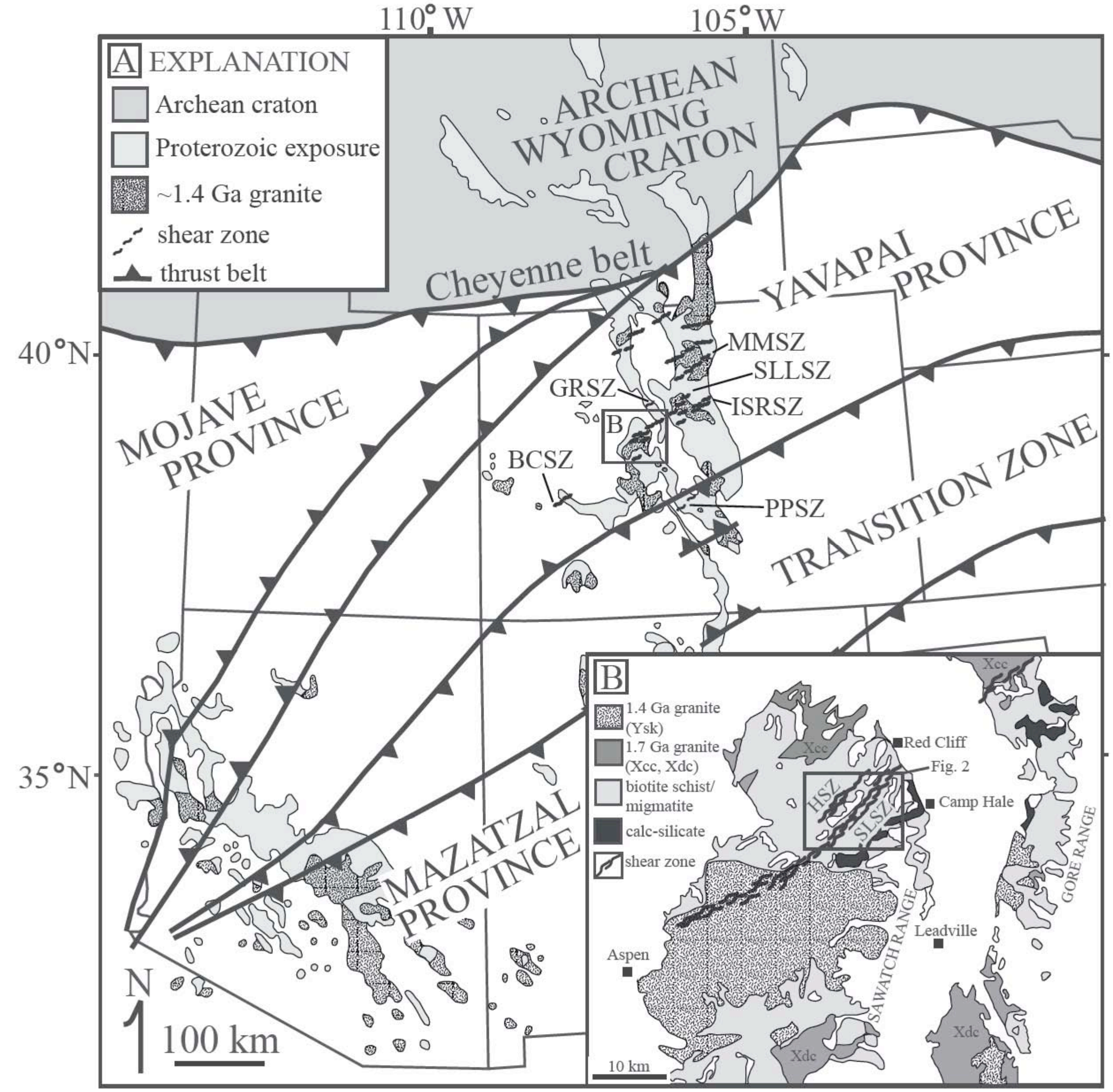

Figure 1. (A) Regional tectonic map of Proterozoic assembly in the southwestern U.S. with Proterozoic boundaries from (Condie, 1986; Bennett and DePaolo, 1987; Karlstrom and Bowring, 1988; Wooden et al., 1988; Wooden and DeWitt, 1991; Jones et al., 2010a). Other shear zones mentioned in this study: BCSZ, Black Canyon shear zone; GRSZ, Gore Range shear zone; SLLSZ, St. Louis Lake shear zone; ISRSZ, Idaho Springs-Ralston shear zone; MMSZ, Moose Mountain shear zone; PPSZ, Poncha Pass shear zone. (B) Inset generalized geologic map of the HSZ and SLSZ area (modified from Shaw and Allen, 2007) with the location of Figure 2.

Williams, 1998; Shaw et al., 2001; McCoy et al., 2005; Shaw and Allen, 2007). These structures comprise the crystalline core of the southern Rocky Mountains and provide an important location to study deformation associated with the growth of Laurentia during the Proterozoic (Figure 1) (e.g. Tweto and Sims, 1963; Karlstrom and Bowring, 1988; Hill and Bickford, 2001). Within this setting, Proterozoic through Phanerozoic deformation has left a record of polyphase deformation that marks the region's assembly and unroofing - from Paleoproterozoic ductile movement at lower to middle crustal levels, to Late Cenozoic upper-crustal brittle fracturing (Figure 1) (Bickford et al., 1989; Bowring and Karlstrom, 1990; Shaw and Karlstrom, 1999; Shaw et al., 2001; Tyson et al., 2002; Jessup et al., 2005; McCoy et al., 2005; Shaw et al., 2005; Jessup et al., 2006; Shaw and Allen, 2007; Caine et al., 2010). Much of this northwest-directed deformation occurred during the Proterozoic and was concentrated along a series of northeast-striking shear zones that traverse the central portion of Colorado (Figure 1A).

The north-northeast striking Slide Lake shear zone (SLSZ) is a 1-km-wide, shallow to moderately dipping mylonite and ultramylonite shear zone that is exposed 3-km-south of the Homestake shear zone (HSZ) near the summit of Homestake Peak (4,023 m) (Figure 1B; 2). The 10-km-wide, steeply dipping HSZ has been mapped as one of the dominant shear zones in the Colorado mineral belt (CMB) and has been mapped extensively (Tweto and Sims, 1963; Tweto, 1974). Timing of regional metamorphism/thermal events (Shaw et al., 2001; Shaw et al., 2005), kinematics, and rheology (Shaw and Allen, 2007) are also well constrained. These studies suggest that the deformed gneiss, mylonite, ultramylonite, and pseudotachylyte of the HSZ record several distinct phases of strain associated with transpression in an exhumed seismogenic zone (Shaw and Allen, 2007). Shaw and others (2001) use monazite ages to suggest that the minor dextral component in D_3 and D_4 could record strike-slip motion associated at ~1

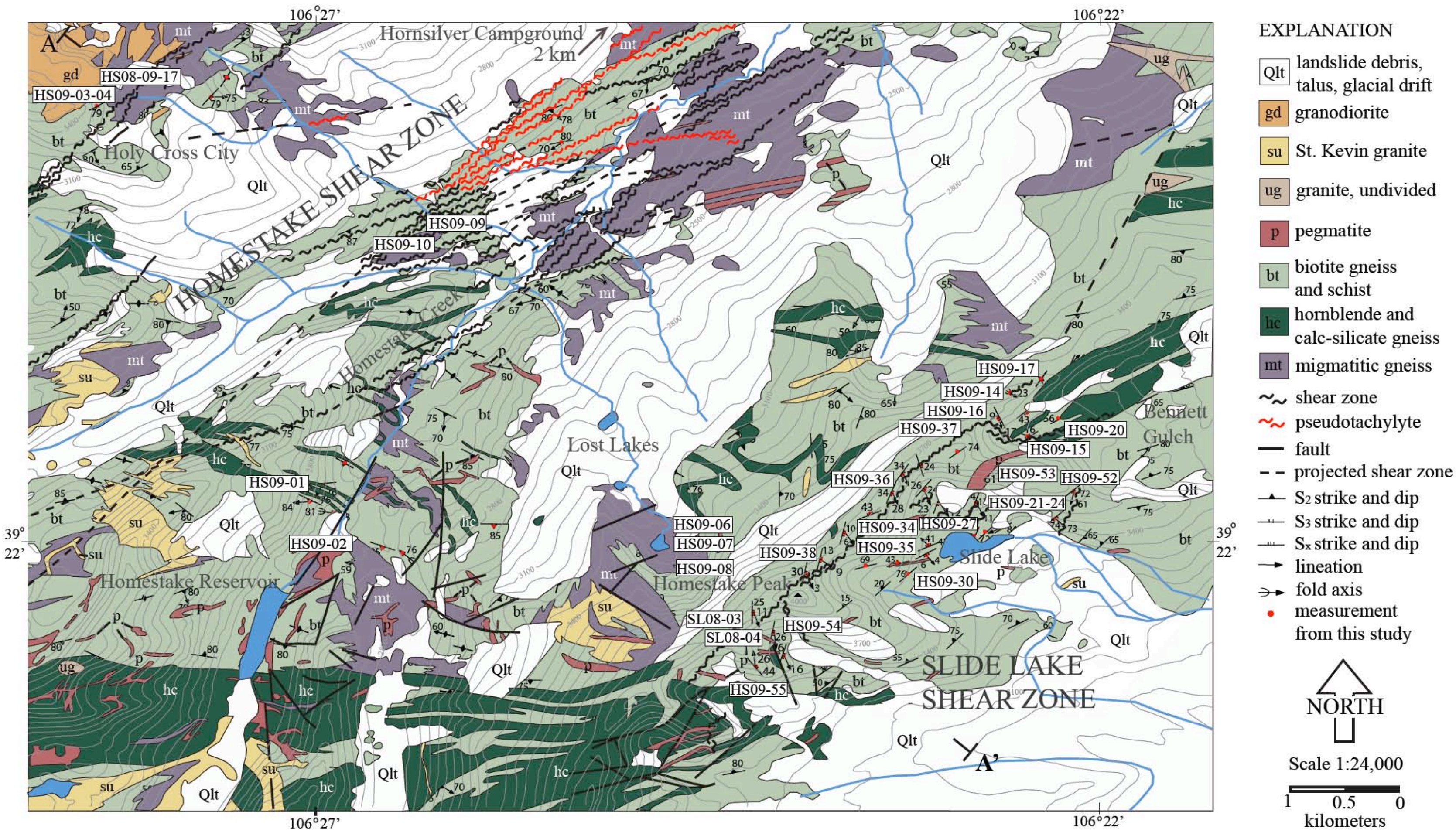

Figure 2. Generalized geologic map of the northern Sawatch Range in the vicinity of Homestake and Slide Lake shear zones, Lake and Eagle County, Colorado. Map was compiled from field mapping in this study, Tweto (1974), Tweto et al. (1978), and Shaw and Allen (2007). Cross-section line A-A' (Figure 6) is taken from this map. Sample locations denoted in white rectangles. A larger, detailed version of this map can be found in Plate I.

The consistency of the strike-slip component within subvertical shear zones along the CMB has led other researchers to suggest that this vertical and horizontal movement is part of a system of transpressional shear zones (Nyman et al., 1994; McCoy et al., 2005; Siddoway et al., 2000; Shaw and Allen, 2007). Due to the spatial proximity between the HSZ and SLSZ (Figure 2), the well-established deformation history of the HSZ will be used to calibrate our new contribution to the deformational history and kinematics of SLSZ as it relates to tectonic-scale processes during the Proterozoic (Shaw et al., 2001; McCoy et al., 2005; Shaw and Allen, 2007).

Due to the slightly less accessible location of Slide Lake and Homestake Peak, relatively little was known about the geometry of the SLSZ, the variability in rock types, consistency in shear-sense indicators, or deformation mechanisms prior to this investigation. To constrain these variables, we created a detailed (1:24,000) map of the SLSZ, (A-1), collected oriented samples from different structural levels, documented fabric relationships to characterize deformation, and quantified strain partitioning across both the HSZ and SLSZ. This project also builds on extensive data from previous investigations, including: (1) detailed structural mapping of the Holy Cross quadrangle (Tweto, 1974), (2) age dates from electron microprobe U-Th-Pb monazite and $^{40}Ar/^{39}Ar$ geochronology (Shaw et al., 2001; Shaw et al., 2005) that constrain Paleo- and Mesoproterozoic metamorphism in the HSZ, and (3) rheologic and kinematic studies of the HSZ (Allen, 1994; Shaw et al., 2001; Shaw and Allen, 2007), as well as the work of others within the Sawatch Range and neighboring shear zones (Figure 1A).

We combine a detailed structural map of the SLSZ with mesoscale observations, microstructural analysis, quartz [c] axis lattice preferred orientation (LPO) patterns derived from electron backscatter diffraction (EBSD), and mean kinematic vorticity (W_m) analysis to constrain the kinematics of the SLSZ and HSZ. As the first major contribution to the SLSZ, this study determines that the low-angle SLSZ records multiple stages of movement in a system that is kinematically linked to the HSZ. Our new data confirms that the HSZ and SLSZ are part of a transpressional system that involved the formation of low-angle shear zones in the mid-crust. Results also provide insights into how strain was partitioned during the ~1.4 Ga tectonism that others have postulated to be analogous to the interior of an orogenic plateau (Shaw et al., 2005).

CHAPTER 2

BACKGROUND

The evolution of a continental crust involves multiple pulses of tectonism, where new crust is assembled onto preexisting crust, and structures associated with shortening, extension, and transcurrent movements are created. Such structures can evolve into persistent intracontinental tectonic zones through repeated reactivation during continental deformation. (Harland, 1971; Molnar, 1988; Molnar and Tapponnier,1975; Bowring and Karlstrom, 1990; Teyssier et al., 1995). Major northeast-striking shear zones throughout the southwestern United States record deformation associated with the assembly and reactivation of structures within the North American continent (Tweto and Sims, 1963; Bowring and Karlstrom, 1990; Karlstrom and Humphreys, 1998; Shaw et al., 2001). Research over several decades has constrained the tectonic history of Colorado's Proterozoic shear zones (Figure 3, 4) (Tweto and Sims, 1963; Tweto, 1974; Shaw et al., 2001; McCoy et al., 2005; Jessup et al., 2005; Shaw and Allen, 2007). Traceable from the Cheyenne belt of southern Wyoming (e.g. Karlstrom and Houston, 1984) southward to New Mexico, the Proterozoic mid-crust that is exposed in central Colorado is part of a ~1200-km-wide swath of juvenile lithosphere and blocks of older material that was assembled onto the southern margin of Laurentia at about 1.8-1.6 Ga (Figure 1A) (Tweto and Sims, 1963; Tweto, 1974; DePaolo, 1981; Karlstrom and Bowring, 1988; Bowring and Karlstrom, 1990; Shaw and Karlstrom, 1999; Hill and Bickford, 2001; Shaw et al., 2001; Tyson et al., 2002; Jessup et al., 2005; McCoy et al., 2005; Shaw and Allen, 2007). A variety of models for this 200-m.y. history of continental growth have been proposed, yet uncertainty remains in defining province boundaries and evidence for moderately dipping shear zones that accommodated crustal shortening across the region (Bickford, 1988; Shaw and Karlstrom, 1999; Hill and Bickford, 2001; Tyson et al., 2002; McCoy et al., 2005).

The Cheyenne belt, Wyoming, defines the southernmost boundary of the Archean craton and the northern extent of a southeastward-younging series of accreted terranes associated with the amalgamation of Laurentia (Karlstrom and Houston, 1984; Duebendorfer et al., 1987; Karlstrom and Bowring, 1988; Bowring and Karlstrom, 1990; Bickford and Hill, 2007). The Yavapai province lies south of the Cheyenne belt and is composed of metamorphic and igneous rocks that are interpreted as a mosaic of arc-derived rocks and fragments of older continental crust that were assembled across a complex system of northeast- and southwest-striking subduction zones between 1.78-1.70 Ga (Duebendorfer et al., 1987; Shaw and Karlstrom, 1999; Hill and Bickford, 2001; Jessup et al., 2005, 2006). Another model suggests that the Cheyenne belt was not the exact suture and that juvenile terranes were reshuffled in a rifted suture zone (Karlstrom and Houston, 1984; Duebendorfer and Houston, 1986; Hill and Bickford, 2001; Tyson et al., 2002; Bickford and Hill, 2007). This model for juvenile crust is supported by Nd isotopic data that suggests the crust of Colorado is derived from ~1.8 Ga mantle differentiation (DePaolo, 1981). U-Pb studies have found Late Archean-Early Proterozoic ages in inherited zircons within plutons of central Colorado, suggesting that some material was derived from the recycling of previously accreted crust (Hill and Bickford, 2001).

The Mazatzal province south of the Yavapai, records deformation and metamorphism at 1.68-1.65 Ga that involved southeastward accretion of terranes onto the Yavapai province along a northeast-striking zone (Figure 1A) (Shaw and Karlstrom, 1999). Shaw and Karlstrom (1999) described this transition zone as a mosaic of tectonostratigraphic terranes, with many sutures marking the progressive addition of material at the convergent margin.

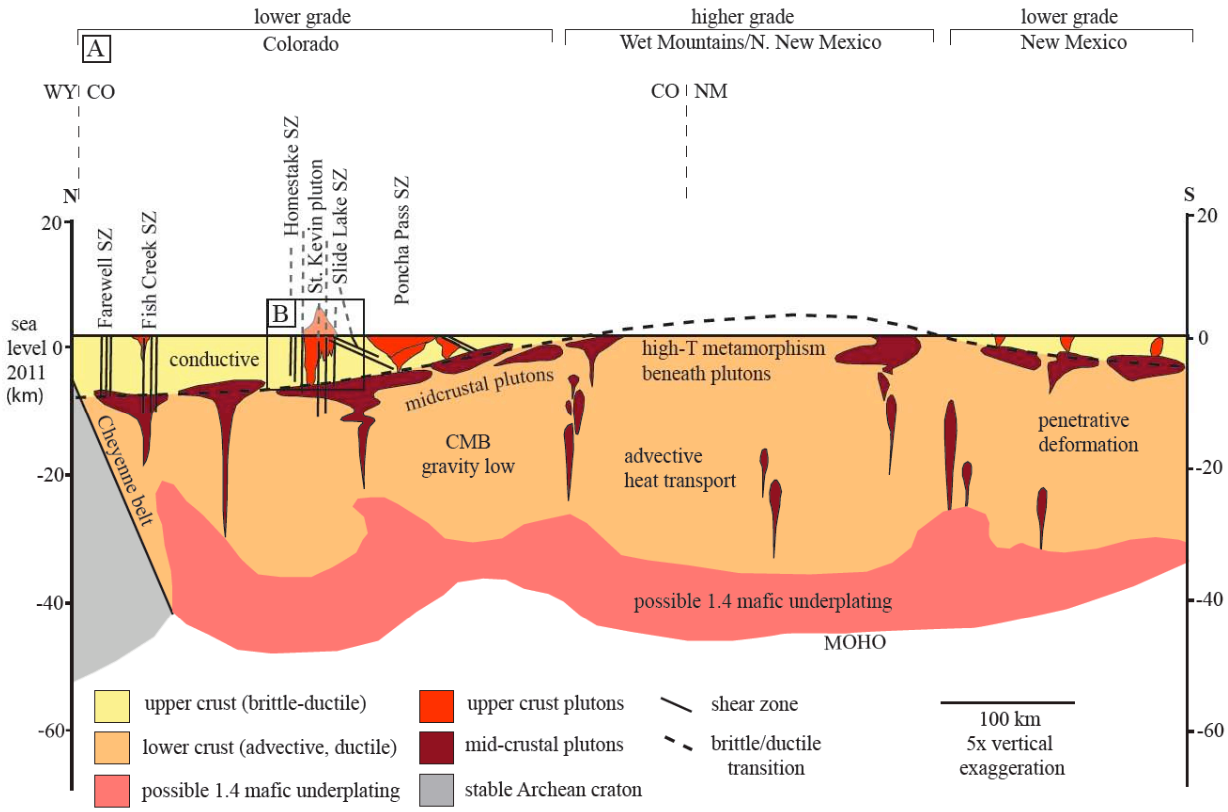

Figure 3. (A) Cartoon cross section illustrating mid-crustal processes that existed in the southwestern U.S. during 1.4 Ga deformation. Figure shows spatial relationship between higher temperature metamorphism and advection in the lower crust and syntectonic emplacment of plutons with ~1.4 Ga mylonite development in major shear zones. Elevation in relation to present day sea level with the dashed line representing the position of the mid-crustal ductile-brittle transition during 1.4 Ga deformation (Modified from Shaw et al., 2005). (B) Box represents field area for HSZ and SLSZ. The two subhorizontal shear zones displayed include the SLSZ and the Poncha Pass shear zone (PPSZ, Figure 1A).

Following the 1.7-1.62 Ga Mazatzal orogeny, a 200-m.y. period of continental stability ensued, with magmatism and the reactivation of earlier structures occurring between 1.47 and 1.36 Ga (Figure 4) (Karlstrom and Bowring, 1988; Williams, 1991; Reed et al., 1993; Nyman et al., 1994; Duebendorfer and Christensen, 1995; Kirby et al., 1995; Karlstrom and Humphreys, 1998; Williams et al., 1999; Jessup et al., 2005, 2006; Jones et al., 2010b). Magma emplacement at ~1.4 Ga was previously described as A-type, occurring in an anorogenic tectonic setting, and related to regional extension in the southwestern U.S. (Anderson, 1983; Hoffman, 1989; Frost et al., 2001). In contrast to anorogenic interpretations based on the geochemical data (Anderson, 1983; Frost et al., 2001), field- and lab-based structural investigations of these granites suggest that emplacement (Figure 3) was accompanied by northwest-directed shortening and strike-slip deformation (Graubard and Mattinson, 1990; Shaw et al., 2001; Jessup et al., 2006; Jones et al., 2010b). This deformation is attributed to far-field stresses invoked by distal subduction or transpression on the southeastern margin of Laurentia (Nyman et al., 1994; Duebendorfer and Christensen, 1995; Ferguson et al., 2004; Jones et al., 2010a).

Many granitic bodies are also associated with northeast-striking shear zones (Bickford, 1988; Bowring and Karlstrom, 1990) that facilitated the emplacement of ~1.4 Ga granites (Figure 3). The 1.44 Ga Mt. Evans batholith is correlated with the reactivation of the Idaho-Springs Ralston shear zone (ISRZ; Figure 1) (Aleinkoff et al., 1993; Nyman et al., 1994). Heat advection related to granite emplacement in the mid-crust may have caused thermal weakening, possibly decreasing the critical shear strength and reactivating the shear zones during the Mesoproterozoic (Figure 3) (Selverstone et al., 2000; Shaw et al., 2005). In central Colorado, the formation of shear zones created an anisotropy (i.e. pre-existing weakness) that possibly controlled the distribution of Mesoproterozoic deformation and the occurrence of granites (e.g.

Davidson et al., 1992; D'Lamos et al., 1997). Reactivation of the Moose Mountain shear zone (MMSZ, Figure 1A) and emplacement of the St. Vrain granite also occurred at 1.4 Ga (Selverstone et al., 2000). In the Northern Sawatch, the St. Kevin granite (1.396 Ga; Doe and Pearson, 1969) occurs in proximity to both the HSZ and SLSZ and has been suggested to be coeval with HSZ development (Shaw and Allen, 2007), however a correlation has yet to be made between 1.4 Ga granite emplacement and SLSZ development.

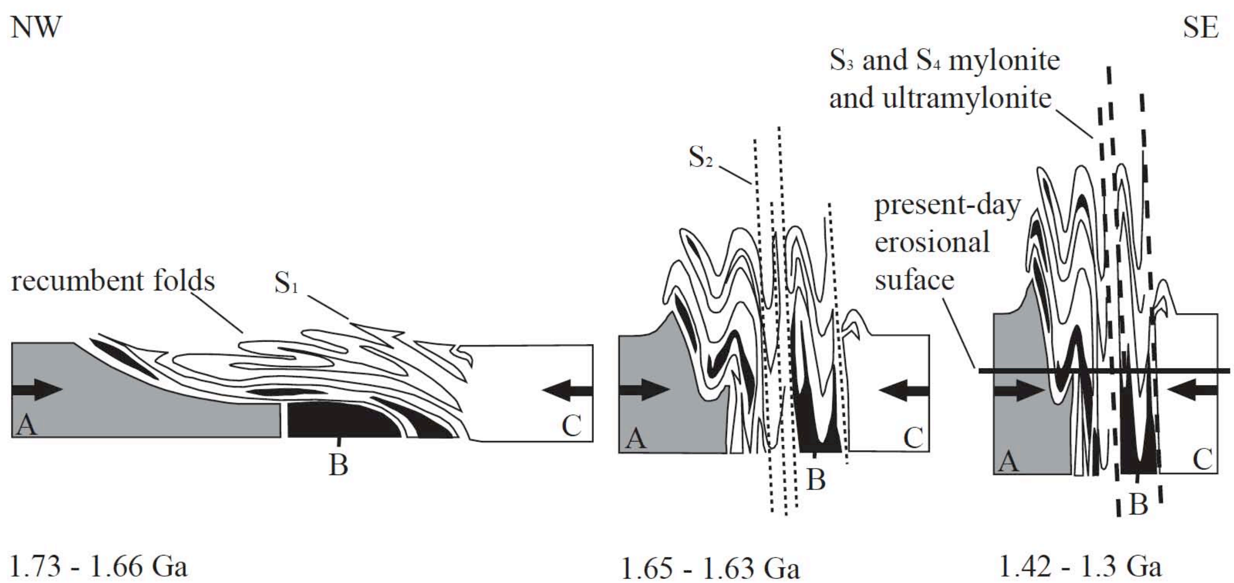

Figure 4. Model for the progressive assembly of the terranes (A, B, C) in central Colorado during the Proterozoic. The first stage (1.73-1.66 Ga) regional shortening and sub-horizontal (S_1) fabric development; oceanic terrane B thrust into large recumbent folds. Continued crustal shortening (1.65-1.63 Ga) steepened earlier folds into S_2 domains. Steep domains accommodated far-field tectonic stresses during the 1.42-1.3 Ga event with mylonite and ultramylonite development. Modified from McCoy et al., 2005.

CHAPTER 3

STRUCTURAL FRAMEWORK

Initial mapping and structural interpretation of the HSZ (Tweto, 1974; Allen, 1994; Shaw et al., 2001, McCoy et al., 2005; Allen, 2005; Shaw and Allen, 2007) defined a regional northeast-striking shear zone system consisting of mylonites, ultramylonites, and pseudotachylyte that cut ~1.8-1.6 Ga Proterozoic high-temperature transposed schist, gneiss, and migmatite. We will use the Proterozoic deformational history of the HSZ (Table 1) and other nearby shear zones (GRSZ, ISRSZ, SLLSZ, BCSZ; see Figure 1A) to calibrate our investigation into the evolution of the SLSZ. Although the chronology of deformation uses the terminology established by Shaw et al. (2001) (D_1 -D_4; Table 1) and associated foliation and lineation development during each phase of deformation, we recognize that these could represent a wide spectrum of timing sequences including distinct and/or protracted events. Shear sense indicators presented in this section are observed in the XZ plane (parallel to lineation and perpendicular to foliation) unless otherwise noted.

Fieldwork was conducted over two summers (2008-2009) and involved mapping and sampling of: (1) SLSZ in the vicinity of Homestake Peak and Slide Lake cirque, (2) a transect from the southeast ridge of Homestake Peak to the southeast ridgeline of Mount of the Holy Cross, and (3) the Continental Divide ridgeline from Homestake Peak to Camp Hale (Hwy 24). From that work, a geologic map (Figure 2 and A-1), lower hemisphere equal area stereonets (Figure 5; A-1), and a cross section (Figure 6; Plates 1 and 2) were compiled with structural data from Tweto (1974) and additional field observations, including lithology, structure, and mesoscale kinematic indicators (Appendix II, III).

Table 1
Summary of deformation episodes for the Homestake shear zone

Episode	Age (Ga)*	Fabric and deformation	Temperature (°C)*	Shear sense
D_1	> 1.7	S_1 sub-horizontal flow	> 500	-
D_2	1.7-1.62	S_2/F_2 NW-SE upright folds	> 500	t-NW
D_3	1.42-1.38	S_3 mylonite	300-500	t-SE, dextral
D_4	~ 1.38	S_4 ultramylonite and pseudotachylyte	250-450	t-NW, dextral

Abbreviations: t-NW, top-up-to-the-NW; t-SE, top-down-to-the-SE
*Ages, temperature, and shear sense after Shaw et al. (2001); Shaw et al. (2005)

3.1. Deformation history and mesoscale structural observations of the HSZ

HSZ (Figure 1B; 2) is exposed on glacially polished outcrops along Homestake Creek as well as above tree line at the old mining locale of Holy Cross City. The valley walls on either side of Homestake Creek are covered by dense vegetation, along with Pleistocene to Holocene glacial drift. HSZ consists of partially migmatized biotite gneiss and schist (bt+grt+sil+qtz+fsp+ ms) and calc-silicate gneiss (hbl+cal+qtz+fsp+ms), all cut by minor pegmatite veins and unclassified Precambrian granites (Figure 2; A-1). The overall northeast-striking shear zone (Figure 5A; 6) is exposed along Homestake Creek as a series of anastomosing splays (0.10 to 3-m-thick) (Figure 2; A-1). Starting at the southwest end of the valley and trending toward the northeast, the shear zone thins and splits into smaller splays toward the northeastern part of Homestake Creek (Figure 7A). Mylonite was observed along Homestake Creek Road and Hornsilver Campground (Shaw et al., 2001), ultramylonite was observed at Holy Cross City, and pseudotachylyte was observed along the Holy Cross Jeep trail and along Homestake Creek (Allen, 2005) (Figure 2; A-1).

Paleoproterozoic deformation

The earliest stage of Paleoproterozoic deformation (D_1) is characterized by high-temperature, melt-present flow. The main foliation (S_1) is subhorizontal and resulted from viscous flow near the granite solidus at ~1708 ± 6 Ma (Shaw et al., 2001). The presence of prismatic sillimanite, biotite, and garnet within HSZ samples implies conditions within the sillimanite isograd. This early foliation (S_1) is present in the HSZ as well as the GRSZ, SLLSZ, and ISRSZ (McCoy et al., 2005). In HSZ, S_1 is characterized by alternating bands of leucosomes and biotite-rich melanosomes in migmatitic gneiss (bt+grt+sil+qtz+fsp+ms) (Figure 7B).

The second stage of deformation (D_2) also occurred during the Paleoproterozoic at amphibolite facies conditions and involved northwest-directed shortening, forming northeast-southwest-trending upright isoclinal folds (Table 1). Within the HSZ, this mid-crustal shortening event steepened and transposed S_1, creating an S_2 axial-surface foliation (Figure 7C) at ~1658 ± 5 Ma (Shaw et al., 2001). The ~1675 Ma Cross Creek granite/granodiorite (Tweto and Lovering, 1977) was emplaced to the northwest of HSZ (Figure 2) during this episode. The Cross Creek granite crosscuts an early foliation (S_1) and follows the general northeast-trend of the HSZ. The steeply dipping foliation (S_2) contains zones of high strain rocks that record general shear in the region at ~1.65 Ga (Shaw et al., 2001). Recumbent nappes (F_1) are preserved in lower strain zones where refolded (F_2), creating fold interference patterns (Shaw et al., 2001).

Mesoproterozoic deformation

Following ~200 m.y. of stability, Mesoproterozoic deformation represents a major shift in deformation style across the region from the distributed high-temperature, melt-present deformation during the Paleoproterozoic into moderate temperature greenschist facies conditions and localized solid-state shear zone development (Table 1). The initial stage of deformation (D_3) is recorded by mylonite development within the HSZ along anastomosing systems (S_3) that reactivated and overprinted the steep foliation (S_2) (Figure 4; 6). Near Hornsilver Campground and Holy Cross City areas (Figure 7D), narrow (1-3-m-thick) bands of quartzofeldspathic rocks that contain interspersed ribbon quartz and phyllosilicate-rich layers with rigid feldspar porphyroclasts make up the pervasive foliation (S_3: 059, 79°SE) that contains an oblique stretching lineation (L_3: 73° → 213) (Figure 5). Narrow (1-10 cm-thick) mylonitic quartz veins occur along some of the mylonite splays. Feldspar porphyroclasts and shear bands record top-down-to-the-southeast sense of shear during mylonite development (D_3) that occurred between 1.45 to 1.38 Ga (Figure 5, 6) (Shaw et al., 2001).

The final stage of reactivation (D_4) involved the development of mylonite and ultramylonite (S_4: 059, 79°SE) that record top-up-to-the-northwest shear sense and pseudotachylyte that overprinted S_3 (Table 1). Analysis of timing, kinematics, and deformation temperatures within both the HSZ (Shaw and Allen, 2007) and GRSZ (McCoy et al., 2005) suggest that mylonite and ultramylonite are spatially and temporally coincident. Pseudotachylyte, cataclasite, and brittle fractures are unique to D_4. D_4 ultramylonite contains a steeply plunging stretching lineation (L_4: 78° → 120) and records dextral and top-up-to-the-northwest (reverse) sense of shear (Figure 5) (Shaw and Allen, 2007). In situ monazite geochronology yields ages for the formation of ultramylonites (S_4) at 1375 ± 14 Ma in the HSZ (Shaw et al., 2001), and more widely with D_4 deformation across the HSZ at 1.38 Ga.

Pseudotachylyte (S_4) occurs as black, discontinuous anastomosing veins in migmatite, biotite gneiss, and alongside ultramylonite (Figure 7E). In the HSZ, pseudotachylyte has been divided into eight northeast-striking, steeply dipping zones (0.2-2.3-km-wide and 1.5-7.3-km-long and varying in thickness 1-15 cm) (Allen, 2005), following and crosscutting the steep, northeast-striking foliation (S_2: 059, 79°SE). The existence of coeval ductile ultramylonite with brittle-frictional pseudotachylyte points to unique conditions, suggesting local changes in temperature, grain size, fluid pressure, and strain rate that affected the prevalence of mid-crustal ductile vs. brittle deformation within an exhumed seismogenic zone (Allen, 2005; Shaw et al., 2005; Shaw and Allen, 2007).

Figure 5: Lower hemisphere equal area stereonets showing foliation and lineation relationships in the field areas. Black planes represent average foliation plane and shaded contours represent poles to foliation for all measured planes. Stretching lineations from this study represented by dashed contour lines. Stretching lineations from Shaw and Allen (2007) denoted with “x” and “o”. (A) HSZ S_3 (056, 79°SE), L_3 (73° → 213), and L_4 (78° → 120). (B) SLSZ low-angle splays, S_x (007, 24°SE) and L_x (09° → 165). (C) SLSZ Bennett ridgeline moderately dipping splay, S_x (048, 60°SE) and L_x (60° → 121).

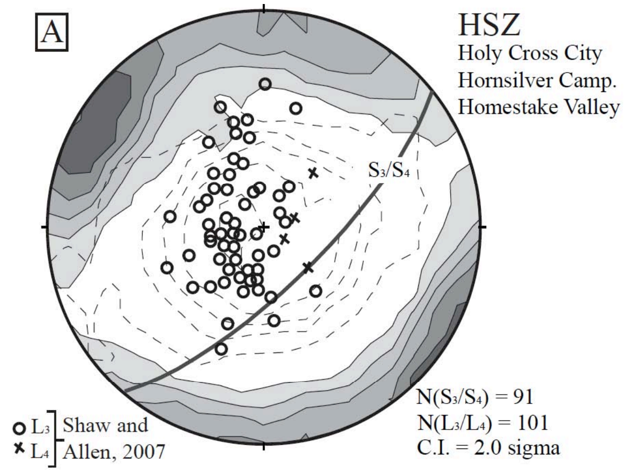

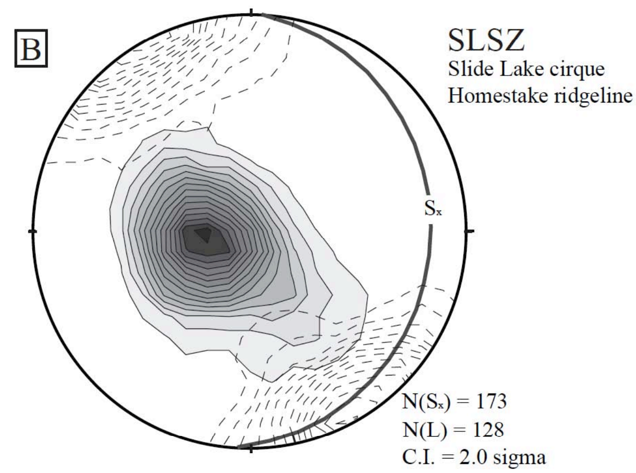

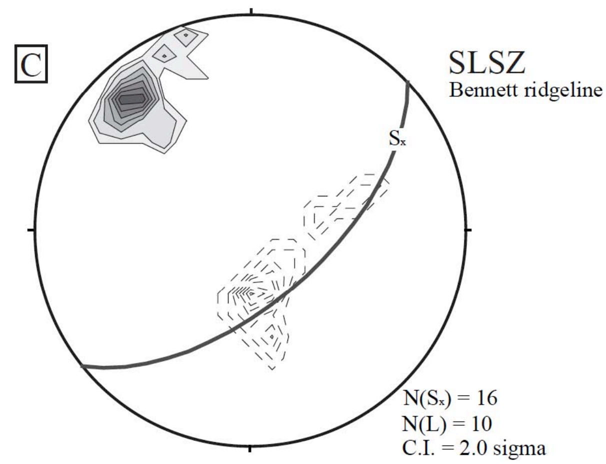

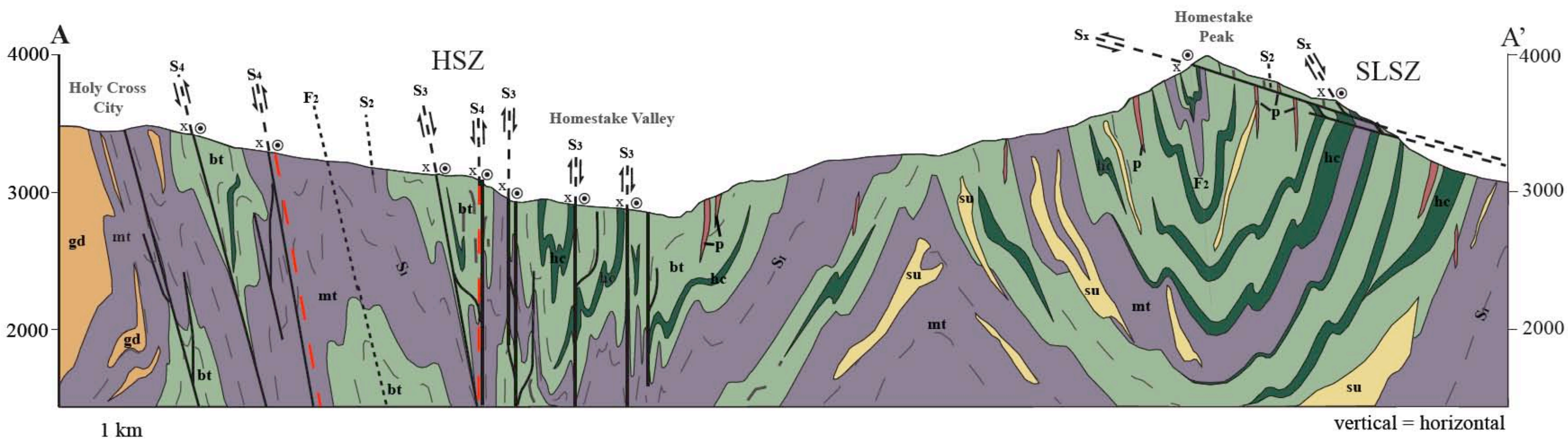

Figure 6. Geologic cross section of the field area (A-A’). Figure shows the multiple generations of foliation exposed in the field area: S_1 early melt present foliation; S_2/F_2 upright folds; S_3 mylonite; S_4 ultramylonite and pseudotachylyte (red-dashed line); and S_x SLSZ fabric. Sense of shear denoted by arrows for vertical motion and “x” and “⊙” for lateral displacement. See Figure 2 and Plate 1 for explanation.

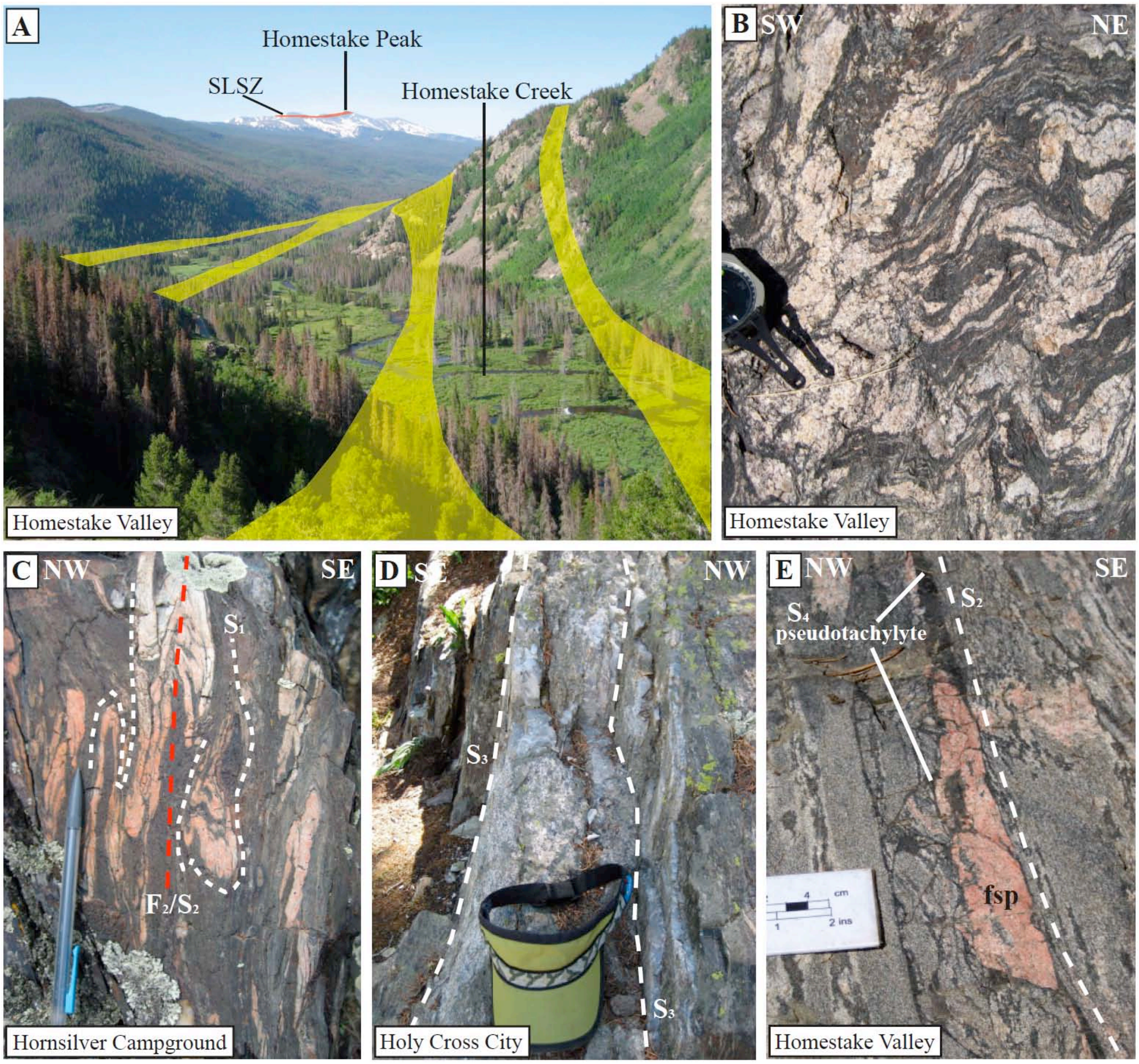

Figure 7. Field observations from the HSZ. (A) View from Hornsilver Campground (Figure 2) towards the southwest along Homestake Creek; yellow bands represent the northeast-striking, subvertical HSZ and the red sliver at skyline represents the upper band of the SLSZ exposed at Homestake Peak. (B) High-temperature (bt+qtz+sil+fsp) migmatite (S_1) characteristic of the region. (C) S_1 fabric folded and transposed into steep S_2 fabric at Hornsilver Campground. (D) Subvertical ultramylonite outcrop near Holy Cross City. (E) Image viewed towards the NE along strike; subvertical S_2 fabric overprinted by pseudotachylyte bounding the feldspar leucosome in the center of the image.

3.2. Mesoscale structural observations of the SLSZ

The shallow to moderately dipping SLSZ exists ~1200-m-above Homestake Valley at and above tree line, and spans two prominent ridges and glacially carved cirques (Figure 2; 8A; A-1). SLSZ occurs as three splays of mylonite and ultramylonite in an area composed of amphibolite facies biotite gneiss (bt+grt+sil+qtz+fsp+ms), quartzofeldspathic gneiss (qtz+fsp+ms+bt), calc-silicate gneiss (hbl+cal+qtz+chl), and migmatite (bt+grt+sil+qtz+fsp+ms), all cut by pegmatite and granite. The overall north-northeast-striking SLSZ occurs as two shallow dipping anastomosing slays that plunge toward the southeast (Figure 5B) and are joined by at least one moderately, southeast-dipping mylonite splay (Figure 5C). Based on field mapping, SLSZ exists as three major mylonite and ultramylonite splays that occur (1) ~10-m-below the summit of Homestake Peak on the Continental Divide, (2) in Slide Lake cirque/Bennett Gulch cirque, and (3) along the Bennett Gulch/Slide Lake ridgeline (Figure 2; 8A). We use the Proterozoic deformational events of the HSZ to calibrate our investigation of the SLSZ, and recognize that these may represent a wide range of timing sequences that include distinct and/or protracted deformational events.

Paleoproterozoic deformation

High-temperature rocks from the first (D_1) and second (D_2) stages of Paleoproterozoic deformation are found in the hanging wall and footwall of the SLSZ. Migmatitic gneiss (bt+grt+ sil+qtz+fsp+ms) is the same as that observed in the HSZ area, with leucosomes and biotite melanosomes characterizing the high-temperature melt-present subhorizontal flow (S_1). The mid-crustal shortening event (D_2) steepened and transposed S_1, creating the axial surface foliation (S_2: 059, 79°SE) similar to that seen in the HSZ. Amphibolite facies gneiss (bt+gt+sil+qtz+fsp+ms) with well-developed biotite foliation overprints older migmatite and are folded into northeast – southwest trending upright folds (F_2).

Mesoproterozoic deformation

~1.4 Ga deformation in the SLSZ represents a change in both metamorphic conditions and kinematics, from high-temperature amphibolite conditions and steep foliation development to moderate-temperature greenschist conditions and the development of a shallow foliation. SLSZ foliation (S_x) is associated with mylonite and ultramylonite development. As absolute timing was not performed in the SLSZ, we refer to 1.4 Ga foliation as S_x. Unlike the HSZ where 1.4 Ga foliation (S_3 and S_4) reactivated and overprinted earlier steeply dipping foliation (S_2), the shallowly dipping 1.4 Ga mylonite and ultramylonite (average low-angle S_x: 007, 24°SE) contains a stretching lineation (average shallow L_x: 011° → 165) in the SLSZ and was found to both truncate and exist parallel to earlier S_2 foliation (059, 79°SE).

The SLSZ is exposed along Bennett ridgeline (Figure 8A; 9A,B) and consists of at least two, ~1-m-thick moderately dipping (048, 60°SE), upper greenschist facies mylonite (qtz+fsp+bt) bands (S_x) bound by high strain zones that consist of grain-size reduced biotite and quartz. Exposure of this splay is isolated to a narrow band of high-strain rock and mylonite interspersed with foliated quartzofeldspathic gneiss on the ridge that divides Bennett gulch from Slide Lake cirque. Moderately dipping mylonite (qtz+fsp+bt) contains rigid, pink feldspars that are set in a matrix of phyllosilicate (bt+ms) and quartz ribbons. Mylonitic foliation (S_x) in the hanging wall and footwall of this shear zone splay is parallel with the moderately dipping earlier high-temperature foliation (Figure 8B). A well-developed, shallow and oblique, southeast

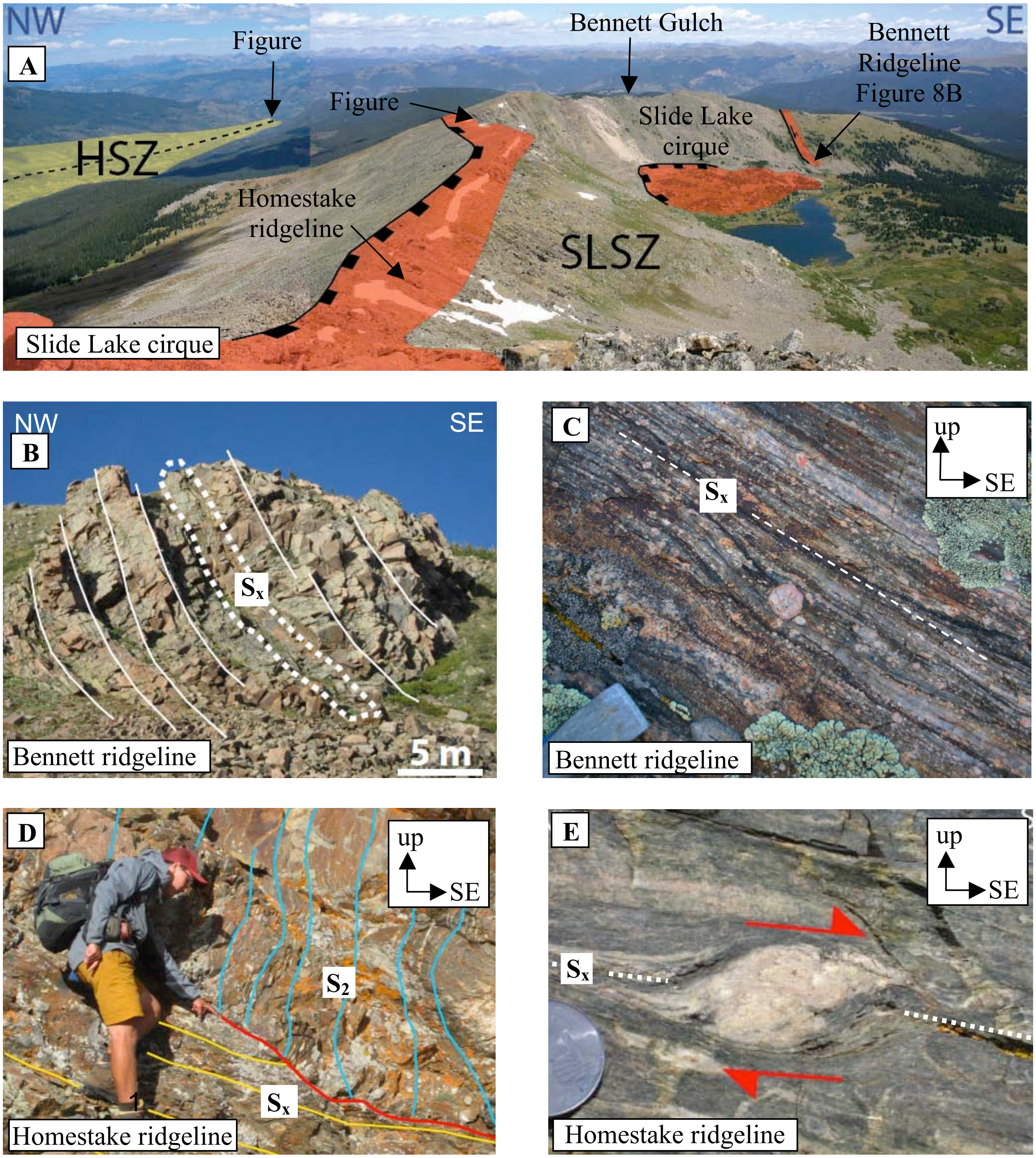

Figure 8. Field observations of the SLSZ. (A)View towards the northeast along the Continental Divide; three major splays (highlighted red) of the SLSZ. (B) Bennett ridgeline outcrop, mylonite splay dashed and parallel to the surrounding foliation (C) Bennett ridgeline mylonite. (D) Fabric truncation between the steep fabric (S_2) within the hanging wall of the upper splay and the subhorizontal fabric (S_x) of the SLSZ. (E) Porphyroclasts within quartz-calcite-biotite mylonite from the upper splay, top-down-to-the-southeast motion.

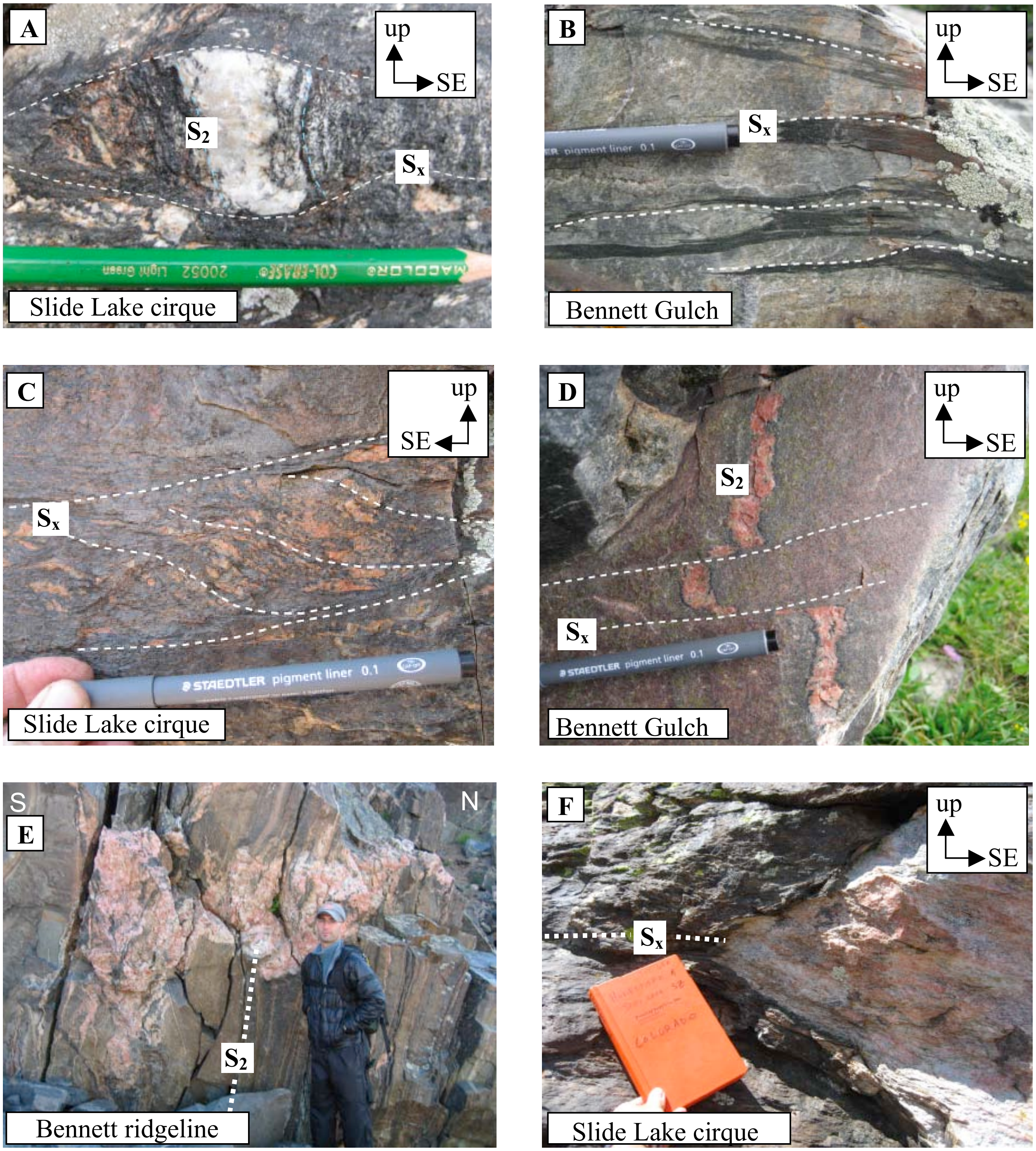

Figure 9. Additional field observations from the Slide Lake shear zone. (A) Fabric relationships in Slide Lake cirque. (B) Grain-size reduced high strain domain in Bennett Gulch. (C) S-C fabric in Slide Lake cirque. (D) Pegmatite offset by high strain domains in Bennett Gulch. (E) Pegmatite cross-cutting steep S_2 fabric. (F) Pegmatite incorporated into shallow S_x SLSZ fabric.

plunging stretching lineation (L_x: 60° → 121) defined by of quartz and feldspar aggregates was observed on the moderately dipping foliation surface (S_x: 048, 60°SE) (Figure 5C). Mesoscale shear-sense indicators (e.g. asymmetric tails on porphyroclasts, shear bands, offset shear bands) reveal dominant top-down-to-the-southeast sense of shear.

Homestake ridgeline (Figure 8A) is the most laterally extensive exposure of the SLSZ that we mapped along the Continental Divide from the saddle southwest of Homestake Peak to the unnamed peak that divides Bennett Gulch and Slide Lake cirque. On the southwestern saddle (southwest of the Homestake summit), the low-angle calc-silicate (cal+qtz+bt+ms+chl) ultramylonite is traceable along-dip for 100+ meters from the saddle down the southeastern side of the Continental Divide. On the northeastern side of Homestake summit, low-angle (S_x: 003, 20°SE), greenschist facies ultramylonite (qtz+bt+fsp+ms ± cal+chl) is traceable along the Continental Divide. Ultramylonite is composed of small feldspar porphyroclasts and ribbon quartz with alternating layers of phyllosilicates (bt+ms+chl). Quartz and feldspar grains form a shallowly plunging lineation (L_x: 006° → 166). Foliation relationships (Figs. 5B; 6) at the northeast end of this splay (Figure 8D) reveal a sharp contact between the low-angle SLSZ splay (S_x: 003, 20°SE) and the overlying steep, high-temperature fabric (S_2: 054, 78°SE). The shear zone appears to truncate the steeply dipping fabric (S_2) that is pervasive across the HSZ (Figure 8B). Mylonite and ultramylonite reveal mesoscopic shear sense indicators (e.g. porphyroclasts, S-C fabric, shear bands) that record both top-up-to-the-northwest and top-down-to-the-southeast (Figure 8E) sense of shear, possibly due to overprinting of earlier fabric.

The structurally lowest splay of the SLSZ was mapped as low-angle (bt+qtz+fsp+ms) mylonite and ultramylonite that occurs on the glacially carved pavement in both Slide Lake cirque and Bennett Gulch (Figure 2; 8A; 9A-D). This splay consists of several thin (1-3-m-strands), shallowly dipping (S_x: 015, 29°SE) greenschist facies ultramylonite strands (bt+fsp+qtz-ms+sil) that display a shallowly plunging southeast-trending stretching lineation (L_x: 16° → 164) (Figure 5B). Ultramylonite contains rigid, pink feldspar, ribbon quartz, and phyllosilicates (bt+ms) in a matrix of bt+ms+chl. Thin strands of ultramylonite occurred as discontinuous, anastomosing splays, bound by sections of migmatitie and biotite gneiss and some high strain domains. High strain domains were extensive in the pavement, consisting of grain-size reduced biotite and quartz that anastomose (i.e. follow and crosscut the foliation) throughout this outcrop. A variety of folds were mapped in the shallowly dipping gneiss that bound splays of the shear zone and included a steep southwest-plunging F_1 (81° → 256) and shallow northwest-plunging fold axis F_2 (41° → 321). Mesoscale structural shear sense indicators (e.g. rigid feldspar porphyroclasts with tails, shear bands) record dominant top-down-to-the-southeast and minor top-up-to-the-northwest sense of shear, similar to the type of shear sense recorded in the Homestake ridgeline splay.

CHAPTER 4

KINEMATICS, DEFORMATION TEMPERATURES, AND VORTICITY

To characterize deformation within the mid-crustal rocks of the SLSZ and HSZ, microscale structural analyses were performed on eleven HSZ samples and thirty-four SLSZ samples (Table 1, 2; Appendix I, IV). Quartz lattice-preferred orientation (LPO) analyses were performed on four samples from the two shear zones. Quartz and feldspar grain boundaries and mineral assemblages were used to estimate temperatures of deformation. Mean kinematic vorticity analyses (W_m) were also performed on four HSZ ultramylonites and six SLSZ mylonites to document the spatial and temporal variability of pure and simple shear across the two shear zones. Oriented samples were collected from Holy Cross City and Hornsilver Campground in the HSZ and from Homestake ridgeline, Bennett ridgeline, Slide Lake cirque, and Bennett Gulch in the SLSZ (Figure 2). The oriented samples were cut parallel to lineation and perpendicular to foliation (XZ), with orientation preserved throughout thin-section preparation.

4.1. Kinematics

Homestake shear zone

Mylonite from the Hornsilver Campground splay of the HSZ is characterized by aligned biotite and muscovite interlayered with quartz-rich domains that define a penetrative foliation (S_x: 059, 79°SE) (Table 2). The well-developed stretching lineation is defined by aggregates of quartz, feldspar, and muscovite (L_x: 73° → 213). In many thin sections, quartz subgrains are elongate into ribbons (S fabric) drawn into shear bands (C fabric) of the aligned biotite and muscovite (Figure 10A). This fabric (S_3) contains σ-type feldspar porphyroclasts with tails of quartz subgrains and biotite mica fish that record top-down-to-the-southeast shear sense with minor top-down-to-the-southwest sense of shear. Varying shear sense indicators within the same sample may suggest different deformational episodes, with the more recent event partially overprinting the previous event (e.g. top-up-to-the-northwest overprints top-down-to-the-southeast shear).

Mylonite and ultramylonite in the Holy Cross City splay of the HSZ contain aligned biotite and muscovite that are interlayered with quartz-rich layers. Rigid porphyroclasts are interspersed within mylonitic quartz veins (Figure 10B) composed of quartz subgrains with isolated muscovite and biotite grains. Two generations of well-developed stretching lineation are defined by quartz, feldspar, and muscovite (L_3: 73° → 213; L_4: 78° → 120). Most porphyroclasts in these mylonites appear as mono- and polycrystalline rounded feldspar porphyroclasts with and without tails. Thin sections of mylonite and ultramylonite from the Holy Cross City splay contain the greatest quantity and variety of shear-sense indicators; both δ- and σ-type porphyroclasts (Figure 10B), rhomboidal (Figure 10C) and lenticular (Figure 10D) mica fish, oblique grain-shape fabric in quartz (Figure 10C, D), C'-type shear bands, boudinage (Figure 10E), and mylonitic textures (Figure 10F). Oblique grain-shape fabric created by quartz subgrain alignment exists at steep angles (32-53°) to foliation and mica fish orientation (Figure 10C, D). Shear sense indicators record top-down-to-the-southeast and top-up-to-the-northwest shear sense, evidence for both S_3 and S_4 deformation.

Table 2

Summary of HSZ shear sense, vorticity, and temperature data

Sample	Rock type	Shear sense	Vorticity (W_m)	% Pure shear	Deformation Temperature (°C)	Temperature indicator[b]
Homestake shear zone - Hornsilver Campground						
HS08-01	qtz my	t-NW	-	-	300-400	q.d., m.a.
Homestake shear zone - Holy Cross City transect						
HS08-07	qtz-fsp my	t-NW	0.58-0.68	60-51	450-500	q.d., m.a.
HS08-08	qtz-fsp my	t-NW	-	-	400-500	q.d., m.a.
HS08-09	qtz my	t-NW	-	-	350-450	q.d., m.a.
HS08-10	qtz my	t-NW	0.45-0.70	60-50	450-500	q.d., m.a.
HS08-11	qtz my	t-NW	-	-	350-450	q.d., m.a.
HS08-12	qv	t-NW	-	-	450-500	q.d., m.a.
HS08-13[a]	qv	t-NW		-	450-500	q.d., m.a.
HS08-14[a]	qtz my	-	-	-	450-500	q.d., m.a.
HS09-03	qtz my	t-NW	-	-	400-500	q.d., m.a.
HS09-04	qtz my	t-NW	-	-	300-450	q.f.d, m.a.

Abbreviations: qtz my, quartz mylonite; c.s. my, calc-silicate mylonite; fsp my, feldspar mylonite; gns, gneiss; mbl, marble; qv, quartz vein; t-SE, top-down-to-the-southeast; t-NW, top-up-to-the-northwest.

[a] Samples analyzed with EBSD

[b] Temperature indicators; all samples used q.d, quartz, and q.f.d quartz and feldspar deformation textures, m.a. mineral assemblage

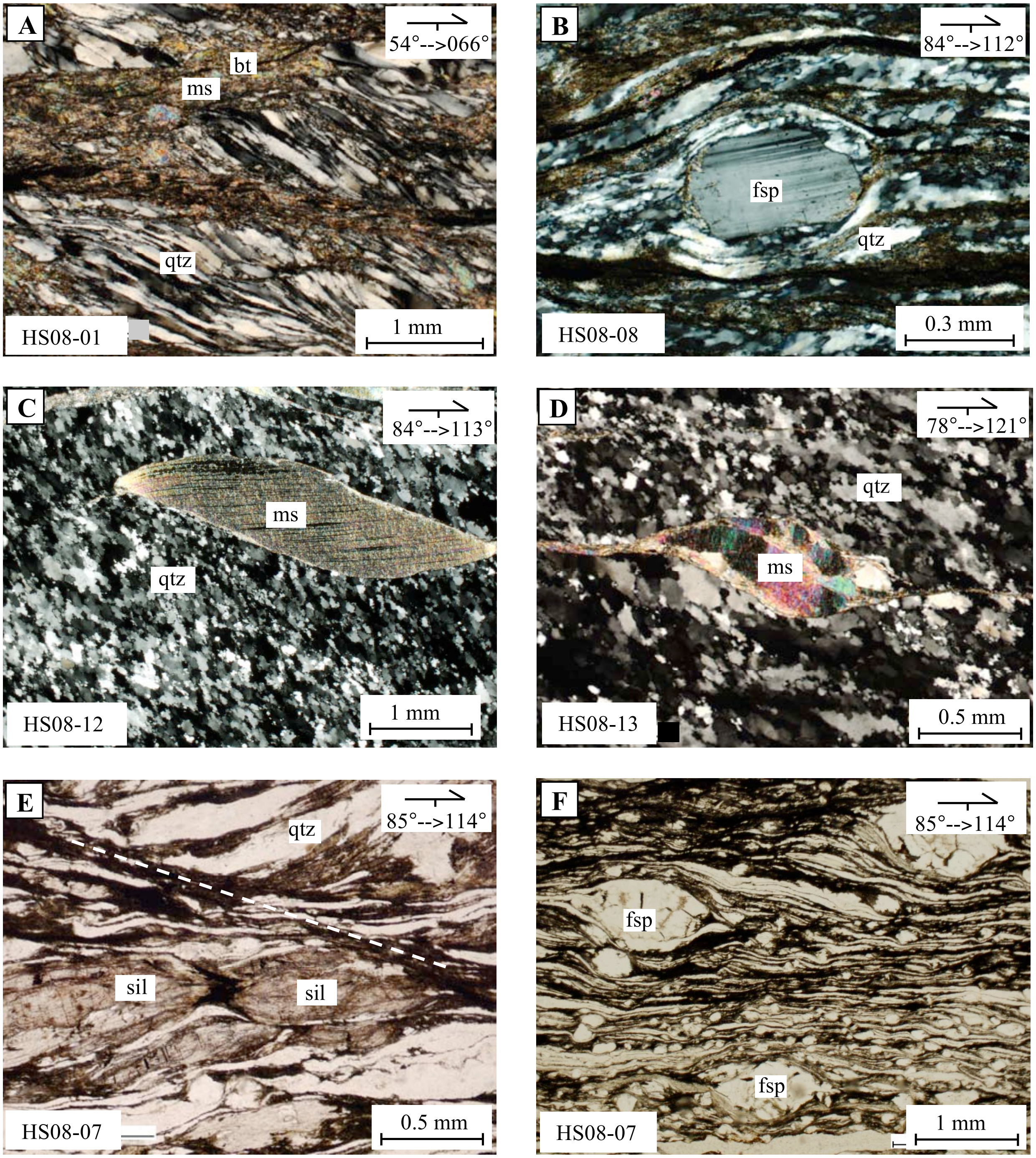

Figure 10. Photomicrographs of HSZ microstructures; crossed polars unless noted. (A) Ultramylonite with S-C fabric with top-up-to-the-SW shear. (B) Mylonite with feldspar porphyroclasts displaying top-down-to-the-SE shear sense. (C) Quartz vein containing oblique grain shape fabric in quartz and mica fish with top-up-to-the-NW shear. (D) Quartz vein with mica fish surrounded by quartz (qtz) subgrains display top-up-to-the-NW shear. (E) Mylonite with sillimanite boudins and shear bands display top-down-to-the-SE; plane light. (F) Mylonite with rigid feldspar porphyroclasts in quartz matrix displays top-up-to-the-NW shear; plane light.

Slide Lake shear zone

Mica fish, asymmetric tails on rigid feldspar porphyroclasts, C- and C'- type shear bands and oblique grain-shape fabric in quartz record both top-down-to-the-southeast and top-up-to-the-northwest shear sense for three major splays of the SLSZ (Figure 11; Table 3; Appendix IV). Twenty-three out of twenty-eight mylonite and ultramylonite samples from the SLSZ record top-down-to-the-southeast shear sense.

The Bennett ridgeline splay of moderately dipping quartzofeldspathic mylonite contains well-defined asymmetric feldspar porphyroclasts (Figure11 A, B), mica fish, and C-type shear bands. This suite of samples from the steeper-dipping mylonite records similar top-down-to-the-southeast shear sense as the other two SLSZ splays, but the mineral assemblage and fabric within the suite is dramatically different. Where the other two splays display qtz+fsp+bt+ms (± cal) mylonite, the Bennett ridgeline splay contains ~80% qtz+fsp with minor bt+ms in the mylonite. The pervasive foliation is defined by bands of quartz and feldspar that alternate with interlayered large white mica laths and biotite grains (Figure 11B) (S_x: 048, 60°SE). Lenticular mica fish are set in a matrix of quartz with polygonal grain boundaries that record high-temperature grain-boundary area reduction. Smaller feldspar and biotite domains also exist with asymmetric-tailed feldspar porphyroclasts domains that pin the high-temperature quartz domains (Figure 11B). In each thin section, the most feldspar porphyroclasts record top-down-to-the-southeast shear sense and a minority of the porphyroclasts record top-up-to-the-northwest sense of shear.

The upper ~100-m-thick Homestake Peak – Continental Divide splay records a large contribution of top-up-to-the-northwest motion along the shallowly dipping shear zone. The pervasive foliation is defined by white mica fish and biotite laths interlayered with quartz and feldspar grains (Figure 11C) (S_x: 003, 20°SE). Quartz and muscovite make up shallowly plunging and weakly developed stretching lineation (L_x: 016° → 166). Between mica-rich domains, quartz and feldspar grains exist in a matrix of calcite, quartz, and biotite. Narrow lenticular mica fish (Figure 11C), C'-type shear bands, and polycrystalline porphyroclasts (Figure 11D) record top-up-to-the-northwest shear sense and a lesser top-down-to-the-SE shear sense component in the upper splay. Sillimanite was also observed in samples from this splay, both in the cores of mica fish and as northwest-southeast oriented boudins. A weak oblique grain-shape fabric in quartz-rich regions developed at a steep angle to foliation (~57°) and records top-up-to-the-northwest shear sense.

The Slide Lake cirque splay is located to the southeast of the ridgeline. Shear sense within the 11 out of the 12 mylonite samples from this part of the shear zone records dominant top-down-to-the-southeast motion. The pervasive foliation in the mylonite is defined by white mica and biotite domains interlayered with quartz and feldspar grains (S_x: 015, 29°SE). A combination of quartz, feldspar, and muscovite make up a weak- to well-developed stretching lineation (L_x: 16° → 164). Mylonite samples display mica fish, S-C' fabric, sillimanite boudins, and δ-type porphyroclasts bound by retrograde muscovite (Figure 11E). Boudins are oriented northwest-southeast. C'-type shear bands record top-down-to-the-southeast sense of shear (Figure 11F). Other samples contain lenticular and rhomboidal mica fish that are set in a matrix of dynamically recrystallized quartz that record top-down-to-the-southeast and minor top-up-to-the-NW shear sense.

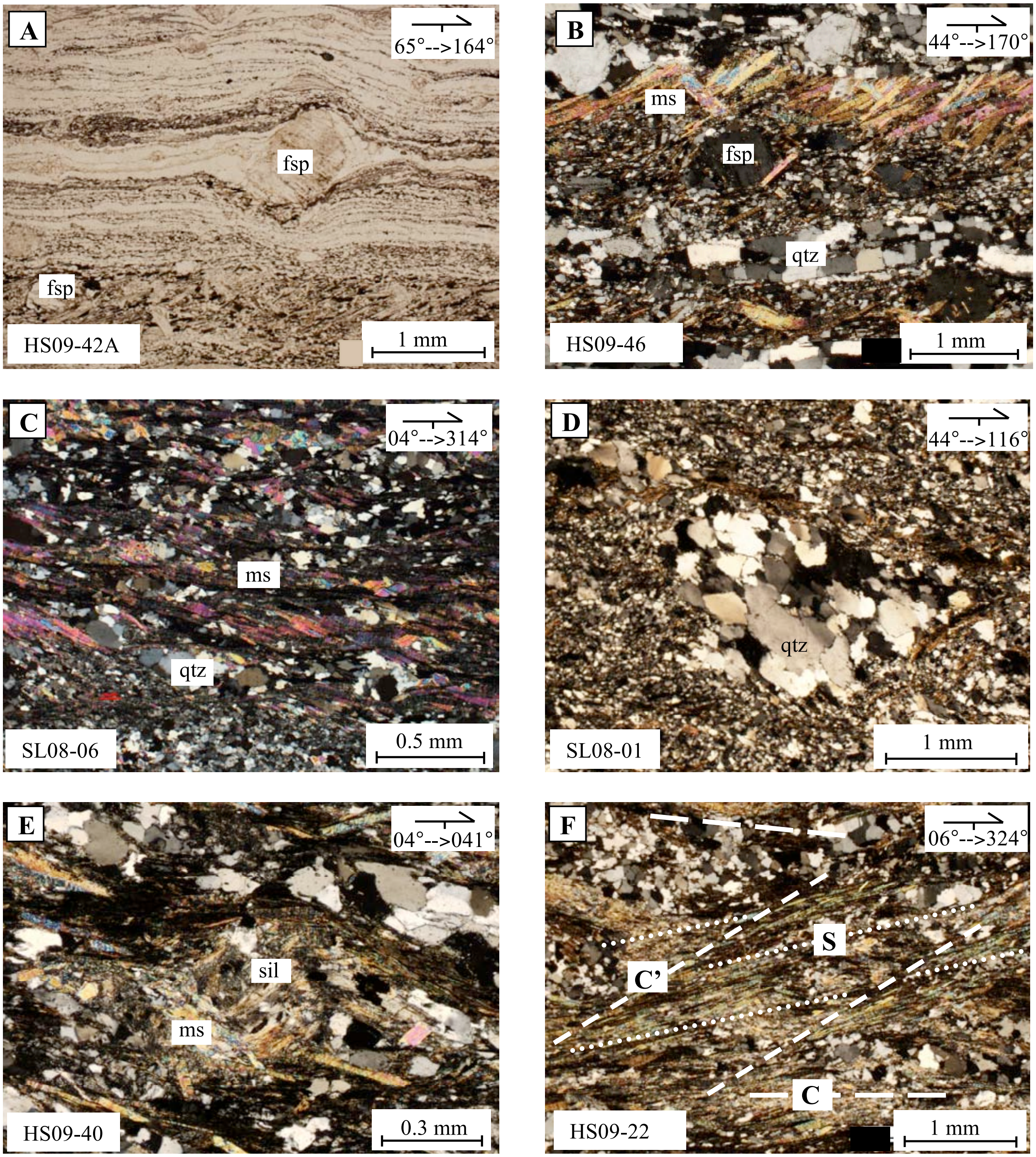

Figure 11. Photomicrographs of SLSZ mylonites; crossed polars unless noted. (A) Quartz-feldspar mylonite with porphyroclasts with asymmetric quartz and biotite tails, top-down-to-the-SE shear; plane light. (B) Mylonite with quartz domains pinned by muscovite laths and biotite, top-down-to-the-SE shear. (C) Ms-bt mylonite with mica fish displaying top-down-to-the-SE shear. (D) Ultramylonite with polycrystalline quartz porphyroclasts displaying top-up-to-the-NW shear. (E) Mylonite showing δ-type sil-porphyroclasts recording top-down-to-the-SE shear. (F) Mylonite with C'- type shear band showing top-down-to-the-SE shear sense.

Table 3
Summary of SLSZ shear sense, vorticity, and deformation temperature data

Sample	Rock type	Shear sense	Vorticity (W_m)	% Pure shear	Deformation Temperature (°C)	Temperature indicator[b]
Slide Lake shear zone - Homestake ridgeline splay						
SL08-08	c.s. my	t-S	-	-	450-550	q.d., m.a.
SL08-07	c.s. my	t-NW	-	-	400-500	m.a..
SL08-06	c.s. my	t-SE	-	-	400-450	q.d., m.a.
SL08-05	mbl	-	-	-	400-450	c.d., m.a.
SL08-04[a]	qv	t-SE		-	350-450	q.d., m.a.
SL08-03	c.s. my	t-SE	-	-	300-400	q.d., m.a.
SL08-02	c.s. my	t-SE	-	-	300-400	q.d., m.a.
SL08-01	c.s. my	t-NW	-	-	300-400	q.d., m.a.
HS09-54	qtz my	t-SE	-	-	350-400	q.d., m.a.
HS09-31	calc my	t-SE	-	-	500-650	m.a..
HS09-32	qtz my	t-NW	-	-	500-650	m.a..
HS09-33	qtz my	t-SE	-	-	650+	q.d., m.a.
HS09-34	qtz my	t-SE	-	-	650+	m.a.
HS09-35	qtz my	t-SE	-	-	450-650	q.d., m.a.
HS09-36	qtz my	t-NW	-	-	650+	q.d., m.a.
HS09-37	gns	t-NW	-	-	300-400	q.d., m.a.
Slide Lake shear zone - Slide Lake cirque splay						
HS09-21	qtz my	t-SE	-	-	350-450	q.d., m.a.
HS09-22	qtz my	t-SE	-	-	300-400	q.d., m.a.
HS09-23	qtz my	t-SE	-	-	450-550	q.d., m.a.
HS09-24	qtz my	t-SE	-	-	450-550	q.d.., m.a.
HS09-25	c.s.my	t-SE	-	-	450-550	q.d., m.a.
HS09-27	qtz my	t-SE	-	-	350-400	q.d., m.a.
HS09-29	qtz my	t-NW	-	-	450-550	q.d., m.a.
HS09-30	qtz my	t-SE	-	-	500-600	q.d., m.a.
HS90-39	qtz my	t-SE	-	-	500-650	q.d., m.a.
HS09-40	qtz my	t-S	-	-	450-500	q.d., m.a.
HS09-41	qtz my	t-SE	-	-	450-500	q.d., m.a.
Slide Lake shear zone - Bennett ridgeline splay						
HS09-17	c.s. my	-	-	-	300-350	q.d, m.a.
HS09-42[a]	qtz-fsp my	t-SE	-	-	450-600	q.d, m.a.
HS09-43	qtz-fsp my	t-SE	-	-	450-600	q.d, m.a.
HS09-44	qtz-fsp my	t-SE	0.65-0.73	47-55	450-600	q.d, m.a.
HS09-45	qtz-fsp my	t-SE	0.67-0.73	47-53	450-600	q.d, m.a.
HS09-46	qtz-fsp my	t-SE	0.63-0.65	55-68	450-600	q.d, m.a.
HS09-47	qtz-fsp my	t-SE	0.58-0.65	55-58	400-600	q.d, m.a.

Abbreviations: qtz my, quartz mylonite; c.s. my, calc-silicate mylonite; fsp my, feldspar mylonite; gns, gneiss; mbl, marble; qv, quartz vein; t-SE, top-down-to-the-SE; t-NW, top-up-to-the-NW.

[a] Samples analyzed with EBSD

[b] Temperature indicators; all samples used q.d, (quartz) and q.f.d. (quartz and feldspar) deformation temperatures, and m.a. (mineral assemblage).

4.2. Deformation temperatures

Deformation temperatures in the HSZ and SLSZ were assessed using a combination of quartz deformation textures (Hirth and Tullis, 1992; Stipp et al., 2002a; Stipp et al., 2002b), feldspar deformation textures (Pryer, 1993), mineral assemblages, and quartz LPOs (Mainprice et al., 1986; Tullis and Yund, 1992). Quartz boundaries deform as temperature is increased during dynamic recrystallization, and assuming constant strain rate and fluid composition, can be used as a proxy for relative temperature conditions during deformation (Figure 12A). The phases of grain-boundary mobility are defined by bulging (BLG, ~280-400°C), subgrain rotation (SGR, ~400-500°C), and grain-boundary migration (GBM, >500°C) (Stipp et al., 2002a; Stipp et al., 2002b). These stages represent the dynamic recrystallization of quartz from dislocation glide and creep (BLG) to climb-accommodated dislocation creep (SGR) and into high-temperature grain boundary migration (GBM), where recrystallization-accommodated creep reduces internal strain energy, and decreases dislocation density. Grain-boundary straightening results in polygonal grain boundaries that allow for the lattice to progress toward a dislocation free lattice (i.e. annealing) and Grain Boundary Area Reduction (GBAR) (Bons and Urai, 1992; Kruhl, 2001; Stipp et al., 2002a).

Quartz LPOs were used to estimate temperature. At lower temperature conditions slip occurs as basal <a> slip associated with 280-400°C, progressing into moderate temperatures (400-500°) where dislocation creep involves prism <a> slip, and lastly into high temperatures (>500 °C), where prism <c> slip dominates deformation (Figure 12A) (Wilson, 1975; Lister and Dorsiepen, 1982; Mainprice et al., 1986; Law, 1990; Tullis and Yund, 1992; Kruhl, 1998). Electron backscatter diffraction (EBSD) was used to obtain LPO diagrams. Diffraction patterns were collected using a Zeiss Supra 55 VP scanning electron microscope coupled with a HKL

Channel 5 EBSD camera at Montana State University. HKL Channel 5 Flamenco software was used to index diffraction patterns.

Feldspar deformation mechanisms were also used to constrain deformation temperatures in the shear zones. Feldspar starts to deform via internal micro-fracturing and dislocation glide beginning at 400-500°C (Pryer, 1993), where feldspar grain boundaries develop core and mantle structures characteristic of bulging and dislocation climb (BLG, 450-600°C) (Borges and White, 1980; Gapais, 1989; Gates and Glover, 1989; Tullis and Yund, 1991; Shigematsu, 1999). Above 600°C feldspar grains deform via SGR and BLG recrystallization that may involve the growth of myrmekite (Vidal et al., 1980; Olsen and Kohlstedt, 1985; Tullis and Yund, 1987; Simpson and Wintsch, 1989; Pryer 1993; Kruse and Stünitz, 1999; Altenberger and Wilhelm, 2000).

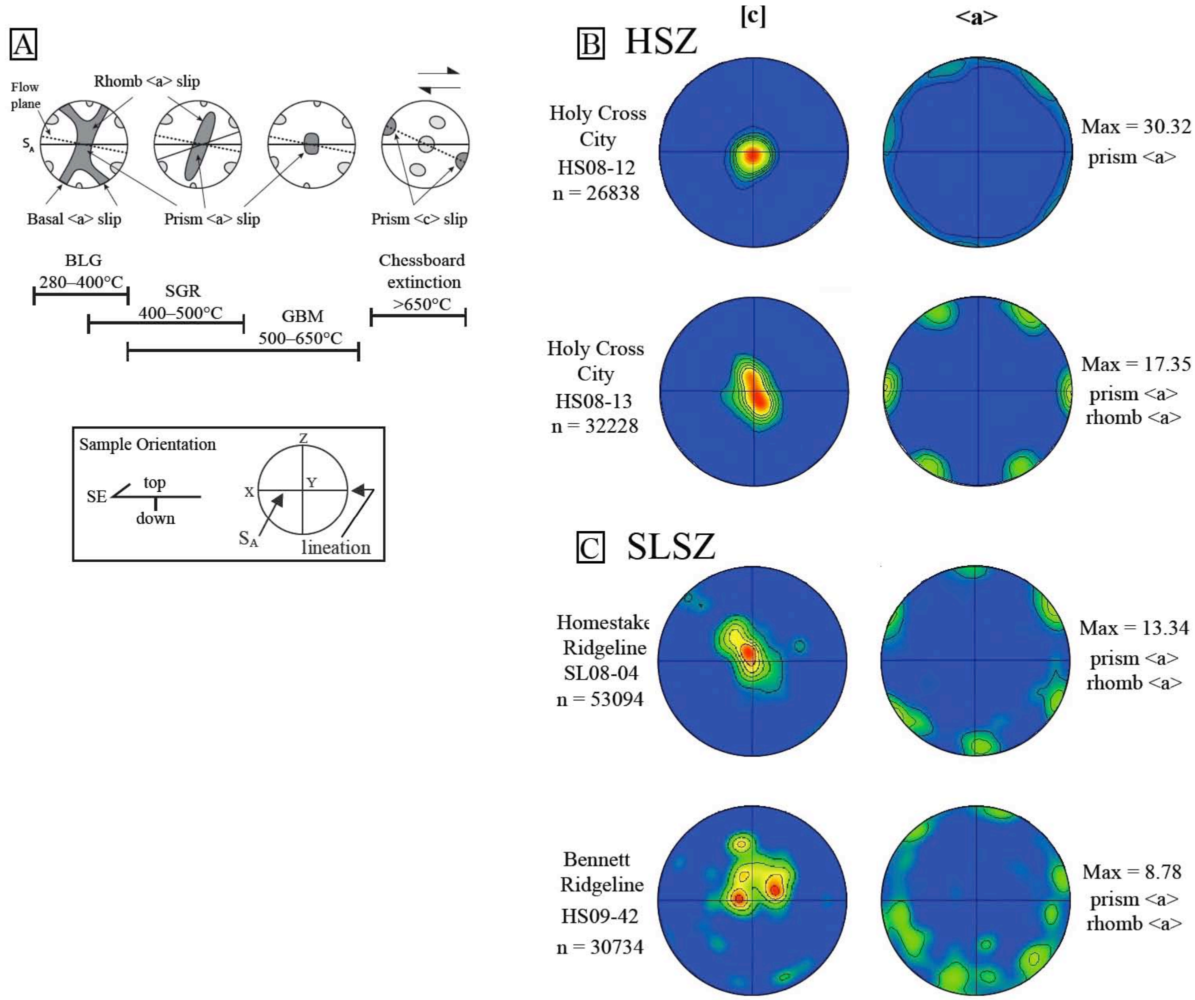

Figure 12. (A) Pole diagrams showing quartz LPO patterns for the [c] axes and <a> axes with increasing temperature for non-coaxial, plane strain deformation (after Stipp et al., 2002b; Passchier and Trouw, 2005; Langille et al., 2010a). (B) EBSD generated lattice-preferred orientations for HSZ (qtz+fsp) mylonite (HS08-12, HS08-13) displaying patterns characteristic of plane strain and prism <a> slip and (C) SLSZ sample SL08-04 displaying prism <a> slip and plane strain patterns and HS09-42 displaying non-plane strain conditions with possible prism <a> and rhomb <a> slip.

Homestake shear zone

Quartz deformation textures within HSZ mylonite and ultramylonite are dominated by subgrains that occur as small, individual grains and elongated ribbon grains, both are evidence for subgrain rotation (SGR, 400-500°C). The mineral assemblage contains minor sillimanite, cordierite, and garnet (Figure 13A) that are legacy to the earlier Paleoproterozoic (D_1) high-temperature, GBAR-dominated flow found throughout the HSZ (Figure 13B). Quartz subgrain development (Figure 13 C, D) varies from the Hornsilver Campground splay into the Holy Cross City splay of the HSZ. Quartz grain boundaries in the Hornsilver Campground (Figure 13D) mylonite contain elongate quartz ribbons with bulging grain boundaries (BLG, 280-400°C) and undulose extinction in the interior of the grain. Holy Cross City mylonite contains ribbon quartz grains and smaller, (Figure 13C) well-defined subgrains (SGR, 400-500°C) that align to form an oblique grain-shape fabric that was used as a shear sense indicator. Feldspar in the Hornsilver Campground mylonite lacks evidence for dynamic recrystallization, however in the Holy Cross City mylonite, some feldspar porphyroclasts display core and mantle structures that are evidence for bulging (BLG, 450-600°C) dynamic recrystallization (Pryer, 1993) and may be part of earlier, high temperature deformation. Feldspar was also observed as fractured porphyroclasts filled with phyllosilicates (Figure 13E) and surrounded by quartz subgrains.

Chlorite, biotite, sillimanite, and muscovite appear within HSZ mylonite and ultramylonite and can be used to interpret metamorphic conditions during deformation. Amphibolite facies migmatite and biotite gneiss (D_1 and D_2) were overprinted by greenschist facies mylonite (D_3) and ultramylonite (D_4). Both fibrous and prismatic sillimanite occur in many of the HSZ sections as shear sense indicators (Figure 13F) and within shear bands. In most sections, sillimanite was fractured or boudinaged and filled with muscovite. This association might record a retrograde reaction (Equation 1, Spear, 1993):

$$\text{K-feldspar} + Al_2SiO_5 + H_2O = \text{muscovite} + \text{quartz}, \quad (1)$$

where quartz subgrains and muscovite encapsulate sillimanite around fibers and between fractures. This sillimanite is likely the product of earlier, high-temperature deformation (D_1/D_2) and during retrogression (D_3 and D_4) subgrains were created (SGR, 400-500°C), sillimanite retrogressed to muscovite, and feldspar porphyroclasts remained rigid (<450°C). Garnet, sillimanite, and minor cordierite are present in some samples outside the main shear band (Figure 13A).

In the Holy Cross City splay (e.g. Figure 13C), quartz subgrains in mylonite can be used as evidence for shear-band development associated with D_3 in the HSZ. Quartz [c] axes plot in the center of the LPOs (Figure 12A), with <a> axes plotting along the primitive circle for two samples analyzed using the EBSD (Figure 12B). One of the Holy Cross City mylonitic quartz veins, HS08-13, contains a well-developed quartz subgrain texture with oblique grain-shape fabric and mica fish that record top-up-to-the-northwest shear sense. LPO plots derived from the (XZ) plane suggest that the [c] axes of quartz subgrains were aligned during plane strain deformation. LPO patterns can also be used to estimate deformation temperature during quartz recrystallization (Stipp et al., 2002b; Langille et al., 2010a, b). Both LPO plots suggest prism <a> slip (>500°C) as the dominant mechanism for deformation, suggesting the possibility of even higher temperatures than the (Figure 12B) quartz textures observed (SGR, 400-500°C).

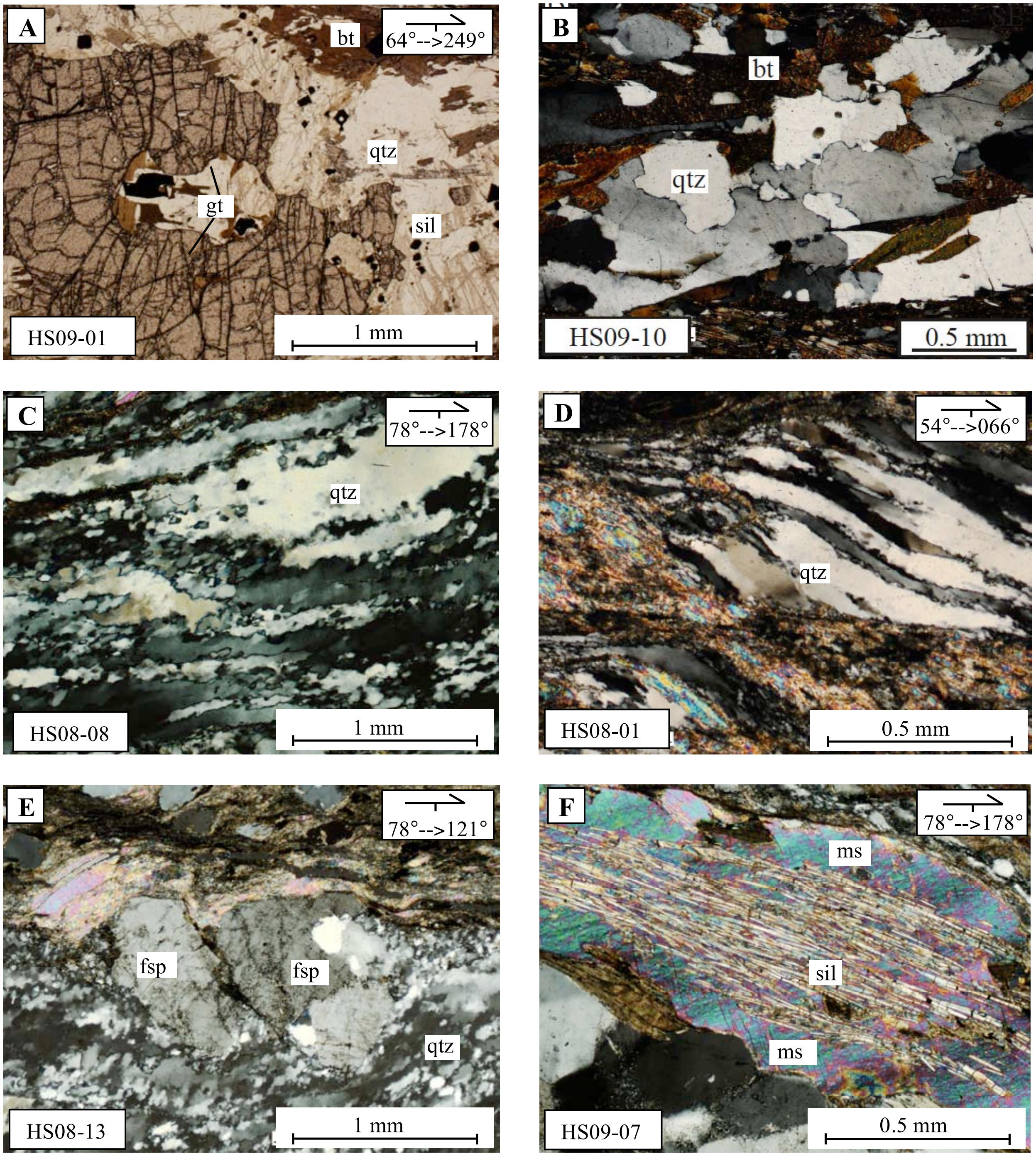

Figure 13. Deformation temperatures within HSZ; crossed polars unless otherwise noted. (A) Undeformed host gneiss; gar, garnet; bt, biotite; sill, sillimanite; qtz, quartz. (B) Grain boundaries displaying high-temperature quartz texture. (C) Quartz mylonite shows well-developed quartz subgrains with top-down-to-the-SE oblique grain-shape fabric. (D) Quartz mylonite boundary with elongated, ribbon quartz subgrains displaying S-C fabric, top-up-to-the-SW shear. (E) Ultramylonite showing quartz subgrains and rigid and fractured feldspar, top-down-to-the-SE. (F) Mylonite with sillimanite porphyroclasts rimmed by muscovite.

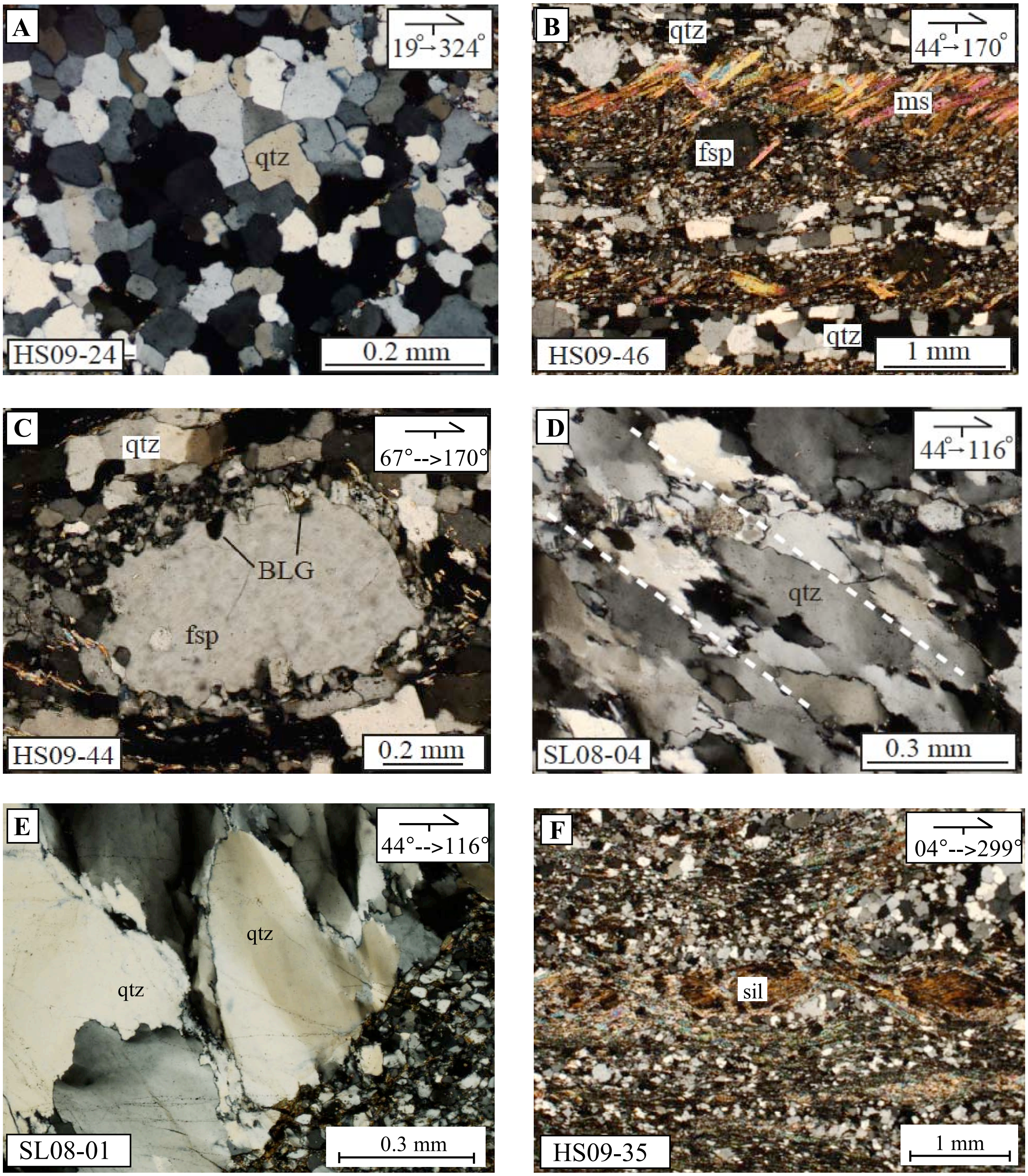

Figure 14. Deformation temperatures within SLSZ; crossed polars unless noted. (A) Annealed quartz (GBAR) in mylonite. (B) Lobate quartz (GBM) domains pinned by micas in mylonite, top-down-to-the-SE shear sense. (C) Core and mantle structures (BLG) in feldspar within mylonite. (D) Aligned quartz subgrains in the mylonite, top-up-to-the-NW shear sense. (E) Bulging quartz grain boundaries in a quartz vein within ultramylonite. (F) Sillimanite boudins from ultramylonite.

Slide Lake shear zone

Bennett ridgeline quartzofeldspathic mylonites contain interlobate quartz-rich domains (5-20 microns thick) that indicate higher-temperature GBM textures (>500°C) (Figure 14A) and are pinned on the foliation plane in some samples (Figure 14B) by aligned biotite and muscovite. Rigid feldspar porphyroclasts, some with asymmetric tails, are set within the quartz matrix composed of quartz grains with polygonal grain boundaries that record semi-annealed fabric. Where the majority of feldspar grains display undulatory extinction, a minority display core and mantle structures (Figure 14C), suggesting the onset of higher temperature (BLG; 450-600°C) feldspar textures (Pryer, 1993). Feldspar subgrains (BLG) only occur as haloes around larger, rigid porphyroclasts and were not found in all the samples, implying either a transition from medium- to higher-grade feldspar textures or legacy to earlier D_1 and D_2 high-temperature deformation.

Mylonite (qtz+fsp+bt+ms+chl) and ultramylonite (qtz+fsp+cal+bt+ ms+chl) from the Homestake ridgeline splay of the SLSZ contain quartz grains that are segregated into narrow bands of alternating feldspar- and calcite-rich domains. Quartz grain boundaries contain small strain free grains with undulose extinction in the interior of grain boundaries that are interpreted to record core and mantle structures (BLG, 280-400°C) (Figure 14 D, E). Similar to the Bennett ridgeline mylonites, earlier (D_1 and D_2) high-temperature deformation is recorded by polygonal quartz grains that display GBAR. Brittle fractures were observed offsetting large quartz grains that displayed high-temperature GBM and are interpreted to be associated with later stage brittle deformation (post 1.4 Ga). Feldspars lack evidence for internal deformation (<450°C), with quartz deformation indicating temperatures ranging from 300-450°C (Pryer, 1993; Stipp et al., 2002a). Similar to sillimanite found within the HSZ, sillimanite retrograded to muscovite was also found in this splay of SLSZ.

Slide Lake cirque ultramylonite and mylonite (qtz+fsp+bt+ms+sil) display well-developed boundaries that record GBM (500-650°C). Phyllosilicates pin quartz grains (Figure 14F), causing the quartz grain boundaries to have migrated within a fixed area and resulting in elongate grain boundaries. The presence of boudinaged sillimanite that is partially retrogressed to white mica is indicative of the older D_1 fabric that was subsequently deformed in late stage ~1.4 Ga deformation (Figure 14F). Similar to feldspar grains observed in the Homestake ridgeline splay, feldspar grain boundaries in Slide Lake cirque also appeared as rigid (<450°C) (Pryer, 1993).

In the two upper splays (Bennett and Homestake ridgeline) of the SLSZ, quartz subgrains can be used as evidence for shear-band development associated with the mylonitic foliation (S_x). Quartz [c] axes LPO data plot in the center of the LPO with <a> axes plotting around the primitive circle for SL08-04, representative of the Homestake ridgeline splay (Figure 12C). This [c] axis pattern is indicative of plane strain deformation conditions. This LPO pattern also suggests rhomb to upper prism <a> slip (~500°C) as the dominant mechanism for deformation, corresponding with the upper end of temperature estimates for quartz subgrain development (SGR; 400-500°C) and feldspar grain boundary immobility (<450°C) (Pryer, 1993; Stipp et al., 2002b; Langille et al., 2010a, b). The other quartz [c] axis LPO plot, HS09-42 (Figure 12C), representative of the Bennett ridgeline mylonite, displays LPO patterns that occur as two distinct groupings of [c] axes data near the middle of the plot, with <a> axes scattered around the outer rim. This pattern may suggest upper prism <a> slip (~500°C) in an undefined strain regime, possibly due to multiple phases of activation within the shear zone splay, with one of the [c] axes partially overprinting [c] axes from an earlier event.

Temperature estimates from deformation mechanisms in both the HSZ and SLSZ are in agreement with broad constraints on ca. 1.4 Ga temperatures for the Homestake Valley and northern Sawatch Range based on $^{40}Ar/^{39}Ar$ thermochronology (Shaw et al., 2005).

4.3. Mean kinematic vorticity

Mean kinematic vorticity (W_m) was used to quantify relative contributions of pure and simple shear within the HSZ and SLSZ. This analysis is important as it allowed us to test models for the HSZ that invoke a combination of pure and simple shear within a transpressional setting (Shaw et al., 2001; Shaw and Allen, 2007) and characterize mylonite development in the SLSZ. A large component of pure shear would indicate a greater percentage of shortening across the shear zone as compared to flow by simple shear. The kinematic vorticity number (W_k) is a measure of the contribution of pure shear (W_k= 0) and simple shear (W_k= 1), where pure and simple components are equal at W_k=0.71 (Figure 15A) (Tikoff and Fossen, 1995; Law et al., 2004). Because vorticity can vary during deformation (non-steady state), we use the mean kinematic vorticity number (W_m) to establish a time-averaged deformation history that assumes plane strain conditions (Fossen and Tikoff, 1997, 1998; Jiang and Williams, 1998). Plane strain is supported by LPO data (also from XZ plane) from samples within both the HSZ and SLSZ. Vorticity (i.e. non-coaxiality) is a parameter for characterizing flow paths (Means et al., 1980; Robin and Cruden, 1994; Fossen and Tikoff, 1997). In an oblique transpressional setting, where fabric may or may not be symmetrical, it is important to note that vorticity, represented by the vorticity vector, can change orientation within the shear zone (Robin and Cruden, 1994). To characterize oblique motion with the SLSZ, micro-scale kinematic analysis within the XY plane would need to be performed to compliment the analyses in the XZ plane in this study (Hudleston, 1999; Giorgis and Tikoff, 2004; Sullivan and Law, 2007).

We applied the rigid-grain technique (Passchier, 1987; Wallis, 1995) to estimate mean kinematic vorticity within four samples from HSZ and six samples from SLSZ. The rigid grain technique involves measuring the rotational component of flow using the aspect ratio of rigid porphyroclasts (e.g. feldspar, garnet, hornblende) as well as the angle between the long axis of the grain and foliation. We used the Rigid Grain Net (RGN), which plots the aspect ratio (R) or shape factor (B*) and the angle (θ) between the long axis of the porphyroclasts with the foliation (Figure 15B) on a net (Figure 15 C, D) constructed using a series of semi-hyperbolas (Jessup et al., 2007).

The necessary conditions for this analysis are: (1) fabric is assumed to be deformed by homogeneous plane-strain, (2) grain size within the matrix is smaller than the porphyroclasts, (3) flow was sufficient for the porphyroclasts to reach stable orientation, (4) measured objects shape is regular and near orthorhombic, (5) porphyroclasts within the sample must contain a wide range of aspect ratios, (6) porphyroclasts must predate the fabric, and (7) measured grains did not interact mechanically (Passchier, 1987; Jessup et al., 2007; Jessup and Cottle, 2010). For a specific combination of W_m and B*, porphyroclasts are predicted to rotate to a range of angles from the foliation. A transition occurs between two areas on the RGN that is defined by the critical aspect ratio (R_c), a unique combination of W_m, B*, and θ. Above the R_c, porphyroclasts will have limited rotation due to pure shear limiting rotation, and below this value, porphyroclasts have the potential to rotate infinitely. From the R_c values, mean kinematic vorticity (W_m) (Wallis et al., 1993):

$$W_m = \frac{R_c^2 - 1}{R_c^2 + 1} \quad (2)$$

Alternatively, the shape factor (B*) for each grain can be used to estimate W_m, where M_x is the long axis and M_n is the short axis as calculated (Passchier, 1987):

$$B^* = \frac{M_x^2 - M_n^2}{M_x^2 + M_n^2} \quad (3)$$

Results from vorticity analyses were plotted on the RGN, and an upper and lower limit of the R_c were used to estimate a range of W_m (Appendix I). W_m values were then plotted to determine percent pure and simple shear for each sample (Figure 15A). Vorticity analyses were performed using a Nikon DS-Fi with Nikon Imaging Systems – Elements 2.3 software that permits measurements to be made on a monitor along with high-resolution image of the thin section.

LPO diagrams (Figure 12 B, C) were used to determine if the strain regime was appropriate for vorticity analysis using the RGN. Quartz (e.g. Mainprice et al., 1986; Tullis and Yund, 1992) [c] and <a> axes patterns were plotted with respect to the lineation and foliation (S_A in Figure 12A). Quartz [c] axis LPOs for the HSZ reveal plane strain, non-coaxial deformation (Figure 12B), and for the SLSZ show patterns for both plane (SL08-04) and potentially non-plane strain (HS09-42) conditions (Figure 12C).

Homestake shear zone

Samples HS08-07 and HS08-08 are ultramylonites that contain rigid feldspar porphyroclasts in a matrix of dynamically recrystallized quartz, and HS08-10 and HS08-13 are mylonitic quartz veins (Table 2; Appendix IV). All samples were collected along a <10-m-thick steeply dipping splay of the HSZ (Figure 16A; Table 2). Of the four samples, only two yielded reliable vorticity estimates. The ultramylonite yielded mean kinematic vorticity estimates of 0.58 to 0.68 (51-58% pure shear). W_m estimates for the mylonitic quartz vein ranged from 0.45 to 0.70 (50-69% pure shear). Quartz LPO patterns (Figure 12B) for HS08-13 show that the mylonite accommodated plane strain, supporting vorticity analyses for pure shear estimates in the Holy Cross City splay of the HSZ. Steep, oblique stretching lineations in the HSZ suggest dextral and vertical movement, which may also suggest a subvertical vorticity vector, parallel to the foliation plane and stretching lineation. If this is the case, measurements to quantify flow would need to be viewed from the plane normal to the vorticity vector, the XY plane. This investigation only extracted data from the XZ plane.

Slide Lake shear zone

The moderately dipping samples from the Bennett ridgeline transect (Figure 16B; Table 3) contain a matrix of dynamically recrystallized quartz, muscovite, and biotite interspersed with rigid feldspar porphyroclasts. Samples were interspersed along 0.5- to 1-m-thick mylonite splays that span ~60 meters of the northeast ridge of the Slide Lake cirque. In the SLSZ, shallowly dipping foliation and shallowly plunging (oblique down-dip) stretching lineations with vertical and minor dextral movement display an along-strike vorticity vector, which would suggest that measurements to quantify flow would need to be viewed in the plane normal to the vorticity vector, the XZ plane, as all of our samples were collected within this study. Mean kinematic vorticity values for these samples range from 0.58 to 0.73 (HS09-44, 0.65-0.73; HS09-45, 0.67-0.73; HS09-46, 0.63-0.65; HS09-47, 0.58-0.65). These results suggest that the Slide Lake shear zone records pure shear (47-59% pure shear), but values are less than those for the HSZ (50-69% pure shear).

Quartz LPO patterns (Figure 12C) for the Bennett ridgeline splay (HS09-42) display two distinct populations of [c] axes, possibly due the sample recording more than one deformational event (i.e. partial overprinting of an earlier fabric), which makes interpreting vorticity results from that particular sample problematic. Sample SL08-04 (Figure 12C) revealed one distinct [c] axis population in the middle of the LPO plot, supporting plane strain conditions in the Homestake ridgeline splay. Based on these findings, W_m data implies that the HSZ records a higher contribution of pure shear within a plane strain dominated system.

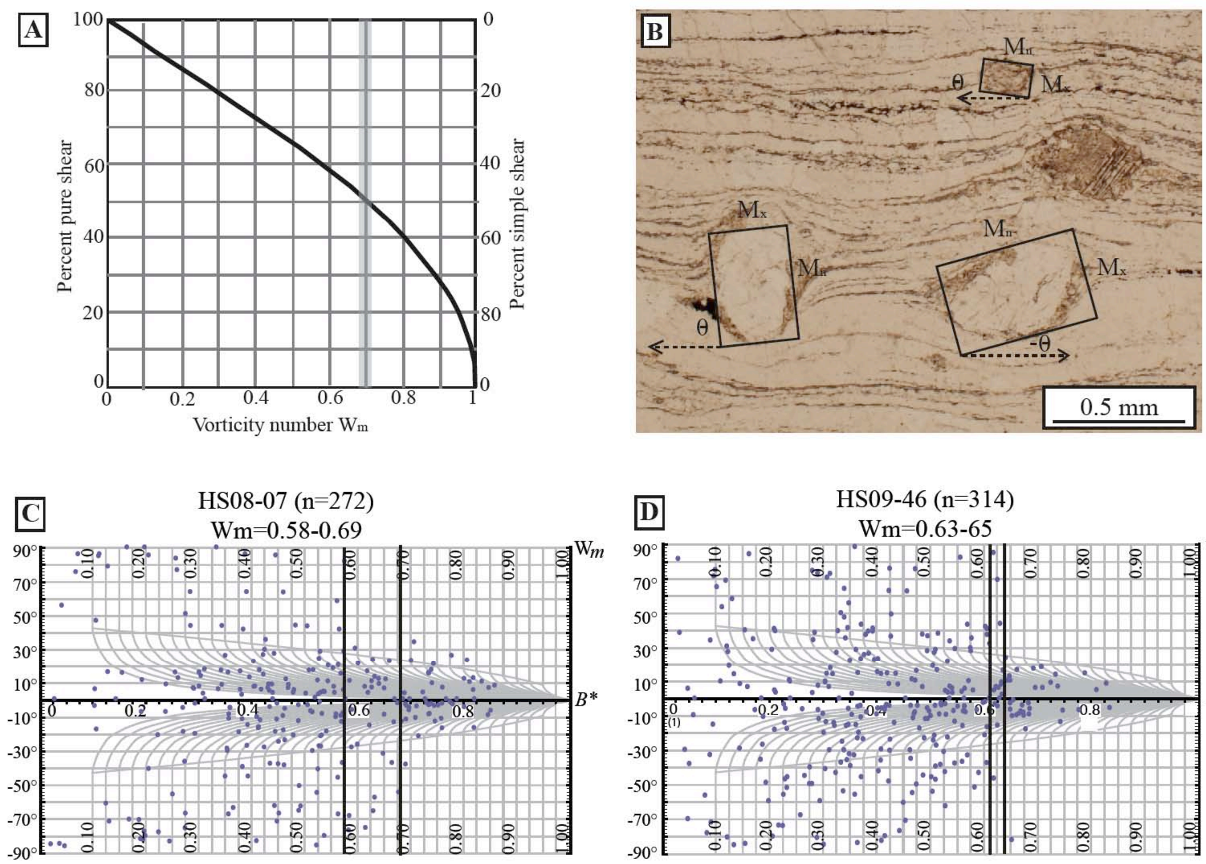

Figure 15. (A) Graph showing the relationship between the vorticity number and pure and simple shear; values are equal when W_m=0.71. After Law et al. (2004). (B) Photomicrograph showing grain axis and angle measurements for vorticity analysis (M_x, long axis; M_n, short axis; θ, angle between the long axis and foliation); top-down-to-the-SE; the clast in the lower right is a back rotator and will thus have a -θ value (see text for details); plane light. (C) Example RGN from HSZ; *n* = number of grains; *B** is the shape factor, y-axis is the angle between the clast long axis and the mesoscopic foliation (refer to text). (D) Example RGN for the SLSZ. Dark vertical marker lines represent the range in W_m for both (C) and (D). See Appendix I for all plots.

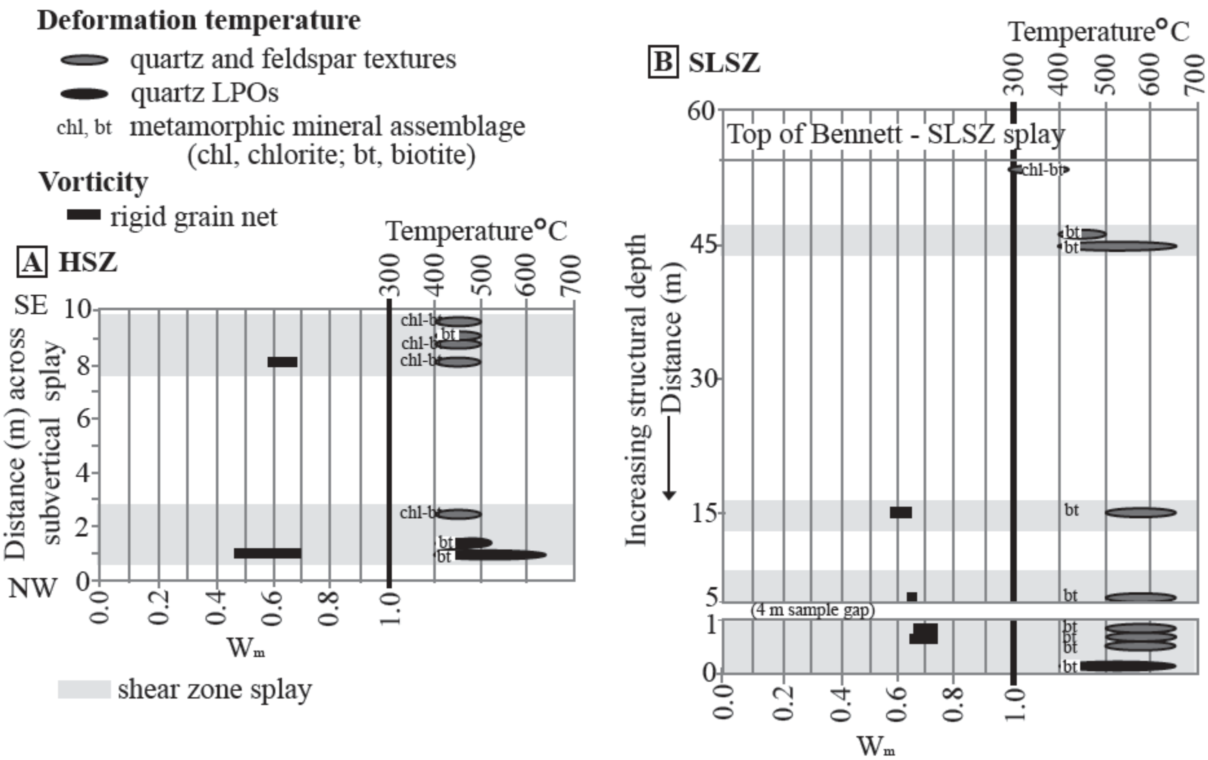

Figure 16. Deformation temperature and vorticity results from (A) HSZ Holy Cross City transect and (B) SLSZ Bennett ridgeline transect. Each rectangle and ellipse represents one sample. Data can be found in Appendix I and IV.

CHAPTER 5

DISCUSSION AND IMPLICATIONS

5.1. Comparison of SLSZ and HSZ deformation history and kinematics

Meso- and microstructural observations of kinematic indicators and fabric relationships in HSZ and SLSZ mylonite and ultramylonite demonstrate that mid-crustal Paleo- and Mesoproterozoic deformation involved shared structural (e.g. shear sense, lineations, strike) and deformational (e.g. pure shear, temperatures, shear sense) components (Table 2; 3). Within the HSZ, 1.4 Ga deformation is subdivided into two events that are characterized by an anastomosing system of steeply dipping (059, 79°SE) mylonite, ultramylonite, and pseudotachylyte that record two stages of movement: (1) D_3 is associated with S_3 mylonite development and a steeply plunging lineation (L_3: 73°→ 213) that records dextral, top-down-to-the-southeast sense of shear and (2) D_4 ultramylonite and pseudotachylyte development and a steeply plunging lineation (L_4: 78° → 120) that records dextral, top-up-to-the-northwest sense of shear (Figure 5A). Comparatively, the SLSZ is a shear system composed of at least two low angle (S_x: 007, 24°SE) splays with a shallow southeast-plunging lineation (L_x: 009°→ 165) (Figure 5B), and one moderate angle (048, 60°SE) mylonite splay with a steeper southeast-plunging lineation (L_x: 60°→ 121) (Figure 5C). All three splays record dextral, top-down-to-the-southeast sense of shear and minor dextral, top-up-to-the-northwest sense of shear. Field mapping at the northeastern part of Homestake ridgeline (Figure 2) found the upper contact of the Homestake ridgeline splay, where the shallowly dipping, north-northeast-striking SLSZ foliation (S_x) truncates the steep high-temperature foliation (S_2) in the hanging wall. In the

Bennett ridgeline splay, the shear zone fabric (S_x) was found to be parallel to the steep, high-temperature fabric (S_2) in the hanging wall and footwall. Consequently, the shear zones splays were interpreted (Figure 2, 6, 17; A-1, 2) to represent two different components of the HSZ and SLSZ system. The oblique steeply plunging HSZ lineations and oblique shallowly plunging SLSZ lineations record right-lateral strike-slip motion that was associated with both the top-down-to-the-southeast and the top-up-to-the-northwest event, respectively (Figure 17).

Mesoscale observations are supported by estimates of deformation temperatures using quartz and feldspar microstructures, quartz [c] axis LPOs, shear sense, and estimates of mean kinematic vorticity. Deformation temperatures derived from quartz and feldspar grain boundaries, metamorphic mineral assemblages, and quartz LPO-derived slip systems range from 280-500°C in the HSZ to 280- >500°C in the SLSZ (Table 2; 3). Temperature estimates in the HSZ are similar to Regime 2 (Hirth and Tullis, 1992) (BLG-SGR transition at ~400°C; Stipp et al., 2002b) estimates from Shaw et al. (2001) for quartz deformation textures. The overwhelming development of quartz subgrains and LPO data from our samples supports a higher temperature range (400-500°C). Assuming an average geothermal gradient of ~25°C/km, constant strain rate and fluids would imply that deformation occurred at similar mid-crustal positions (~12-24 km). 47-69% pure shear estimates from representative splays of the HSZ and SLSZ demonstrate that components of coaxial (50-69% in HSZ and 47-59% in SLSZ) as well as non-coaxial (31-50% HSZ and 41-53% in SLSZ) strain were associated with deformation at ~1.4 Ga. Quartz LPO plots (Figure 12B) (Lister et al., 1978; Law, 1990) indicate that the Holy Cross City ultramylonites within the HSZ experienced 50-69% pure shear during plane strain-dominated flow associated with top-up-to-the-northwest sense of shear. Quartz [c] axis LPO patterns within the SLSZ Homestake ridgeline mylonites (Figure 12C) yield plane strain conditions, whereas [c] axes in the Bennett ridgeline splay experienced non-plane strain. Therefore the estimates of W_m (47-59% pure shear) from our analyses in a single plane (XZ) are likely to be modestly in uncertainty for describing the overall deformation because the lack of a plane strain state may lead to overestimates of up to 0.05 (Tikoff and Fossen, 1995); a relatively minor amount when compared with the errors associated with the technique (Langille et al, 2010a, b; Jessup and Cottle, 2010).

5.2. Relative age of the SLSZ

Although it is impossible to directly establish a relative chronology of HSZ/SLSZ deformation, the physical proximity, kinematic compatibility, and similarity in deformation mechanisms indicate that the two systems formed at similar crustal levels. $^{40}Ar/^{39}Ar$ data for the area (Shaw et al., 2005) suggests that temperatures were 400-550°C at ~1.4 Ga. Monazite ages from HSZ mylonite (Shaw et al., 2001; Shaw et al., 2005) and field-derived fabric relationships provide a proxy for the age of the onset of mylonite development within the SLSZ to be ~1.4 Ga. Monazite ages from both top-down-to-the-southeast mylonite and top-up-to-the-northwest ultramylonite within the HSZ are indistinguishable, although morphology and microstructures suggest that they were formed either during two separate events (D_3/D_4) or as phases of a single tectonic event involving a reversal of dip-slip shear sense – with the same strike-slip shear (Shaw et al., 2001). Because D_3 mylonite (top-down-to-the-southeast) and D_4 ultramylonite (top-up-to-the-northwest) development within SLSZ cannot be uniquely related to the D_3/D_4 (1.42-1.38 Ga) chronology and kinematics of the HSZ, we group these into a ~1.4 Ga event based on similarity of inferred temperatures and kinematics.

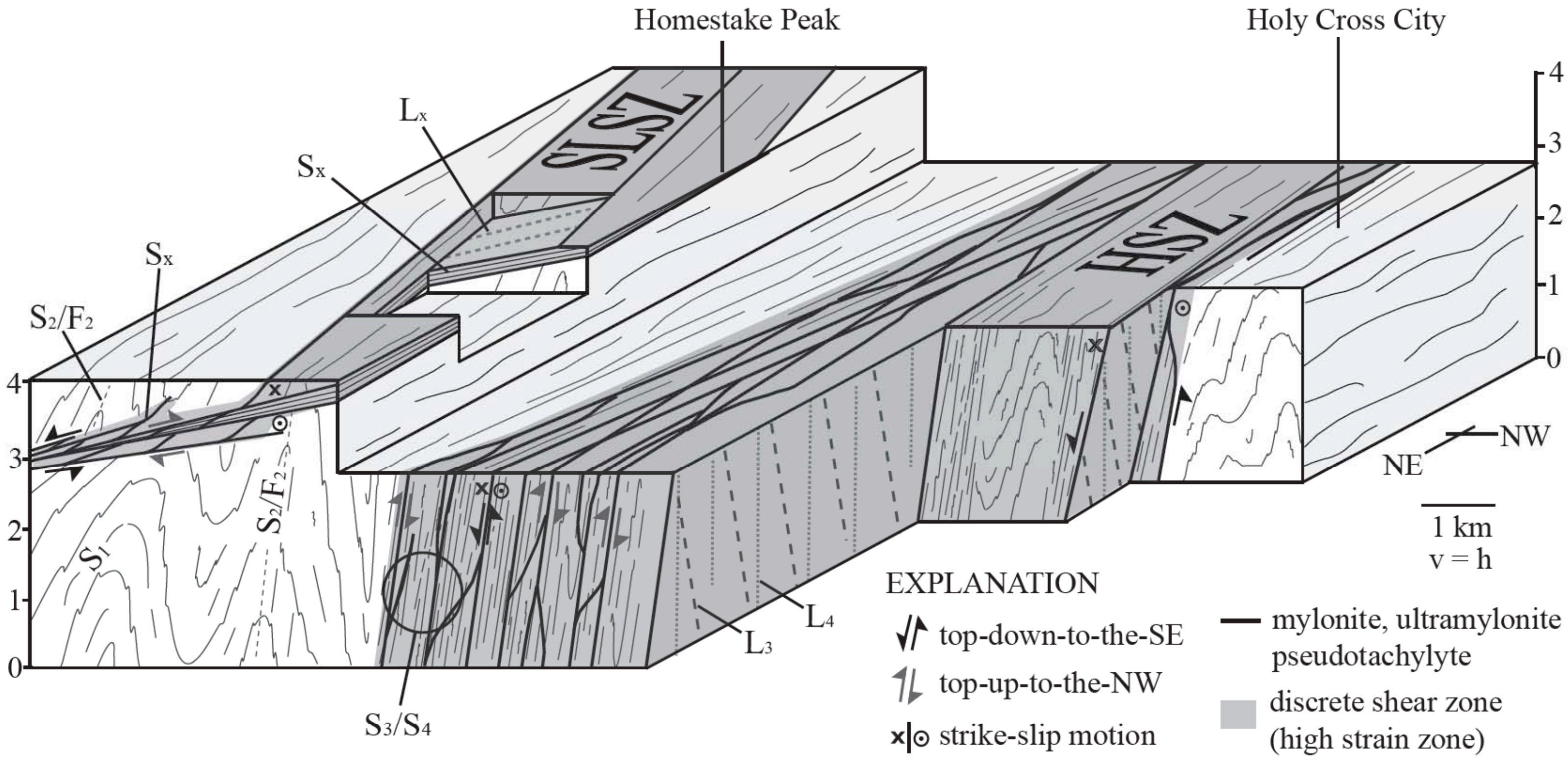

Fig. 17. Block diagram of the SLSZ and HSZ viewed to the south. Lineation-foliation relationships and shear sense are displayed within the figure. Black arrows represent top-down-to-the-SE, gray arrows represent top-up-to-the-NW sense of shear. Note orientation and style of SLSZ deformation. Zones of mylonite, ultramylonite, pseudotachylyte, and high strain domains highlighted in dark gray.

5.3. Mid-crustal heterogeneity and anisotropy

1.4 Ga shear zone development and magmatism in intracontinental Laurentia is inferred to represent an inboard response to far-field shortening between southern Laurentia and a continental landmass farther south (Nyman et al., 1994; Duebendorfer and Christensen, 1995; Karlstrom and Humphreys, 1998; Jones et al., 2010a). Thermal structure beneath an orogenic plateau (e.g. modern Tibet, Andean Antiplano) at 1.4 Ga may explain magma emplacement near the brittle-ductile transition as well as reshuffling of thermally weakened blocks via oblique and dip slip motion (Andronicos, et al., 2003; Shaw et al., 2005). In the northern Sawatch Range, 1.4 Ga mid-crustal deformation is recorded by the shuffling of crustal blocks within the HSZ and SLSZ as well as the emplacement of the St. Kevin granite (Figure 18) (Doe and Pearson, 1969; Shaw and Allen, 2007). Shear zone development is attributed to a varied ductile-brittle transition (12-24-km-depth) that acted as a barrier for magma ascent and accommodated crustal oscillations (Shaw et al., 2001; Shaw et al., 2005) caused by gravitationally driven extension and tectonic contraction that we relate to top-down-to-the-southeast and top-up-to-the-northwest, respectively (Figure 3).

Anisotropy may have also contributed to shear zone development. Low-angle structures similar to the SLSZ have been documented in modern collisional settings where strain is partitioned in an unstable middle crust (Yin, 1989; Wernicke, 1992). Studies from the Tibetan Plateau show low-angle shear zones that cut across anisotropic structures that developed during shortening, suggesting that low-angle structures can develop without preexisting features (Kapp et al., 2008) and may provide a modern analog to SLSZ development.

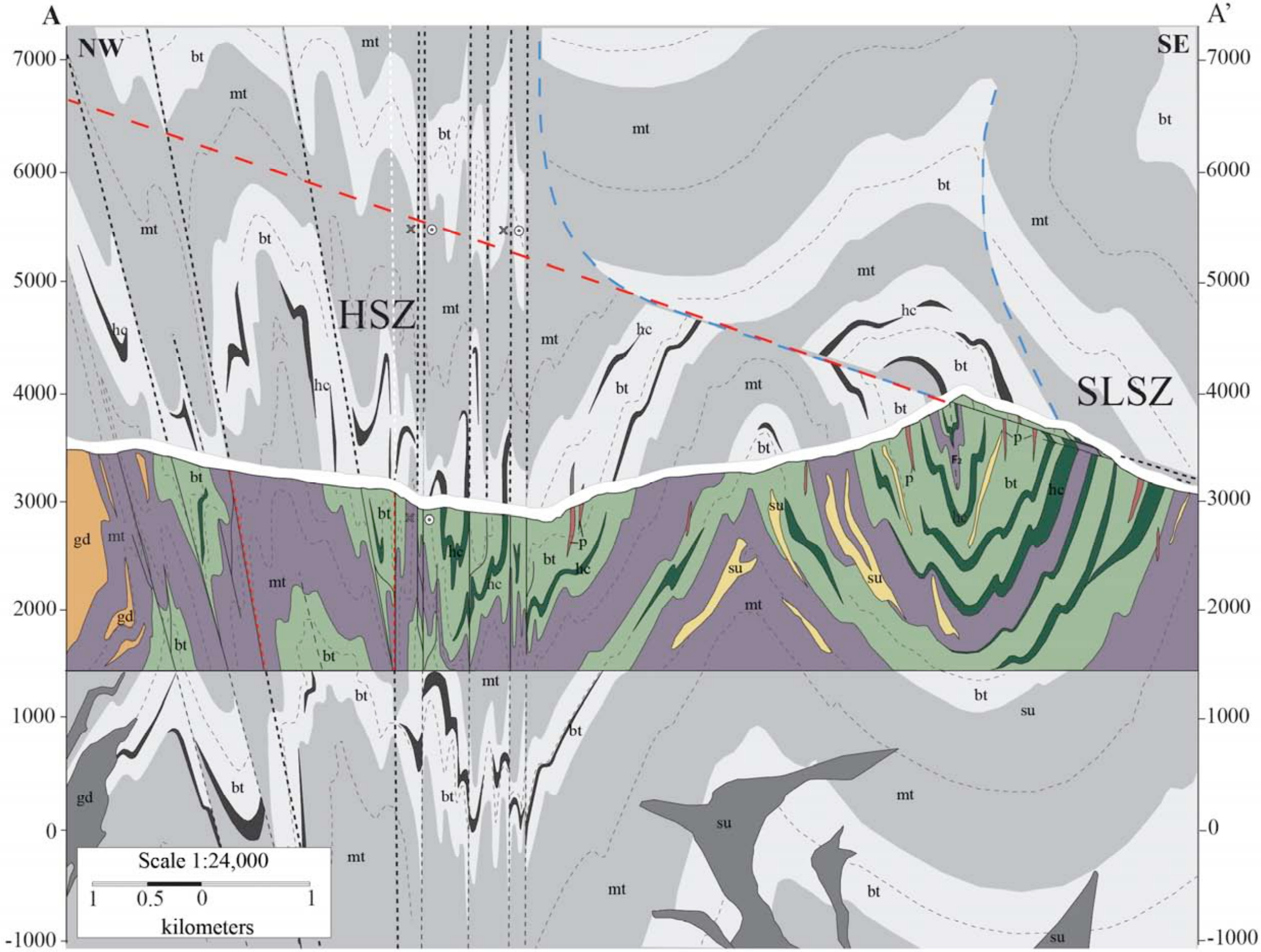
A
A'
NW
SE
HSZ
SLSZ
7000
6000
5000
4000
3000
2000
1000
0
-1000
mt
bt
hc
gd
su
p
Scale 1:24,000
1
0.5
0
1
kilometers

Figure 18. (Previous page) Geologic cross section of the boxed HSZ and SLSZ in color with interpretation in gray scale. (see A-1 for larger version). Red and blue dashed lines represent two possible models for 1.4 Ga HSZ and SLSZ interaction. Note position of the St. Kevin granite (su) in the lower right. Refer to Figure 3 for mid-crustal position. Explanation of units and symbols found in A-1.

5.4. ~1.4 Ga transpression

Stretching lineations can be used to determine flow movement, but should be used with caution in transpressional (i.e. 3D) systems (Tikoff and Greene, 1997; Tessyier and Tikoff, 1999). Subvertical stretching lineations will ultimately form in high-strain transpressional shear zones that are dominated by pure shear, and have, in many studies, been found to occur with a subvertical foliation (e.g. Hudleston, 1999; Robin and Cruden, 1994; Tikoff and Greene, 1997; Tessyier and Tikoff, 1999). The oblique stretching lineations occur as steeply plunging (HSZ: L_3, 73° → 213, top-down-to-the-southeast shear sense; L_4, 78° → 120, top-up-to-the-northwest shear sense) and shallowly plunging (SLSZ: L_x, 9° → 165, top-down-to-the-southeast and top-up-to-the-northwest shear sense) (Figure 17; 19). Variation in the orientation of stretching lineations across two shear zones (Figure 19) has been documented in other transpressional models (Tikoff and Greene, 1997) where fabric symmetry has been attributed to cause the differences in the plunge of lineations and vorticity across a shear system (Lister and Williams, 1983; Robin and Cruden, 1999).

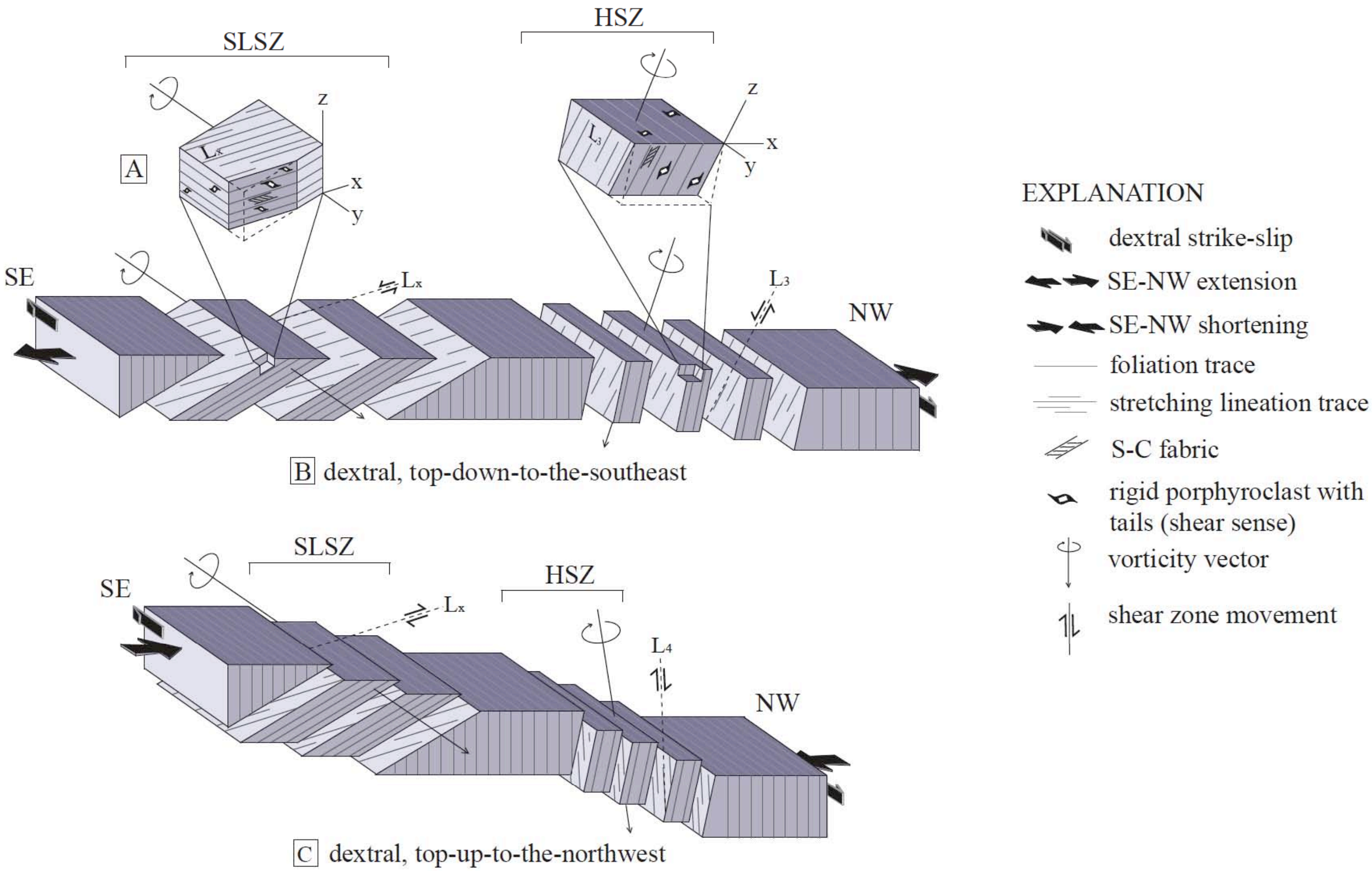

Figure 19. Schematic block diagrams illustrating the kinematics of the HSZ and SLSZ during ~1.4 Ga deformation. (A) Oriented blocks from each shear zone and the XZ plane used to determine kinematics with shear sense indicators and vorticity vector denoted on the XZ plane. (B) Kinematics of dextral, top-down-to-the-SE deformation. (C) Kinematics of dextral, top-up-to-the-NW deformation. Not to scale.

Based on relative timing constraints, we are unable to determine whether or not the HSZ and the SLSZ were active during the same transpressional event. Kinematic investigations presented herein have defined the meso- and microstructural components of the SLSZ and HSZ (Figure 17; 19), independent of timing. Vorticity and shear sense analyses (Figure 19A) from the Bennett ridgeline splay of the SLSZ and Holy Cross City splay of the HSZ suggest one possible model for similar contributions (50-69% in HSZ; 47-59% in SLSZ) of pure shear associated with two types of shear zone movement: 1) top-down-to-the-southeast, dextral general shear (Figure 19B) and 2) top-up-to-the-northwest, dextral general shear (Figure 19C) at similar mid-crustal positions (12-24 km) (Figure 19). Our model supports suggestions by other workers that instability in the middle crust influenced the development of discrete shear zones at around 1.4 Ga and may be associated with transpression (e.g. Nyman et al., 1994; Duebendorfer and Christensen, 1995; Shaw et al., 2001; McCoy et al., 2005, Shaw et al., 2005).

5.5. Implications

SLSZ is a low-to-moderate-angled structure that accommodated normal (top-down-to-the-southeast), reverse (top-up-to-the-northwest), and dextral movement. This study documents the north-northeast-striking SLSZ as sharing similar deformational styles as the subvertical, northeast-striking HSZ. Mylonite and ultramylonite from both shear zones record top-down-to-the-southeast, top-up-to-the-northwest, and dextral movement at similar mid-crustal ductile deformation temperatures (HSZ: ~280-500°C; SLSZ ~280-600°C) and W_m values (47-69% pure shear) in both plane and non-plane strain conditions. General shear deformation occurred along discrete mylonite and ultramylonite bands in both the shallow SLSZ and steep HSZ that suggests mid-crustal heterogeneity, possibly influenced by anisotropic D_1/D_2 foliation, may have partitioned transpression into the ~1.4 Ga shear zones of central Colorado. This data contributes towards previous work (McCoy et al., 2005; Shaw et al., 2005) performed on shear zones within on the Colorado mineral belt that suggests Mesoproterozoic deformation was associated with the transpressional reshuffling of blocks to accommodate far-field deformation along the evolving margin of Laurentia.

REFERENCES CITED

Allen, J.L. III, 2005, A multi-kilometer pseudotachylyte system as an exhumed record of earthquake rupture geometry at hypocentral depths (Colorado, USA): Tectonophysics, v. 402, p. 37-54.

______1994, Stratigraphic variations, fault rocks, and tectonics associated with brittle reactivation of the Homestake shear zone, central Colorado [Ph.D. dissert.]: Lexington, University of Kentucky, 294 p.

Aleinkoff, J.N., Reed, J.C. Jr., and DeWitt, J.L., 1993, The Mount Evans batholith in the Colorado Front Range: Revision of its age and reinterpretation of its structure: Geological Society of America Bulletin, v. 105, p. 791-806.

Altenberger, U., and Wilhelm, S., 2000, Ductile deformation of K-feldspar in dry eclogite facies shear zones in the Bergen Arcs, Norway: Tectonophysics, v. 320, p. 107-121.

Anderson, J.L., 1983, Proterozoic anorogenic granite plutonism of North America, *in* Medaris, L.G., Jr., Kyers, C.W., Mickelson, D.M., and Shanks, W.C., eds., Proterozoic geology: selected papers from an international proterozoic symposium: Boulder, Colorado, Geological Society of America Memoir 161, p. 133-154.

Anderson, T.B., Jamtveit, B., Dewey, J.F., and Swensson, E., 1991, Subduction and education of continental crust: major mechanisms during continent-continent collision and orogenic extensional collapse, a model based on the Norwegian Caledonides: Terra Nova, v. 3, p. 303-310.

Andronicos, C.L., Chardon, D.H., Hollister, L.S., Gehrels, G.E., and Woodsworth, G.J., 2003, Strain partitioning in an obliquely convergent orogen, plutonism, and synorogenic collapse: Coast Mountains Batholith, British Columbia, Canada: Tectonics, v. 22, doi:10.1029/2001TC001312.

Bennett, V.C., and DePaolo, D.J., 1987, Proterozoic crustal history of the western United States as determined by neodymium isotopic mapping: Geological Society of America Bulletin, v. 99, p. 674-685.

Bickford, M.E., and Hill, B.M., 2007, Does the arc accretion model adequately explain the Paleoproterozoic evolution of southern Laurentia? An expanded interpretation: Geology, v. 35, p. 167-170.

Bickford, M.E., 1988, The accretion of Proterozoic crust in Colorado: Igneous, sedimentary, deformational, and metamorphic history, *In* Ernst, W.G., ed., Metamorphism and crustal evolution of the western United States [Rubey Volume]: Prentice Hall, Englewood Cliffs, New Jersey, v. 7, p. 411-430.

Bickford, M.E., Shuster, R.D., and Boardman, S.J., 1989, U-Pb geochronology of the Proterozoic volcanic plutonic terrane in the Gunnison and Salida areas, Colorado, *in* Grambling, J.A., and Tewksbury, B.J., eds., Proterozoic geology of the southern Rocky Mountains: Geological Society of America Special Paper 235, p. 33–48.

Bons, P.D., and Urai, J.L., 1992, Syndeformational grain growth: microstructures and kinetics: Journal of Structural Geology, v. 14, p. 323-334.

Borges, F.S., and White, S.H., 1980, Microstructural and chemical studies of sheared anorothosites, Roneval, South Harris: Journal of Structural Geology, v. 2, p. 273-280.

Bowring, S.A., and Karlstrom, K.E., 1990, Growth, stabilization, and reactivation of Proterozoic lithosphere in the southwestern United States, Geology, v. 18, p. 1203-1206.

Burchfiel, B.C., Chen, Zhiliang, Hodges, K.V., Yupling, L., Royden, L.H., Deng, C., and Xu, J., 1992, The south Tibetan detachment system, Himalayan orogen: Extension contemporaneous with parallel to shortening in a collisional mountain belt: Geological Society of America Special Paper, v. 269, 41 p.

Caine, J.S., Ridley, J., and Wessel, Z.R., 2010, To reactivate or not to reactivate – Nature and varied behavior of structural inheritance in the Proterozoic basement of the eastern Colorado Mineral Belt over 1.7 billion years of earth history, *In* Morhan, L.A., and Auane, S.L., eds., Through the Generations: Geologic and Anthropogenic Field Excursions in the Rocky Mountains from Modern to Ancient: Geological Society of America Field Guide 18, p. 119-140.

Condie, K.C., 1986, Geochemistry and tectonic setting of early Proterozoic supracrustal rocks in the southwestern United States: Journal of Geology, v. 94, p. 845-864.

Davidson, C., Hollister, L.S., and Schmid, S.M., 1992, Role of melt in the formation of a deep-crustal compressive shear zone: The Maclaren Glacier metamorphic belt, south central Alaska: Tectonics, v. 11, p. 348-359.

D'Lamos, R.S., Schofield, D.I., Holdsworth, R.E., and King, T.R., 1997, Deep crustal and local rheological controls on the sitting and reactivation of fault and shear zones, northeastern Newfoundland: Journal of the Geological Society, London, v. 154, p. 117-121.

DePaolo, D.J., 1981, Neodymium isotopes in the Colorado Front Range and crust-mantle evolution in the Proterozoic: Nature, v. 291, p. 193-196.

Doe, B.R., R.C., Pearson, 1969, U-Th-Pb chronology of zircons from the St. Kevin Granite, northern Sawatch Range, Colorado, Geological Society of America Bulletin, v. 80, p. 2495-2502.

Duebendorfer, E.M., and Houston, R.S., 1986, Kinematic history of the Cheyenne belt, Medicine Bow Mountains, southeastern Wyoming: Geology, v. 14, p. 171-174.

Duebendorfer, E.M., Chamberlain, K.R., and Jones, C.S., 1987, Proterozoic tectonic history of the Cerbat Mountains, northwestern Arizona; implications for crustal assembly in the Southern United States, Geological Society of America Bulletin, v. 98, p. 544-568.

Duebendorfer, E.M., and Christensen, C., 1995, Synkinematic (?) intrusion of the “anorogenic” 1425 Ma Beer Bottle Pass pluton, southern Nevada: Tectonics, v. 14, p. 168-184.

Ferguson, C.B., Duebendorfer, E.M., and Chamberlain, K.R., 2004, Synkinematic intrusion of the 1.4-Ga Boriana Canyon Pluton, Northwestern Arizona: Implications for ca. 1.4-Ga regional strain in the Western United States: Journal of Geology, v. 112, p. 165-183.

Fossen, H., Tikoff, B., 1997, Foward modeling of non-steady-state deformation and the ‘minimum strain path’: Journal of Structural Geology, v. 19, p. 987-996.

Frost, B.R., Barnes, C.G., Collins, W.J., Arculus, R.J., Ellis, D.J., and Frost, C.D., 2001, A geochemical classification for granitic rocks: Journal of Petrology, v. 42, p. 2033-2048.

Gapais, D., 1989, Shear structures within deformed granites: mechanical and thermal indications: Geology, v. 17, p. 1144-1147.

Gates, A.E., and Glover, L., 1989, Alleghanian tectono-thermal evolution of the dextral transcurrent Hylas Zone, Virginia Piedmont, USA: Journal of Structural Geology, v.11, p. 407-419.

Giorgis, S., and Tikoff, B., 2004, Constrains on kinematics and strain from feldspar porphyroclast populations, *in* Alsop, I., and Holdsworth, R., eds., Transport and flow processes in shear zones: Geological Society [London] Special Publication, v. 224, p. 265-285.

Graubard, C.M., and Mattinson, J.M., 1990, Syntectonic emplacement of the approximately 1440-Ma Mt. Evans Pluton and history of motion along the Idaho Springs-Ralston Creek shear zone, central Front Range, Colorado: Geological Society of America Abstracts with Programs, v. 22, p. 12.

Harland, W.B., 1971, Tectonic transpression in the Caledonian Spitsbergen: Geological Magazine, v. 108, p. 27-42.

Hill, B.M., and Bickford, M.E., 2001, Paleoproterozoic rocks of central Colorado: Accreted arcs or extended older crust: Geology, v. 29, no. 11, p. 1015-1018.

Hirth, G., and Tullis, J., 1992, Dislocation creep regimes in quartz aggregates: Journal of Structural Geology, v. 14, p. 145–159.

Hoffman, P.F., 1989, Speculations on Laurentia’s first gigayear (2.0-1.0 Ga): Geology, v. 17, p. 135-138.

Hudleston, P., 1999, Strain compatibility and shear zones: is there a problem? : Journal of Structural Geology, v. 21, p. 923-932.

Jessup, M.J., and Cottle, J.M., 2010, Progression of South-Directed Extrusion to Orogen-Parallel Extension in the Southern Margin of the Tibetan Plateau, Mount Everest Region, Tibet: Journal of Geology, v.118, p. 467-486.

Jessup, M.J., Jones, J.V.III, Karlstrom, K.E., Williams, M.L., Connelly, J.N., and Heizler, M.T., 2006, Three Proterozoic orogenic Episodes and an intervening exhumation event in the Black Canyon of the Gunnison region, Colorado: The Journal of Geology, v. 114, p. 555-576.

Jessup, M.J., Law, R.D., Frassi, C., 2007, The Rigid Grain Net (RGN): An alternative graphical approach for estimating mean kinematic vorticity (Wm): Journal of Structural Geology, v. 29, p. 411-421.

Jessup, M.J., Karlstrom, K.E., Connelly, J., Williams, M., Livaccari, R., Tyson, A., and Rogers, S.A., 2005, Complex Proterozoic crustal assembly of southwestern North America in an arcuate subduction system: the Black Canyon of the Gunnison, southwestern Colorado, *In* Karlstrom, K.E., and Keller, G.R., eds., American Geophysical Union Monograph 154: The Rocky Mountain region: An evolving lithosphere tectonics, geochemistry, and geophysics: American Geophysical Union Monograph 154, p. 1-19.

Jiang, D., and Williams, P.F., 1998, High-strain zones: a unified model: Journal of Structural Geology, v. 20, p. 1105-11120.

Jones, J.V. III, Rogers, S.A., and Connelly, J.N., 2010a, U-Pb geochronology of Proterozoic granites in the Sawatch Range, central Colorado, U.S.A.: Rocky Mountain Geology, v. 45, no. 1, p. 1-22.

Jones, J.V., III, Siddoway, C.S., and Connelly, J.N., 2010b, Characteristics and implications of Ca. 1.4 Ga deformation across a Proterozoic mid crustal section, Wet Mountain, Colorado, USA: Lithosphere, v. 2, p. 119-135.

Kapp, P., Taylor, M., Stockli, D., and Ding, L., 2008, Development of active low-angle normal fault systems during orogenic collapse: Insight from Tibet: Geology, v. 36, no. 1, p. 7-10.

Karlstrom, K.E., and Bowring, S.A., 1988, Early Proterozoic assembly of tectonostratigraphic terranes in southwestern North America: Journal of Geology, v. 96, p. 561–576.

Karlstrom, K.E., and Houston, R.S., 1984, The Cheyenne belt: analysis of a Proterozoic suture in southern Wyoming: Precambrian Research, v. 25, p. 415-446.

Karlstrom, K.E., and Humphreys, E.D., 1998, Persistent influence of Proterozoic accretionary boundaries in the tectonic evolution of southwestern North America: Interaction of cratonic grain and mantle modification events: Rocky Mountain Geology, v. 33, p. 161-179.

Karlstrom, K.E., and Williams, M.L., 1998, Heterogeneity of the middle crust: Implications for strength of continental lithosphere: Geology, v. 26, no. 9, p. 815-818.

Kirby, E., Karlstrom, K.E., Andronicos, C.L., and Dallmeyer, R.D., 1995, Tectonic setting of the Sandia Pluton; an orogenic 1.4 Ga granite in New Mexico: Tectonics, v. 14, p. 185-201.

Kruhl, J.H., 1998, Reply: prism- and basal-plane parallel subgrain boundaries in quartz: a microstructural geothermobarometer: Journal of Metamorphic Petrology, v. 16, p. 142-146.

Kruhl, J.H., 2001, Crystallographic controls on the development of foam textures in quartz, plagioclase and analogue material, *In* Dresen, G., Handy, M., eds., Deformation mechanisms, rheology and microstructures. International Journal of Earth Science, v. 90, p. 104-117.

Kruse, R., and Stünitz, H., 1999, Deformation mechanisms and phase distribution in mafic high-temperature mylonites from the Jotun Nappe, Southern Norway: Techonophysics, v. 303, p. 223-249.

Langille, J., Lee, J., Hacker, B., Seward, G., 2010a, Middle crustal ductile deformation patterns in southern Tibet: Insights from vorticity studies in Mabja Dome, Journal of Structural Geology, v. 32, p. 70-85.

Langille, J.M., Jessup, M.J., Cottle, J.M., Newell, D., Seward, G., 2010b, Kinematic evolution of the Ama Drime Detachment: Insights into orogen-parallel extension and exhumation of the Ama Drime Massif, Tibet-Nepal: Journal of Structural Geology, v. 32, p. 900-919.

Law, R.D., 1990, Crystallographic fabrics: a selective review of their applications to research in structural geology, *In* Knipe, R.J., Rutter, E.H., eds., Deformation mechanisms, rheology, and tectonics: Geological Society Special Publication 54, p. 335-352.

Law, R.D., Searle, M.P., and Simpson, R.L., 2004, Strain, deformation temperatures, and of flow at the top of the Greater Himalayan Slab, Everest Massif, Tibet: Journal of the Geological Society of London, v. 161, p. 305-320.

Lister, G.S., and Davis, G.A., 1989, The origin of metamorphic core complexes and detachment faults formed during Tertiary continental extension in the northern Colorado river region, U.S.A.: Journal of Structural Geology, v. 11, p. 65-94.

Lister, G.S., and Dornsiepen, U.F., 1982, Fabric transitions in the Saxony granulite terrain: Journal of Structural Geology, v. 41, p. 81-92.

Lister, G.S., and Williams, P.F., 1983, The partitioning of deformation in flowing rock masses: Tectonophysics, v. 92, p. 1-33.

Mainprice, D., Bouchez, J.L., Blumenfeld, P., and Tubia, J.M., 1986, Dominant c-slip in naturally deformed quartz: implications for dramatic plastic softening at high-temperature: Geology, v. 14, p. 819-822.

McCoy, A.M., Karlstrom, K.E., Williams, M.L., Shaw, C.A., 2005, The Proterozoic ancestry of the Colorado mineral belt: 1.4 Ga shear zone system in central Colorado, *In* Karlstrom, K.E., and Keller, G.R., eds., The Rocky Mountain region: An evolving lithosphere tectonics, geochemistry, and geophysics: American Geophysical Union Monograph 154, p.71-90.

Means, W.D., Hobbs, B.E., Lister, G.S., and Williams, P.F., 1980, Vorticity and non-coaxiality in progressive deformations: Journal of Structural Geology, v. 2, p. 371-378.

Molnar, P., 1988, Continental tectonics in the aftermath of plate tectonics: Nature, v. 335, p. 131-137.

Molnar, P., and Tapponier, P., 1975, Cenozoic tectonics of Asia: Effects of a continental collision: Science, v. 189, p. 419-462.

Murphy, M.A., Yin, A., Kapp, P., Harrison, T.M., Manning, C.E., Ryerson, F.J., Lin, D., and Jinghui, G., 2002, Structural evolution of the Gurla Mandhata detachment system, southwest Tibet: Implications for the eastward extent of the Karakoram fault system: Geological Society of America Bulletin, v. 114, no. 4, p. 428-447.

Nyman, M. W., Karlstrom, K. E., Kirby, E., and Graubard, C. M., 1994, Mesoproterozoic contractional orogeny in western North America: Evidence from ca. 1.4 Ga plutons: Geology, v. 22, p. 901–904.

Olsen, T.S., and Kohlstedt, D.L., 1985, Natural deformation and recrystallization of some intermediate plagioclase feldspars, v. 111, p. 107-131.

Passchier, C.W., and Trouw, R.A.J., 2005, Microtectonics, 2nd Ed: Berlin, Springer, 366 p.

Passchier, C.W., 1987, Stable positions of rigid objects in non-coaxial flow: a study in vorticity analysis: Journal of Structural Geology, v. 9, p. 679-690.

Pryer, L.L., 1993, Microstructures in feldspars from a major crustal thrust zone: the Grenville Front, Ontario, Canada. Journal of Structural Geology, v. 15, p. 21-36.

Reed, J.C., Jr., Bickford, M.E., and Tweto, O., 1993, Proterozoic accretionary terranes of Colorado and southern Wyoming, *in* Reed, J.C., Jr., and six others, eds., Precambrian: Conterminous U.S., Volume C-2: The Geology of North America: Boulder, Colorado, Geological Society of America, p. 110-121.

Robin, P.Y.,and Cruden, A.R., 1994, Strain and vorticity patterns in ideally ductile transpression zones: Journal of Structural Geology, v. 16, p. 447-466.

Sanderson, D.J., and Marchini, W.R.D., 1984, Transpression: Journal of Structural Geology, v. 6, p. 449-458.

Selverstone, J., 1988, Evidence for east-west crustal extension in the Eastern Alps: implications for the unroofing history of the Tauern Window: Tectonics, v. 7, p. 87-105.

Selverstone, J., Hodgins, M., Aleinkoff, J.N., and Fanning, C.M., 2000, Mesoproterozoic reactivations of a Paleoproterozoic transcurrent boundary in the northern Colorado Front Range: Implications for ~1.7- and 1.4-Ga tectonism: Rocky Mountain Geology, v. 35, p. 139-162.

Shaw, C.A., and Allen, J.L., 2007, Field rheology and structural evolution of the Homestake shear zone, Colorado: Rocky Mountain Geology, v. 42, no. 1, p. 31- 56.

Shaw C., and Karlstrom, K., 1999, The Yavapai- Mazatzal crustal boundary in the Southern Rocky Mountains: Rocky Mountain Geology, v. 34, p. 37–52.

Shaw, C.A., Karlstrom, K.E., Williams, M.L., Jercinovic, M.J., McCoy, A.M., 2001, Electron-microprobe monazite dating of ca. 1.71-1.63 Ga and ca. 1.45-1.38 Ga deformation in the Homestake shear zone, Colorado: Origin and early evolution of a persistent intra-continental tectonic zone: Geology, v. 29, p. 739-742.

Shaw, C.A., Heizler, M.T., and Karlstrom, K.E., 2005, 40Ar/30Ar thermochronologic record of 1.45-1.35 Ga intracontinental tectonism in the southern Rocky Mountains: Interplay of conductive and advective heating with intracontinental deformation, *in* Karlstrom, K.E. and Keller, G.R., eds., The Rocky Mountain region: An evolving lithosphere: American Geophysical Union Geophysical Monograph 154, p. 163-184.

Shigematsu, N., 1999, Dyanmic recrystallization in deformed plagioclase during progressive shear deformation: Tectonophysics, v. 305, p. 437-452.

Siddoway, C.S., Givot, R.M., Bodle, C.D., and Heizler, M.T., 2000, Dynamic versus anorogenic setting for Mesoproterozoic plutonism in the Wet Mountains, Colorado: Does the interpretation depend on level of exposure? : Rocky Mountain Geology, v. 35, p. 91-111.

Simpson, C., Wintsch, R.P., 1989, Evidence for deformation-induced K-feldspar replacement by myrmekite. Journal of Metamorphic Geology, v. 7, p. 261-275.

Spear, F., 1993, Metamorphic phase equilibria and pressure-temperature-time paths: Mineralogical Society of America Monograph, Washington, D.C., 799 p.

Stipp, M., Stünitz, H., Heilbronner, R., Schmid, S.M., 2002a, The eastern Tonale fault zone:

a ‘natural laboratory’ for crystal plastic deformation of quartz over a temperature range from 250 to 700°C: Journal of Structural Geology, v. 24, p. 1861-1884.

Stipp, M., Stünitz, H., Heilbronner, R., Schmid, S.M., 2002b, Dynamic recrystallization of quartz: correlation between natural and experimental conditions, *in* De Meer, S., Brury, M.R., De Brasser, J.H.P., and Pennock, G.M., eds., Deformation mechanisms, rheology and tectonics: Current status and future perspectives: Geological Society of London Special Publications, v. 200, p. 171-190.

Sullivan, W.A., and Law, R.D., 2007, Deformation path partitioning within the transpressional White Mountain shear zone, California and Nevada: Journal of Structural Geology, v. 29, p. 583-598.

Teyssier, C., and Tikoff, B., 1999, Fabric stability in oblique convergence and divergence: Journal of Structural Geology, v. 21, p. 969-974.

Teyssier, C.,Tikoff, B., and Markley, M., 1995, Oblique plate motion and continental tectonics: Geology, v. 23, no. 5, p. 447-450.

Tikoff, B., and Teyssier, C., 1994, Strain modeling of displacement-field partitioning in transpressional orogens: Journal of Structural Geology, v. 16, no. 11, p. 1575-1588.

Tikoff, B., and Fossen, H., 1995, The limitations of three-dimensional kinematic vorticity analysis: Journal of Structural Geology, v. 17, p. 1771-1784.

Tikoff, B., and Greene, D., 1997, Stretching lineations in transpressional shear zones: an example from the Sierra Nevada Batholith, California: Journal of Structural Geology, v. 19, p. 29-39.

Tullis, J., and Yund, R.A., 1991, Diffusion creep in feldspar aggregates: experimental evidence: Journal of Structural Geology, v. 13, p. 987-1000.

Tullis, J., and Yund R., 1992, The brittle-ductile transition in feldspar aggregates: an experimental study*, in*: Evans, B., and Wong, T.F., eds., Fault mechanics and transport properties in rocks: Academic Press, New York, p. 89-118.

Tullis, J., and Yund, R., 1987, Transition from cataclasite flow to dislocation creep of feldspar: mechanisms and microstructures: Geology, v. 15, p. 606-609.

Tweto, O., 1974, Geologic map and sections of the Holy Cross Quadrangle, Eagle, Lake, Pitkin, and Summit Counties, Colorado. United States Geological Survey Miscellaneous Investigations Map I-830, scale 1:24,000.

Tweto, O.L., Moench, R.H., and Reed, J.C., Jr., 1978. Geologic map of the leadville 1° x 2° qudrangle, northwestern Colorado. United States Geological Survey Miscellaneous Investigatons Map I-999, scale 1:250,000.

Tweto, O.L., and Sims, P.K., 1963, Precambrian ancestry of the Colorado mineral belt: Geological Society of America Bulletin, v. 74, p. 991-1014.

Tyson, A.R., Morozova, E.A., Karlstrom, K.E., Chamberlain, K.R., Smithson, S.B., Dueker, K.G., and Foster, C.T., 2002, Proterozoic Farwell Mountain-Lester Mountain suture zone, northern Colorado: Subduction flip and progressive assembly of arcs: Geology, v. 30, no. 10, p. 943-946.

Vidal, J.L., Kubin, L., Debat, P., and Soula, J.L., 1980, Deformation and dynamic recrystallization of K-feldspar augen in orthogneiss from Montagne Noire, Occitania, southern France: Lithos, v. 13, p. 247-244.

Wallis, S.R., Platt, J.P., and Knott, S.D., 1993, Recognition of syn-convergence extension in accretionary wedges with examples from the Calabrian Arc and the Eastern Alps: American Journal of Science, v. 293, p. 463-495.

Wallis, S.R., 1995, Vorticity analysis and recognition of ductile extension in the Sanbagawa belt, SW Japan: Journal of Structural Geology, v. 17, no. 8, p. 1077-1093.

Wernicke, B., and Axen, G.J., 1988, On the role of isostasy in the evolution of normal fault systems: Geology, v. 16, p. 848-851.

Wernicke, B., 1992, The fluid crustal layer and its implications for continental dynamics, *in* Salsbury, M.H., and Fountain, D.M., eds., Exposed cross-sections of the continental crust: Netherlands, Kluwar Academic Publishers, p. 509-544.

Wheeler, J., and Butler, R.W.H., 1994, Criteria for identifying structures related to true crustal extension in orogens: Journal of Structural Geology, v. 16, p. 1023-1027.

Williams, M.L., 1991, Heterogeneous deformation in a ductile fold-thrust belt: The Proterozoic structural history of the Tusas Mountains, New Mexico: Geological Society of America Bulletin, v. 102, p. 171-188.

Williams, M.L., Karlstrom, K.E., Lanzirotti, A., Read, A.S., Bishop, J.L., Lombardi, C.E., Pedrick, J., and Wingsted, M.B., 1999, New Mexico middle crustal cross sections: 1.65-Ga macroscopic geometry, 1.4-Ga thermal structure, and continued problems in understanding crustal evolution: Rocky Mountain Geology, v. 34, p. 53-66.

Wilson, C.J.L., 1975, Preferred orientation in quartz ribbon mylonites: Geological Society of America Bulletin, v. 86, p. 986-974.

Wooden, J.L., Stacey, J.S., Howard, K.A., Doe, B.R., Miller, D.M., 1988, Pb isotopic evidence for the formation of Proterozoic crust in the southwestern United States, *in* Ernst, W.G., eds., Metamorphism and crustal evolution of the western United States [Rubey Volume]: Prentice Hall, Englewood Cliffs, New Jersey, v. 7, p. 68-86.

Wooden, J.L., and DeWitt, E., 1991, Pb isotopic evidence for the boundary between the Early Proterozoic Mojave and central Arizona crustal provinces in western Arizona, i*n* Karlstrom, K.E., ed., Prtoterozoic geology and ore deposits of Arizona: Tuscon, Arizona, Arizona Geological Society Digest, v.19, p. 27-50.

Yin, A., 1989, Origin of regional, rooted low-angle normal faults: A mechanical model and its tectonic implications: Tectonics, v. 8, p. 469-48.

APPENDIX I

RIGID GRAIN NETS

(FULL EXCEL DATA SETS IN PLATE 3)

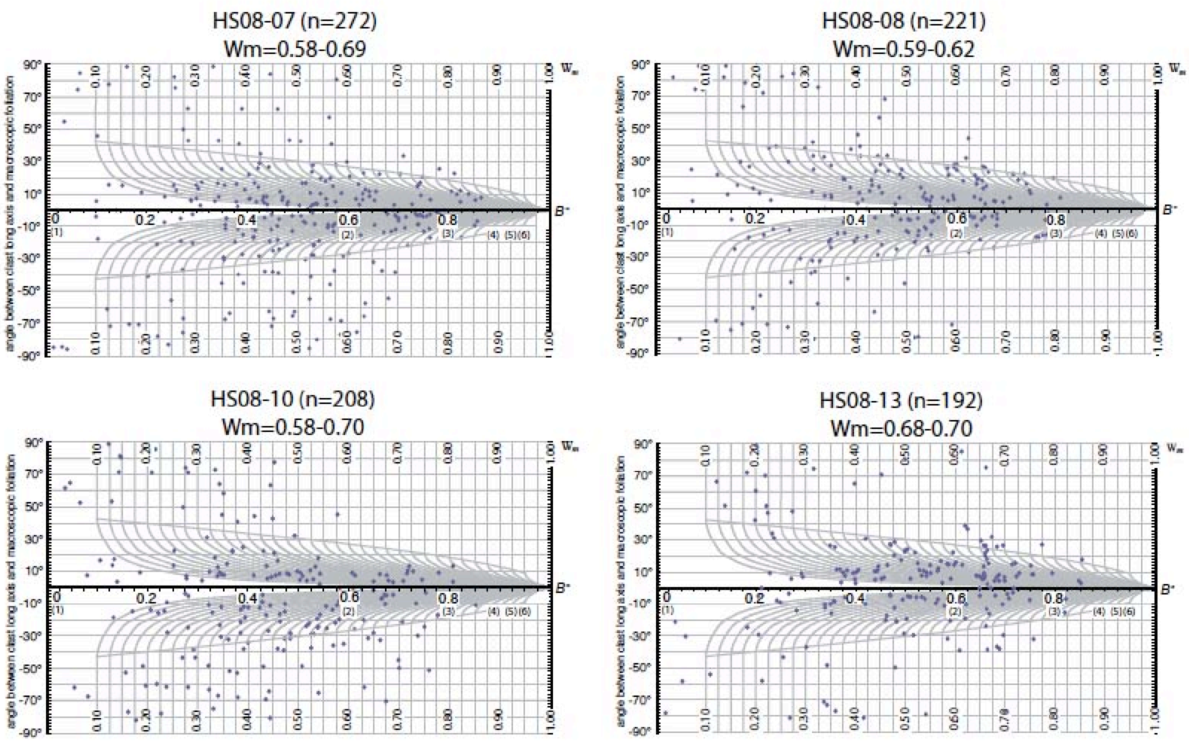
HS08-07 (n=272)
Wm=0.58-0.69
HS08-08 (n=221)
Wm=0.59-0.62
HS08-10 (n=208)
Wm=0.58-0.70
HS08-13 (n=192)
Wm=0.68-0.70
angle between clast long axis and macroscopic foliation

HS09-42 (n=461)
Wm=0.72-0.79

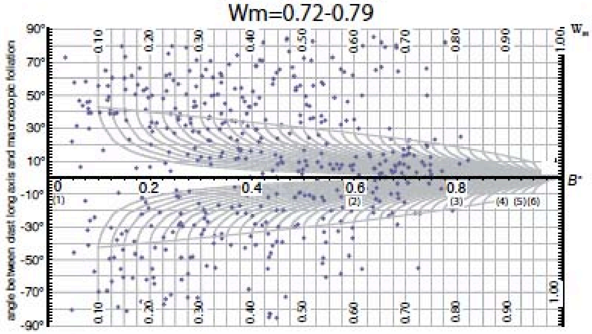

HS09-43 (n=318)
Wm=0.71-0.72

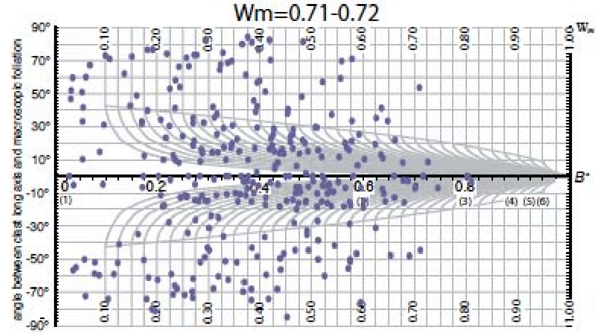

HS09-44 (n=461)
Wm=0.70-0.72

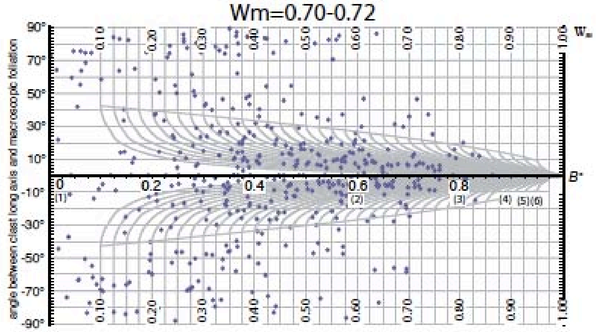

HS09-45 (n=357)
Wm=0.68-0.73

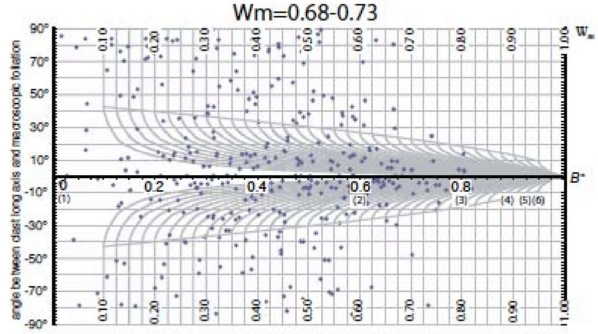

HS09-46 (n=314)
Wm=0.63-65

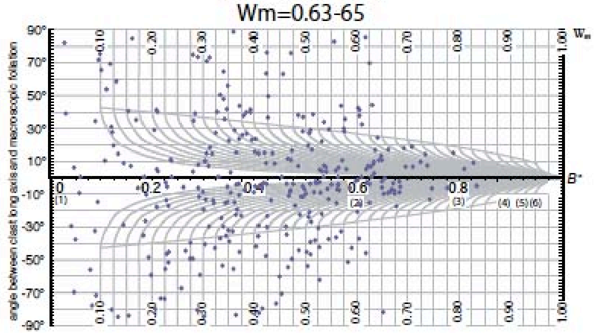

HS09-47 (n=223)
Wm=0.58-0.65

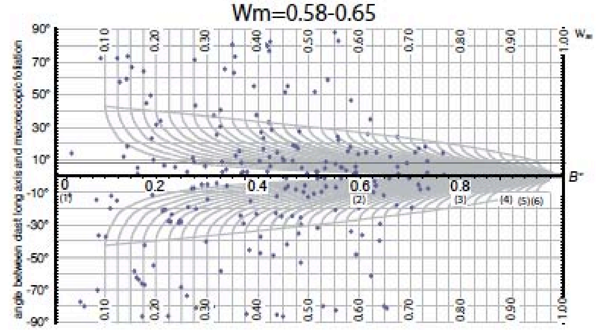

APPENDIX II

FIELD DATA

2008

2008 Colorado Mineral Belt Fieldwork

Sample	Location	Date	Coordinates	Waypoint	Elevation	Strike, Dip	Plunge→Trend	Sample Description
HS08-01	Hornsilver Campground	7/3/08	N39°29'16.4" W106°21'50.9"		9278ft	026, 75SE	54 - 66	ultramylonite towards the NE. Quartzofeldspathic schist with shea
HS08-02	Hornsilver Campground	7/3/08	N39°29'13.1" W106°21'46.6"	97	9260ft	035, 63SE	N/A	XYG Proterozoic Granite
HS08-03	Hornsilver Campground	7/3/08	N39°29'15.5" W106°21'49.6"	99	9236ft	018, 97SE	undefined	ultramylonite, high srain part of the shear zone
HS08-04	Hornsilver Campground	7/3/08	8m NW of last site			021, 80SE	97 - 95, weak	quartz vein within shear zone
HS08-05	Hornsilver Campground	7/3/08	3m NW of quartz vein			038, 69SE	68 - 105	ultramylonite with strong foliation
HS08-06	Hornsilver Campground	7/3/08	N39°29'15.9" W106°21'41.5"	100	9248ft	027, 84SE	86 - 114	ultramylonite, 10 m up from #9
HS08-07	Holy Cross City	7/4/08	N39°29'15.9" W106°31'49.5"	102	10791ft	005, 86SE	85 - 114	mylonite within migmatized gneiss. Fine grained mylonite with fel
HS08-08	Holy Cross City	7/4/08	25m NNE of last sample (downslope)			019, 83SE	84 - 112	mylonite downslope of above sample
HS08-09	Holy Cross City	7/4/08	2.5m SE of HS08-07			342, 90SE	90 - 75	mylonite
HS08-10	Holy Cross City	7/4/08	6.5m NNW of last sample			030, 83SE	down dip	mylonite
HS08-11	Holy Cross City	7/4/08	N39°25'08.06" W106°28'23.8" (1.5n	103	11,231ft	021, down dip	down dip - 90	mylonite
HS08-12	Holy Cross City	7/4/08	2m SE of 11			023, 84SE	down dip	Quartz vein within mylonite
HS08-13	Holy Cross City	7/4/08	0.3mSE from 12			031, 78SE	down dip	Quartz vein within mylonite
HS08-14	Holy Cross City	7/4/08	0.4m SE of 13			025, 78SE	Down dip	fine grained mylonite with clasts
HS08-15	Holy Cross City	7/4/08	0.3m SE of 13			024, 79SE	down dip	fine grained mylonite
HS08-16	Holy Cross City	7/4/08	0.2m SE of 13			030, 76SE	down dip	fine grained mylonite
HS08-17	Holy Cross City	7/4/08	N39°25'06.0"W106°28'24.5"	104	11,254ft	016, 69NW	down dip	mylonite within high strain zone with migmatitic gneiss. Mylonite
SL08-01	Slide Lake	7/7/08	N39°22'00.5"W106°25'04.3"	108	12988ft	002, 69SE	44-116	representative sample of calc mylonite
SL08-02	Slide Lake	7/7/08	N39°22'01.5"W106°25'03.3"	110	12,964ft	010, 42SE	26-039	calc mylonite with approzimate stretching lineation
SL08-03	Slide Lake	7/7/08	N39°22'01.5"W106°25'03.1"	111	12,987ft	358, 59SE	weak lineation	calc mylonite-thinly lamitated with folding features
SL08-04	Slide Lake	7/7/08	.3m from sample 3			002, 65SE	weak lineation	quartz vein
SL08-05	Slide Lake	7/7/08	N39°22'01.7"W106°25'02.6"	113	12,999ft	020, 15SE	06-039	marble lens
SL08-06	Slide Lake	7/7/08	N39°22'01.5"W106°25'01.6"	114	13,035ft	059, 006NW	004-314	calc silicates
SL08-07	Slide Lake	7/7/08	4mSE of last sample			330, 21NE	11-128	calc silicates
SL08-08	Slide Lake	7/7/08	N39°22'01.5"W106°25'01.0"	115	13,042ft	332, 26NE	06-128	?
SL08-09	Slide Lake	7/7/08	N39°22'01.5"W106°25'00.7"	116	13,050ft	341, 29NE	009-143	?
CC08-01	Golden Gate State Park	7/10/08	N39°51'06.8"W105°23'00.7"	127	8,539ft	029, vertical	weak	basal quartzite conglomerate
CC08-02	Golden Gate State Park	7/10/08	N39°51'38.7" W105°21'26.1"	128	8,148ft	185, 52SE	38 - 151 (approx)	shear zone-mylonites and ultramylonites near contact of granodioı
CC08-03	Golden Gate State Park	7/10/08	few m from last sample			190, 54SE	36 - 334	shear zone-mylonites and ultramylonites near contact of granodioı
CC08-04	Golden Gate State Park	7/10/08	N39°51'37.4"W105°21'29.1"	129	8,095ft	206, 51SE	38 - 162	granodiorite/quartzite mylonite
CC08-05	Golden Gate State Park	7/10/08	N39°51'35.4"W105°21'31.3"	130	7,965ft	050, 86SE	81 - 154, near dow	shear quartz zone within mylonite quartzite
CC08-06	Golden Gate State Park	7/10/08	N39°51'35.4"W105°21'31.3"	130	7,965ft	228, 84SE	down dip	quartzite next to quartz vein
CC08-07	Golden Gate State Park	7/10/08	N39°51'35.2"W105°21'31.3"	131	7,934ft	214, 85SE	74 - 121 weak	quartzite with strong foliation, 2m from last sample
CC08-08	Golden Gate State Park	7/10/08	N39°51'28.563"W105°21'30.692"		7,908FT	221, 74SE	on backside lineati	Quarzite

APPENDIX III

FIELD DATA

2009

SLSZ/HSZ Fieldwork: August 2009

Date	Location	Lat	Long	Elev	Strike	Dip	Trend	Plunge	Lineation t	Type	Sample #	Misc	Fold Axis
4-Aug	NW HS Creek	39.38431	106.45367	3048m	99	86SW				bt gneiss			
		39.3848	106.45403	3028m	66	89SE	245	35		bt gneiss			
		39.38551	106.45472	3023m	106	84SW				bt gneiss			
					71	65SW				bt gneiss			
					52	82SW	230	18	SL	bt gneiss			
		39.38554	106.45546	3016m	99	66SW	209	59	SL-weak	bt gneiss			
					68	80SE				bt gneiss			
		39.38561	106.45579	3015m	68	83SW				bt gneiss		Higher strain zone	
		39.38552	106.45611	3028m	89	86SW	220	86	SL	bt gneiss			
					85	76SW	209	76	SL/ML?	bt gneiss			
		39.38507	106.45831	3161m	81	89SW	255	51	SL	bt gneiss			F1: 101, 88
		39.38619	106.45611	3155m	111	81SW	249	64	ML	bt gneiss	HS09-01		
	SE HS Creek	39.38131	106.44994	3129m	101	89SW	295	59	WD SL	bt gneiss	HS09-02		
		39.382	106.44942	3080m	110	85SW	292	56	ML	bt gneiss			
					109	81SW				bt gneiss			F1: 300, 76
		39.38157	106.94953	3049m	118	87SW				bt gneiss			
					135	90SW				bt gneiss			
					135	71SW				bt gneiss			
					135	67SW				bt gneiss			
					70	86SE				bt gneiss			
		39.38061	106.4514	2988m	129	84SW				bt gneiss			
5-Aug	NW, en route	39.39535	106.47063	2936m	84	85NW				mt			F1: 250, 81
	to Holy Cross				58	90NW				bt gneiss			
		39.41612	106.48242		173	70NE				bt in granodiorite			
		39.41486	106.48163		35	84SE				foliated Cross Creek			
					30	89SE				foliated Cross Creek			
		39.41398	106.48176		25	89SE	132	75	SL	mylonite-bt	HS09-03		F1:190, 75SW
		39.41408	106.48135		9	89NW	289	88	SL	mylonite-bt	HS09-04	good porphyroclasts	F1: 348, 66
					3	87NW	115	85	SL	mylonite-bt			
		39.41536	106.47909	3478m	40	77SE	95	75	SL	mylonite-bt		diff. strand-weaker	
					8	86NW				mt		70 s/se of last	
		39.41798	106.47304	3473m	35	90NW				mt			
		39.41692	106.46578	3471m	41	83NW	286	83	SL-weak	mt		shear bands	
		39.41589	106.46387	3265m	315	87NW	226	83	SL-weak	mt-bt			
		39.4122	106.45752	3262m	59	89SE	205	69	?	mt			
6-Aug	NW HS Creek	39.39922	106.44746	3260m	69	77SE	165	77	ML	bt gneiss			
		39.39981	106.44854	2976m	145	90NW				bt-gt gneiss			
		39.40202	106.45111	9725ft	79	76SE				bt-gt gneiss			
8-Aug	Lost Lakes	39.38088	106.44704	9885ft	115	89SW	304	43	ML	mt		boudins PIC	
		39.38029	106.4454	10098ft	120	68SW	215	68	?	qtzite/bt gneiss		S2 SS indicators PIC	
		39.38129	106.44239	10469ft	94	83SW				bt gneiss-higher strain		Macro PICS SS indicators	
		39.37924	106.43521	11085ft						bt/gt/sil schist-gneiss			
		39.37776	106.43206	11043ft	100	81SW				bt gneiss		boudinage	
		39.37527	106.42998	11056ft	124	73SW				bt gneiss		multiple generations exposed	
		39.37509	106.4289	11072ft	295	84SW	20	73	SL	bt gneiss	HS09-05	crenulation, multiple lineations	
		39.37429	106.42839	11225ft	229	74SE	40	80	SL	mt	HS09-06	another folitiation: 155/54NW?	
		39.37174	106.42297	11565ft	5	75SE				bt gneiss	HS09-07	lin??	F1: 88, 70
		39.37081	106.4229	11665ft	353	76NE	178	78	SL	calc-sil w/ bt	HS09-08	large scale fold	FA: 241, 41
				11800ft	25	89NW				bt gneiss			
		39.36835	106.42848	11680ft	100	76NE				bt gneiss			
9-Aug	NW HS Creek	39.39981	106.44854	2976m	115	84NW				gt/bt gneiss	HS09-09	overhanging-oblique to foliation	
					281	80SW				gt/bt/sil? Gneiss	HS09-10		
					65	74NW						PICS: on top of outcrop-shear bands	
	Camp Hale	Tweto SZ			27	53NW				calc-sil		just below unconformity with upper Paleoz	
		climbing area			55	74NW				calc-sil		3.5m peg x-cuts-10/65SE	
11-Aug	Bennett Cirque I	39.39777	106.38004	11833ft	30	17SE	212	30	SL-weak	bt gneiss	HS09-11		
		39.3903	106.38653	11786ft	41	78SE	41	46	SL-weak	marble	HS09-12	lithology change (diagram)	
			just downhill from abo		80	88SE	89	34	SL	bt gneiss			
		39.38884	106.38818	11704ft	43	84SE				calc-sil			
		39.38668	106.39079	11812ft	32	47SE	121	41	SL	bt schist, maybe gt?	HS09-13	Low ange SZ contact! Pavement in cirque	
		39.3838	106.39273	11880ft	41	43SE	66	21	SL	bt gneiss	HS09-14	sinistral, top to SE	
		39.38285	106.39455	11919ft	55	16NW	287	17	SL	mt	HS09-15	mega-shear zone-macro pics	
		39.38233	106.39613	12054ft	140	9NW	159	7	SL	bt schist	HS09-16	feldspar melted	
		39.38708	106.39329	12185ft	55	44SE							
					53	35SE	72	17	SL	sil meta-seds		"z" fold-PIC-plunging SE	FA: 120, 21
		39.38872	106.38979	11984ft	38	90	163	75	SL	calc-sil mylonite	HS09-17	mylonite zone 2-3m wide	
12-Aug	Wurts Ditch	39.3733	106.36902	11201ft	35	86SE				bt gneiss			
		39.37361	106.36971	11325ft	58	87NW				bt gneiss			
		39.37477	106.37021	11369ft	85	55SE				bt gneiss			
			8 m up		125	47SW				bt w/more melt			
		39.37542	106.37037	11376ft	94	55SW				mt			
		39.37621	106.7301	11385ft	94	75NE				mt			
		39.37917	106.36278	11336ft	10	40NW				mt-bt			
		39.38542	106.33851	10437ft	15	60NW				bt gneiss			
			200-300m downslope		71	11NW				bt gneiss			
			100m down		350	40NW				bt gneiss			
13-Aug	Highway 24 I	39.4265	106.32162	9278ft								strained quartzite w/ bt-shear bands	
					44	76NW	44	57	SL	qtzite-bt			
		39.42691	106.3217	9288ft	53	77NW				mylonite)PIC		top to the NW shear sense	FA: 354, 78
			S part of outcrop		16	64NW							
					46	76NW				calc-sil		disconformity? See PICS	
			100m N of outcrop		15	57SE	165	75		calc-sil			
14-Aug	Bennett Cirque II	39.39001	106.38839		61	89SE	71	29	SL	calc-sil		Just before mylonite outcrop	
		39.38872	106.38979	11984ft	44	79SE	50	52	SL	mylonite		SE my. Zone	
					38	73SE	63	58	SL	mylonite		NW zone-brittle fracture in my. Zone	
		39.383	106.39841	12512ft	55	74NW				mt		W of cornice	
		39.38128	106.39923	12688ft	127	21NE				bt schist		SZ sub-horizontal	
					140	36NE							
					126	40NE							
					150	24NE	118	21	SL	bt gneiss	HS09-19		
		39.38079	106.39709	12399ft	71	49NW	305	87	SL	bt gneiss		melt starts	
		39.38274	106.39385	11873ft	74	56NW	57	25	SL	bt gneiss	HS09-20		
		39.38302	106.39353	11869ft	22	39SE	156	25	SL	bt gneiss		K-spar rich intrusions	
16-Aug	Hwy 24 II	39.42746	106.32186	9275ft	229	81NW	237	79	Int. Lin	bt-mylonite			FA: 76, 25 FA:50, 81
			railroad tracks	9520ft	94	81NE	84	15	SL	hc			
		39.42634	106.32462	9716ft			5	66	IL	phyllite			

17-Aug	Slide Lake pavem	39.37381	106.39568	11741ft	45	84NW	234	63	SL	bt gneiss			
			5m up		81	34NW				bt gneiss			
			2 more m up		24	84NW				bt/mt			
		39.37391	106.39566	11775ft	40	70NW	319	68	IL	bt gneiss		S and Z part of larger fold FA: 256, 81	
	outcrop b	39.37578	106.39728	11908ft	120	16NE	320	7	SL	mylonite	HS09-21	TONS of Pics of shear sense and fabric gen	
					50	14NW	324	6	SL	mylonite	HS09-22		
					123	7NE	324	6	SL	mylonite	HS09-23		
					95	19NE	324	19	SL	mylonite	HS09-24		
					201	30SE	170	55	SL				
					39	19SE	160	10					
					194	33SE	151	15					
					10	14SE	169	9					
					13	34SE	166	11					
					51	11SE	169	7					
					14	20SE	141	13					
					3	12SE	170	3					
					18	24SE	149	13					
					8	21SE	151	9					
					146	11NE	355	4					
					30	17SE	157	11					
					42	14SE	148	8					
					128	12SE	351	5					
					78	15NE	335	14					
	outcrop c	39.37591	106.39806	11978ft	41	32SE				mt, S2		T Hinge-Pic in book-part of large fold	
					20	27SE	145	12	SL	mylonite		shear sense pics	
					160	12NE	326	5					
					164	23NE	130	22					
					113	17NE	320	14					
					90	22N	315	14					
					133	14NE	332	4					
					172	22NE	139	20					
	outcrop d	39.37729	106.39939	11748ft	65	11SE	154	10		bt gneiss			
		39.3775	106.39908	11797ft	26	69SE	119	64	SL	bt gneiss			
		39.377719	106.39879	11902ft	42	82SE	134	77	SL	mt with epidote?			
		39.37717	106.39893	11978ft	24	46SE				bt gneiss			
					30	60SE							
		39.37712	10639927	12002ft	62	12NW	351	9	SL	calc-sil mylonite	HS09-26	sub-horizontal	
					75	14NW	351	9	SL-weak				
					34	14NW	341	12	SL				
		39.37729	106.39939	11748ft	40	84NW							
					61	9SE	161	6	SL-weak				
					319	16SW	12	18	SL-weak				
					106	8SW	163	5				part of large W-plunging fold	
		39.39603	106.39919	12012ft	44	87NW				mt (sil pods?)			
		39.37487	106.3983	11907ft	92	44NE				bt gneiss			
		39.37466	106.3983	11907ft	59	64NW				more bt-bt gneiss			
		39.37423	106.39911	11853ft	79	20NW	325	4	SL-well de	mylonite		cliff above lake	
		39.37365	106.39875	11805ft	45	81NW	40	81	ML	mt			
		39.37356	106.39745	11691ft	45	72NW				bt gneiss			
18-Aug	Slide Lake cirque	39.37421	106.39898	11848ft	342	38NE	324	9	SL-WD	qtzo-feldspathic gneiss			
					349	32NE	327	8	SL-WD	qtz-feld gneiss			
					329	33NE	332	6	SL-WD	qtzo-feldspathic gneiss			
					83	39NW						higher strain domains	
					170	13NE	148	4	SL-WD	mylonite zone		lots of pics and drawings of shear bands	
					148	22NE	144	2	SL-WD	mylonite zone			
					156	21NE	147	3	SL-WD	mylonite zone			
					177	19NE	146	6	SL-WD	mylonite zone			
					16	7SE	165	6	SL-WD	mylonite zone			
					148	21NE	144	2	SL-WD	calc-sil mylonite	HS09-27		
		39.37417	106.40135	11756ft	71	79SE	100	76	ML	mt			
					57	62SE							
		39.37499	10640121	11836ft	47	79NW							
					59	77NW						transition from mt to bt-not as much melt p	
		39.37554	106.4025	11999ft	138	32NE	128	7		calc-sil			
					160	34NE	129	15		calc-sil			
					214	12SE	150	11		calc-sil			
					159	12NE	125	9		calc-sil			
					165	38NE				calc-sil			
							147	4		calc-sil			
							131	12		calc-sil			
					41	15SE	162	8		calc-sil			
		39.37547	106.40302	12076ft	61	81NW							
		39.37632	106.4044	12327ft	180	29E	141	12	SL-WD	calc-sil w/ bt			
					147	21NE	145	5		calc-sil w/ bt			
					147	16NE	345	7					
					172	22NE	142	11					
					30	20SE	130	18					
					53	24SE	152	23		mylonite	HS09-28	shear sense pics-top to the NW	
		39.37671	106.40539	12578ft	20	34SE	158	28	SL-WD	bt gneiss-higher strain			
		39.37772	106.40554	12611ft	46	32SE	164	26					
		39.37747	106.40996	12494ft	15	17SE	154	5		mt			
		39.37704	106.4038	12262ft	85	43NW				mt			
19-Aug	Slide Lake cirque	39.37183	106.4027	11738ft	65	43NW	312	41		mt	HS09-29		
					118	9NE							
					72	20NW							
					73	34NW	342	34					
					59	19NW	305	18					
		39.37161	106.40327	11805ft	40	72NW							
					55	36NW							
					45	2SE	121	1	SL				
					80	6SE	134	4	SL	mylonite	HS09-30	top-to-the-NW-shear sense	
		39.37128	106.40362	11843ft	42	81SE	153	80	SL	mt			
		39.37106	106.40422	11971ft	30	556NW							
					39	76NW				mt			
		39.37097	106.40513	12112ft	75	43NW				mt w/ high strain domain			
		39.37061	106.40721	12222ft	42	66NW				mt			FA:321, 41
		39.37068	106.40791	12265ft	25	55NW				mt			
		39.37012	106.40958	12309ft	46	43NW				mt			
		39.36995	106.41109	12472ft	55	66NW				mt			

					48	53NW				mt		
		39.36984	106.41229	12670ft	145	25NE				calc-sil		
		39.36959	106.4126	12709ft	23	88SE				bt gneiss		
		39.3694	106.41354	12879ft	172	30SW	155	3	SL	calc-sil-higher strain		
		39.38977	106.41329	12917ft	20	13SE	150	9	SL	calc-mylonite	HS09-31	
					44	10SE	153	10	SL			
		39.37041	106.41274	12853ft	42	35NW				mt		
					28	26NW	291	23		qtz layer		
					75	17NW	334	11		qtz layer		
		39.37096	106.41206	12796ft	14	36SE	155	20	SL	mylonite-calc		
				3 m N	359	24SE	330	13	SL	mylonite-calc		
					20	29SE	165	9	SL	mylonite-calc		
		39.3711	106.41167	12778ft	120	11NE	323	7	SL-WD	mylonite		
					165	17NE	345	17	SL	mylonite	HS09-32	Top to the SE SS
		39.37208	106.41035	12825ft	5	36SE	176	4	SL	mt		
		39.37256	106.4095	12826ft	359	30E	331	16	SL	amph/mylonite layered		
		39.37324	106.40826	12810ft	149	15NE	141	3	SL	mt, near mylonite		
					155	10NE	123	6	SL	mylonite	HS09-33	
				2m dow	159	16NE	133	3	SL	my		
				4.5m dc	140	20NE	135	4	SL	mylonite		
		39.37344	106.40819	12826ft	156	27NE	332	6	SL	mylonite	HS09-34	
		39.37399	106.40766	12833ft	32	43NW				pebbly horizon?		
		39.37583	106.40716	12763ft	118	35NE	324	9	SL	mt, small my zones		
					106	17NE	333	8	SL	my		Top to the NW SS
				near PE	102	22NE	299	4	SL	my?	HS09-35	
		39.37631	106.40668	12721ft	79	23NW	314	19	SL	my		
		39.37685	106.40639	12710ft						my in float		
		39.3772	106.40593	12687ft	48	46NW				bt schist. Crap.		
		39.37876	106.40499	12618ft	123	28NE						
					164	37NE						
					135	26SE						
				7m dow	156	24NE	150	4	SL	calc-mylonite		
				W-side (	14	69SE	165	54	SL	calc-mylonite		
		39.37876	106.40499	12546ft	139	28NE	8	23	SL	my?	HS09-36	not super mylonitic/S-C fabric?
					158	29NE	320	15		mylonite-calc		
				5 m NE	159	23NE	139	4		mylonite		
		39.38004	106.40353	12543ft	142	16NE	139	3	weak SL	calc-mylonite		
		39.38011	106.40336	12539ft	153	33NE	132	8	weak SL	calc-mylonite		
		39.38017	106.40304	12551ft	154	78SW				bt-gneiss		CONTACT
					40	24SE				mylonite-SZ		CONTACT
				7 m bel	145	27NE						
					149	29NE						
		39.37971	106.40302	12441ft	161	46NE	347	38 ?	same??	mylonite	HS09-37	near contact-below it~10m
	Micah's notes	39.02224	106.24253		70	8SE				mt		
		39.22232	106.24283	11951ft	17	61NW						
		39.22268	106.24343	12196ft	266	64NW	330	45		mt		
		39.22269	106.24342	12172ft	237	46NW	275	43	moderate	mt		
		39.22298	106.24411	12379ft	250	79NW			NO lin	qtz-feld schist		
		39.22337	106.24451	12554ft	279	50NE			NO lin	qtz-feld schist		
				3 m upl	255	65NW	330	61				
		39.22358	106.24483	12666ft	260	51NW	341	50		bt schist/gneiss		
		39.22376	106.24506	12763ft	20	11SE	351	1	SL-WD	bt schist		
		39.2238	106.24504	12803ft	290	55SE	165	3	SL-WD	mylonite		Micah has SS indicator-Top to the SE
		39.22382	106.24521		290	50NE				20 ft from top of mylonite zone		
		39.22329	106.24604	12863ft	325	9NE	20	11		mylonite		
		39.22307	106.24664	12834ft	280	54NE			No lin	mt		
		39.22265	106.24702	12786ft	20	18SE	225	1				
					133	21NE	357	12		mylonite	HS09-38	
		39.22201	106.24785	12864ft	161	32NE			NO lin			
		39.2215	106.2482	12990ft	269	82SE			NO lin	qtz-feld schist		
		39.21929	106.24473	12527ft	55	54SE				mig		
		39.21949	106.24473	12527ft	11	26SE	145	15	WD Lin	mylonite		
		39.22001	106.24319	12043ft	250	58NW				mig		
20-Aug	N-side of lake	39.43272	106.41431		50	88SE				bt schist		
					54	87SE				gt-bt schist		
		39.37807	106.39624	12169ft	22	22SE				mt		
					15	30SE				mt		
							40	29	IL			in fold
		39.37517	106.39431	11941ft	53	21NW	310	19	SL	mylonite		
					86	12NW	315	9	SL	mylonite		
					35	13NW	325	13	SL	mylonite	HS09-39	
					15	9NW	324	5	SL	mylonite		
				9 m dov	115	16NE	335	11	SL	mylonite		
		39.37509	106.39489	11915ft	52	27NW				isolated shear band		FA: 33-7 mylonite wrapped in fold
					57	28NW				mylonite	HS09-40	Axial surface-58/57NW
					70	37NW	4	41		mylonite	HS09-41	Top to the SE
	killer mylonite!	39.37498	106.39156	11438ft	45	61SE				feldspar/bt/qtzose		
					51	75SE				feldspar/bt/qtzose		
				2m E	51	68SE	164	65	SL-WD	mylonite	HS09-42 a/b	
					52	73SE	125	74	SL-WD	mylonite		
		39.3749	106.39131	11597ft	48	52SE						limb of fold
21-Aug	N-side of lake	39.37378	106.39246	11502ft	51	70SE	175	54	SL	mylonite	HS09-43	
	killer mylonite!				35	67SE	170	69	SL	mylonite	HS09-44	
					225	75SE	170	64	SL	mylonite	HS09-45	
					50	50SE	170	44	SL	mylonite	HS09-46	
		39.3749	106.39115	11872ft	39	73SE	189	59	SL	mylonite	HS09-47	
		39.37488	106.39124	11831ft	42	69SE	76	61	SL	mylonite	HS09-48	
					48	63SE	70	44	SL	mylonitized qtz ribbc	HS09-49	
		39.37474	106.39105	11831ft	65	82SE	42	69	SL-WD	mylonite		
		39.37466	106.39091	11821ft								
		39.37445	106.39024	11810ft	70	64SE				bt gneiss		
		39.3742	106.38978	11779ft	71	78SE				sil-bt gneiss		
					60	75SE				sil-bt gneiss		
27-Aug	Bennett/SL ridge	39.35585	106.40575	12030ft	89	44SE	148	34	SL-weak	bt gneiss/qtz		
		39.369	106.40208	11965ft	100	59SW						
				2 m dov	112	50SW	176	48	SL-WD	qtz/feld		
					108	44SW	170	41	SL	mylonite	HS09-51	
		39.3777	106.38593	11959ft	50	74SE	229	20	SL-weak	high strain in mt		
				5 m dov	56	78NW	325	74	SL-WD	bt/qtz ribbons		

		39.37774	106.38674	11961ft	43	66NW					bt gneiss/qtz		
		39.37775	106.3879	12132ft	39	75SE					bt/plag coarser grained		
					65	81NW					bt/plag coarser grained		
				5 m up	65	72SE	212		61	SL	calc-sil mylonite	HS09-52	
		39.37967	106.39381	12520ft	48	71SE					bt gneiss		
		39.37469	106.39423	12524ft	74	73SE					bt gneiss w/kspar		
		39.37967	106.39461	12522ft	76	61SE	194		59	WD-SL	qtz-feld gneiss	HS09-53	
		39.37873	106.39524	12515ft	57	49SE				no lin	bt gneiss		
28-Aug	Homestake Cirque	39.36666	106.40375	11948ft	62	74NW					bt gneiss/qtz		
					35	82SE					bt gneiss		
					36	76SE					bt gneiss		
				4 m up	23	46NW	310		43	SL	bt gneiss with gt		
		39.36576	106.40674	12263ft	345	11NE					high strain in mt		
					340	28NE					S2 defined by mica		
		39.36574	106.40736	12389ft	4	40SE	156		25	SL	mt		top to the SE
		39.36701	106.41695	12953ft	23	40SE	158	DD		SL	calc-mylonite		
					1	25SE	160		11	SL-WD	mylonite		top to the SE
					10	31SE	155		24	SL	calc-mylonite		
		39.36641	106.41822	12945ft	6	26SE	172		9	SL	qtz-feld gneiss		
				5 m dov	1	34SE	169		11	SL	bt gneiss		
		39.36592	106.41887	12977ft	152	48NE							
					161	65NE					calc-sil gneiss		
		39.36603	106.41779	12843ft	140	33NE							
				3 m dov	136	21NE	348		11		calc-mylonite		
		39.36621	106.41617	12773ft	36	28SE	155		28	SL	mylonite	HS09-54	
		39.36592	106.4159	12755ft	3	29SE	144		12	SL	mylonite		
				6 m dov	150	28NE					qtz-feld gneiss		
		39.36568	106.41566	12708ft	5	27SE	143		18	SL	calc-mylonite		
		39.36549	106.4155	12641ft	14	15SE	156		16	SL	bt mylonite		
				12 up	40	3SE	164		1	SL	bt gneiss		
		39.36512	106.41509	12634ft	45	61NW					qtzo-feldspathic gneiss		
		39.36391	106.41665	12301ft	164	37NE					qtz feld gneiss		part of large fold-diagram in book
				10 m dc	125	50NE					qtzo-feldspathic gneiss		same fold above
		39.36224	106.41756	12614ft	122	71NE					qtzo-feldspathic gneiss		
		39.36119	106.41799	12325ft	144	44NE	351		26	SL	mylonite	HS09-55	
		39.3606	106.40866	11826ft	131	39NE					mt		
29-Aug	Slide Lake pavemı	39.37194	106.39291	11725ft	71	62NW				no lin	bt gneiss		
				20 m SE	15	46SE					bt gneiss		
		39.37125	106.39297	11704ft	51	71NW					bt gneiss		
		39.37017	106.39616	11778ft	100	54NE					bt gneiss		
		39.36823	106.3997	11739ft	70	74NW					bt gneiss into Mt		
		39.36772	106.40041	11737ft	45	72NW					bt gneiss		
					54	64NW	286		59		bt gneiss		
		39.36613	106.40183	11846ft	12	54NW	340		48		calc-sil gneiss		
		39.36449	106.40121	11926ft	45	60NW							
					73	55NW					qtz-feldspathic gneiss with calc		
		39.3648	106.40078	11894ft	62	82SE					qtzo-feldspathic gneiss		
					50	89NW					qtzo-feldspathic gneiss		
		39.36521	106.40045	11858ft	28	79NW					qtzo-feldspathic gneiss		
				10 m dc	40	54NW					qtzo-feldspathic gneiss		

APPENDIX IV

THIN SECITONS

Appendix IV

Homestake and Slide Lake petrographic and microstructural analysis

Collected during the 2008-2009 field seasons

Sample	Locati	Latitude	Longitude	Strike	Dip	Trend	Plung	Lithology	Mineral assemblage	Met. grade	Def. mech.	Def. T °C[1]	Shear sense	Vorticity	Monazite/Zircon
HS08-01	HC	39°29'16.4"	106°21'50.9"	26	75 SE	66	54	ultramylonite	qtz, fsp, chl, plag, musc, zr	chl	BLS-SGR	300-400	-	-	
HS08-02	HC	39°29'13.1"	106°21'46.6"	35	63 SE			granite	qtz, plag, ksp, musc, chl	chl	BLG	300	-	-	
HS08-03	HC	39°29'15.5"	106°21'49.6"	18	97 SE			ultramylonite	qtz, fsp, plag, musc, bt, op	bt	SGR	450-500	-	-	
HS08-04	HC	39°29'15.5"	106°21'49.6"	21	80 SE	95	97	quartz vein	qtz, little chl	chl	SGR	400-450	-	-	
HS08-05	HC	39°29'15.5"	106°21'49.6"	38	69 SE	105	68	ultramylonite	qtz, fsp, plag, bt, musc, chl	bt-chl	SGR	300-400	-	-	
HS08-06	HC	39°29'15.9"	106°21'41.5"	27	84 SE	114	68	ultramylonite	qtz, fsp, bt	bt	SGR	450-500	-	-	
HS08-07a/b	HCC	39°29'15.9"	106°31'49.5"	5	86 SE	114	85	mylonite	qtz, fsp, plag, sil, musc, bt	bt	SGR	450-500	t-NW	0.58-0.69	
HS08-08	HCC	39°29'15.9"	106°31'49.5"	19	83 SE	112	84	proto-mylonite	qtz, bt, plag, fsp, sil, musc,	sil-musc, (-chl)	SGR	400-500	t-NW	0.59-0.62	
HS08-09	HCC	39°29'15.9"	106°31'49.5"	342	90 SE	75	90	proto-mylonite	qtz, bt, plag, fsp, musc, chl	bt-chl	BLG-SGR	350-450	-	-	
HS08-10	HCC	39°29'15.9"	106°31'49.5"	30	83 SE	120	DD	mylonite	qtz, musc, bt, fsp, plag, mus	bt	SGR	450-500	-	0.58-0.70	
HS08-11	HCC	39°25'08.06	106°28'23.8"	21	DD	111	DD	proto-mylonite	qtz, musc, bt, fsp, plag, bt,	bt-chl	BLG-SGR	350-450	-	-	
HS08-12	HCC	39°25'08.06	106°28'23.8"	23	84 SE	113	DD	quartz vein	qtz, musc, fsp, ,bt	bt	SGR	450-500	t-NW	-	
HS08-13	HCC	39°25'08.06	106°28'23.8"	31	78 SE	121	DD	quartz vein	qtz, musc, fsp, ,bt	bt	SGR	450-500	t-NW	0.68-0.70	
HS08-14	HCC	39°25'08.06	106°28'23.8"	25	78 SE	115	DD	proto-mylonite	qtz, fsp, plag, musc, bt	bt	SGR	450-500	-	-	
HS08-15	HCC	39°25'08.06	106°28'23.8"	24	79 SE	114	DD	proto-mylonite	qtz, mic, plag, bt	bt	BLG-SGR	350-450	-	-	
HS08-16	HCC	39°25'08.06	106°28'23.8"	30	76 SE	120	DD	proto-mylonite	qtz, plag, bt, musc	bt	SGR	450-500	-	-	
HS08-17	HCC	39°25'06.0"	106°28'24.5"	16	69 NW	106	DD	bt gneiss	bt, qtz, fsp, musc	bt	BLG-SGR	300-500	-	-	
SL08-01	HP	39°22'00.5"	106°25'04.3"	2	69 SE	116	44	proto-mylonite	qtz, bt, plag, bt, chl	chl	BLG	300-400	t-NW	-	monazite - (1) centra
SL08-02	HP	39°22'01.5"	106°25'03.3"	10	42 SE	39	26	calc-sil marble	qtz, cal, chl	chl	BLG	300-400	t-SE	-	
SL08-03	HP	39°22'01.5"	106°25'03.1"	358	59 SE			calc mylonite	qtz, plag, chl	chl	BLG	300-400	-	-	
SL08-04	HP	39°22'01.5"	106°25'03.1"	2	65 SE			quartz vein	qtz, fsp, cal, epi, chl	chl	GBM	350-450	-	-	
SL08-05	HP	39°22'01.7"	106°25'02.6"	20	15 SE	13	6	marble lens	qtz, fsp, cal (no alignment)	bt	cal BLG (?)	~ 400-450	-	-	
SL08-06	HP	39°22'01.5"	106°25'01.6"	59	6 NW	314	4	calc silicates	qtz, musc, qtz, cal, chl	chl	SGR	400-450	t-SE	-	
SL08-07	HP	39°22'01.5"	106°25'01.6"	330	21 NE	128	11	ultramylonite	qtz (GSR), bt, chl, musc	bt-chl	SGR	400-500	t-NE	-	monazite- (1) in alig
SL08-08	HP	39°22'01.5"	106°25'01.0'	332	26 NE	128	6	bt gneiss	qtz, bt, fsp,	bt	GBM	450-550	t-SW	-	
SL08-09	HP	39°22'01.5"	106°25'00.7"	341	29 NE	143	9	bt gneiss	qtz, bt, fsp, musc	bt	BLG	400-450	-	-	
HS09-01	HV	39.38619	106.45611	111	81SW	249	64	bt gneiss	qtz, mus, bt, plag, zr, fsp,	bt	BLG	400-450	-	-	
HS09-02	HV	39.38131	106.44994	101	89SW	295	59	bt gneiss	qtz, fsp, mus, bt (minor)	bt	BLG-SGR	400-500	-	-	
HS09-03	HCC	39.41398	106.48176	25	89SE	132	75	ultramylonite-b	qtz, bt (minor), fsp	bt	SGR	400-500	t-NW	-	
HS09-04	HCC	39.41408	106.48135	9	89NW	289	88	mylonite-bt	fsp, plag, qtz, bt, musc, chl	b-chl	BLG-SGR	300-450	-	-	
HS09-05	LL	39.37509	106.4289	295	84SW	20	73	bt gneiss	no thin section	-	-	-	-	-	
HS09-06	LL	39.37429	106.42839	229	74SE	40	80	mt	qtz, bt, chl, sil, fsp	sil-musc, bt-chl	GBAR	650+ (retro 350-400)		-	
HS09-07	LL	39.37174	106.42297	5	75SE			bt gneiss	qtz, bt, musc, ser	bt	GBAR	650+ (retro	-	-	
HS09-08	LL	39.37081	106.4229	353	76NE	178	78	calc-sil w/ bt	bt, cal, hbl, qtz	hbl-bt	GBAR	650+ (retro	-	-	
HS09-09	HV	39.39981	106.44854	115	84NW			gt/bt gneiss	bt, gt, sil, crd, qtz, kpar, mu	bt-gt-sil-crd	GBAR	600-700	-	-	monazite
HS09-10	HV	39.39981	106.44854	281	80SW			gt/bt/sil gneiss	bt, gt, sil, crd, qtz, kpar, mu	bt-gt-sil-crd	GBAR	600-700	-	-	monazite
HS09-11	BC	39.39777	106.38004	30	17SE	212	30	bt gneiss	qtz, fsp, sil, bt, chl, mus (op	sil-musc, bt-chl	GBAR	650+ (retro	-	-	
HS09-12	BC	39.3903	106.38653	41	78SE	41	46	marble	cal, amp? (minor qtz)	chl-bt	P sol'n	350-400	-	-	
HS09-13	BC	39.38668	106.39079	32	47SE	121	41	bt schist, mayb	qtz, bt, gt, chl, rt, zr, musc	bt, gt-chl	GBAR	~500-600 re	-	-	zircon in garnets
HS09-14	BC	39.3838	106.39273	41	43SE	66	21	bt gneiss	qtz, fsp, bt, plag,	bt	BLG	350-450	-	-	
HS09-15	BC	39.38285	106.39455	55	16NW	287	17	mt	qtz, bt, fsp, mus	bt	BLG	350-450	-	-	
HS09-16	BC	39.38233	106.39613	140	9NW	159	7	bt schist	qtz, bt, fsp	bt	BLG	350-450	-	-	
HS09-17	BC	39.38872	106.38979	38	90	163	75	proto-mylonite	qtz, chl, musc	chl	BLG	300-350	-	-	
HS09-18	Hwy 2	39.42691	106.3217	56	83NW	45	76	quartzite	qtz, fsp, bt	bt	GBAR	650+ (retro	-	-	
HS09-19	BC	39.38128	106.39923	150	24NE	118	21	bt gneiss	qtz, zr, rt, mus, bt, fsp	bt	GBAR	650+ (retro	-	-	
HS09-20	BC	39.38274	106.39385	74	56NW	57	25	bt gneiss	qtz, zr, rt, mus, bt, fsp, plag	plag-musc	GBAR	650+	-	-	
HS09-21	SLC	39.37578	106.39728	120	16NE	320	7	mylonite	qtz, fsp, bt, epi, zr	bt	BLG	350-450	-	-	

HS09-22	SLC	39.37578	106.39728	50	14NW	324	6	mylonite	qtz, sil, mus, bt,	sil-to-musc	high T overprinted by BI		t-SE	-	
HS09-23	SLC	39.37578	106.39728	123	7NE	324	6	mylonite	qtz, musc, bt, sil	bt-sil to musc	GBAR	650+ (retro	t-SE	-	
HS09-24	SLC	39.37578	106.39728	95	19NE	324	19	mylonite	qtz, fsp, sil, bt, musc, ap,	bt, sil to musc,	GBM to GB	650+ (retro	t-SE	-	monazites - (1) g
HS09-25	SLC	39.37578	106.39728	20	27SE	145	12	mylonite	qtz, cal, musc, bt, rt, minor	bt minor sil	GBM	650+ (retro	t-SE	-	
HS09-26	SLC	39.37712	10639927	62	12NW	351	9	calc-sil mylonit	qtz, hbl, bt, cal, sphene	bt	SGR-GBM	450-600	t-SE	-	
HS09-27	SLC	39.37421	106.39898	148	21NE	144	2	mylonite	qtz, bt, musc, fsp, chl	bt, chl	GBAR	650+ (retro	t-SE	-	
HS09-28	SLC	39.37632	106.4044	53	24SE	152	23	mylonite	qtz, musc, bt	bt	GBM	500-600	t-SE	-	
HS09-29	SLC	39.37183	106.4027	65	43NW	312	41	migmatite	qtz, bt, musc, sil, rt	sil-musc, bt	GBAR	650+ (retro	t-NW	-	
HS09-30	SLC	39.37161	106.40327	80	6SE	134	4	mylonite	qtz, bt, musc, sil, rt, sil	sil-musc, bt	GBM	500-600	t-SE	-	
HS09-31	SLC	39.38977	106.41329	20	13SE	150	9	calc-mylonite	qtz, musc, bt, minor hbl, sil	bt-sil to musc	GBM	500-650	t-SE	-	
HS09-32	SLC	39.3711	106.41167	165	17NE	345	17	mylonite	qtz, musc, bt, mag, chr, sil	bt-sil to musc	GBM	500-650	t-NW	-	
HS09-33	SLC	39.37324	106.40826	155	10NE	123	6	mylonite	qtz, bt, musc, sil, opq,	bt-sil to musc	(earlier high	650+	t-SE	-	
HS09-34	SLC	39.37324	106.40826	156	27NE	332	6	mylonite	qtz, fsp, bt, chl	chl	GBAR	650+ (retro	t-SE	-	
HS09-35	SLC	39.37583	106.40716	102	22NE	299	4	my?	qtz, sil, musc,	bt, sil to musc	GBM	450-650	t-SE	-	
HS09-36	SLC	39.37876	106.40499	139	28NE	8	23	my?	qtz, bt, musc, fsp, bt	bt	high T over	650 overpri	t-NW	-	monazite - (1) m
HS09-37	SLC ((	39.37971	106.40302	161	46NE	347	38 ?	mylonite	qtz, fsp, bt, musc, chl (lots!	chl	BLG	300-400	t-NW	-	
HS09-38	SLC	39.22265	106.24702	133	21NE	357	12	mylonite	qtz-fsp (dom.)musc, bt, sil	bt	GBAR	650+ (retro	t-NW	-	
HS09-39	SLC	39.37517	106.39431	35	13NW	325	13	mylonite	qtz, musc, bt, minor chl	bt	BLG	450-500	t-SE	-	
HS09-40	SLC	39.37509	106.39489	57	28NW			mylonite	qtz, fsp, bt, musc, sil, ap, ch	chl, sil-to-musc	BLG	450-500	t-S	-	
HS09-41	SLC	39.37509	106.39489	70	37NW	4	41	mylonite	qtz, bt, musc, sil	bt, sil to musc	GBAR	650+ (retro	-	-	
HS09-42 a/b	BR	39.37498	106.39156	51	68SE	164	65	mylonite	qtz, fsp, bt, mus, zr,	bt	GBM	450-600	t-SE	0.72-0.79	big zr in the fabr
HS09-43	BR	39.37378	106.39246	51	70SE	175	54	mylonite	qtz, musc, bt, fsp, zr	bt	GBM	450-600	t-SE	0.71-0.72	
HS09-44 a/b	BR	39.37378	106.39246	35	67SE	170	69	mylonite	qtz, fsp, musc, bt, zr, sphen	bt	GBM	450-600	t-SE	0.70-0.72	
HS09-45	BR	39.37378	106.39246	225	75SE	170	64	mylonite	qtz, fsp, zr, musc	bt	GBM	450-600	t-SE	0.68-0.73	monazite - (1) al
HS09-46	BR	39.37378	106.39246	50	50SE	170	44	mylonite	qtz, fsp, zr, musc, cr, bt	bt	GBM	450-600	t-SE	0.63-0.65	zircon
HS09-47	BR	39.3749	106.39115	39	73SE	189	59	mylonite	qtz, fsp, bt, chl, zr	chl-bt	SGR-GBM	400-600	t-SE	0.58-0.65	monazite
HS09-48	BR	39.37488	106.39124	42	69SE	76	61	mylonite	qtz, bt, musc, fsp	bt	BLG-SGR	350-450	-	-	
HS09-49	BR	39.37488	106.39124	48	63SE	70	44	mylonitized qtz	qtz, fsp, bt, musc	bt	SGR-GBM	450-550	-	-	
HS09-50	BR	39.37488	106.39124	75	88SE	191	86	mylonite	qtz, bt, fsp, zr, minor chl	bt	BLG-SGR	350-450	-	-	monazite - (1) m
HS09-51	BR	39.369	106.40208	108	44SW	170	41	mylonite	qtz, bt, fsp	bt	GBM	450-600	t-NW	-	
HS09-52	BR	39.37775	106.3879	65	72SE	212	61	calc-sil mylonit	qtz, chl, bt, musc, cal	chl-bt	GBAR	650+ (retro	t-SE	-	
HS09-53	BR	39.37967	106.39461	76	61SE	194	59	qtz-feld gneiss	qtz, fsp, zr, chl, gt, sil	chl-bt-gt-sil	GBAR	650+ (retro	-	-	
HS09-54	SLC	39.36621	106.41617	36	28SE	155	28	mylonite	qtz, fsp, musc, bt	bt	BLG	350-400	t-SE	-	
HS09-55	SLC	39.36119	106.41799	144	44NE	351	26	mylonite	qtz, fsp, bt, sil, musc	sil-to-musc, bt	GBAR	650+ (retro	-	-	
CC08-01	GGSP	39°51'06.8"	105°23'00.7"	29	vertical	weak	0	basal quartzite (	qtz, op, sil, bt	sil	BLG-SGR	250-400	-	-	
CC08-02	GGSP	39°51'38.7"	105°21'26.1"	185	52SE	151	38	mylonite	qtz, fsp, bt, ms, ms, ser	bt	BLG	<250	t-NW	-	
CC08-03	GGSP	39°51'38.7"	105°21'26.1"	190	54SE	334	36	mylonite	qtz, fsp, plag, ms, bt, ser	bt	BLG	<250	t-SE	-	
CC08-04	GGSP	39°51'37.4"	105°21'29.1"	206	51SE	162	38	ultramylonite	qtz (micro), ksp, op	bt	BLG	<250	t-NW	-	
CC08-05	GGSP	39°51'35.4"	105°21'31.3"	50	86SE	154	81	quartz vein	qtz, ms, bt, ksp	bt	BLG	<250	t-SE (lt. m f	-	
CCO8-06	GGSP	39°51'35.4"	105°21'31.3"	228	84SE	down dip		quartzite	qtz, ms, bt, zr, op,	bt	BLG+	250-300	t-NW (ogsf)	-	
CC08-07	GGSP	39°51'35.2"	105°21'31.3"	214	85SE	121	74	quartzite	MIA	-	-	-	-	-	
CC08-08	GGSP	39°51'28.56	105°21'30.69	221	74SE	down dip		quarzite	qtz, ms, op	chl	BLG	<250	-	-	

Location abbreviations: (HC) Hornsilver campground, (HCC) Holy Cross City, (HP) Homestake Peak, (LL) Lost Lakes, (HV) Homestake Valley, (BC) Bennett Cirque, (SLC) Slide Lake Cirque, (BR) Bennett Ridgeline, (GGSP) Golden Gate State Park.

Mineral abbreviations: (qtz) quartz, (bt) biotite, (fsp) feldspar, (musc) muscovite, (chl) chlorite, (sil) sillimanite, (zr) zircon, (cal) calcite, (gt) garnet, (crd) cordierite, (ap) apatite, (hbl) hornblende, (rt) rutile, (plag) plagioclase

Deformation temperatures: derived from quartz and feldspar texures from Stipp et al., 20002 (qtz) and Pryer, 1993 (fsp), and Spear (1993)

Shear sense: from oriented samples, indicators include: mica fish, rigid tails on porphyroclasts, oblique grain shape fabric, shear bands…

Vorticity: Mean kinematic vorticity (Wm) derived from the Rigid Grain Net technique (see text for methodology)

[1]Deformation temperatures derived from quartz textures (Stipp et al., 2002a,b) feldspar textures from (Pryer, 1993), metamorphic mineral assemblage (Spear, , and quartz LPOs

VITA

Patricia Elizabeth (Liz) Lee was born in Richmond, Virginia, in February 1983 to Mary Ackerly Lee and James Merrill Lee. She attended Douglas S. Freeman High School and graduated in 2001. She then attended Sewanee: The University of the South and graduated in 2005 with Bachelors of Science in Geology as a member of the Order of the Gownsmen, a NCAA All-Academic cross-country athlete, and an active student leader with the Sewanee Outdoor Program. Post-undergraduate years were spent as a ski instructor, medic at an outdoor science school, rock climbing and running in the mountains of Colorado, and serving as the Director of Sewanee Outdoor Program. She began her Masters of Science at the University of Tennessee, Knoxville in July of 2008. While at UT, she had the opportunity to be part of a research team (including M. Jessup and J. Langille) that spent June-July 2009 investigating the structure of the Leo Pargil shear zone in the Indian Himalaya. She also spent two field seasons performing MS-based research in the northern Sawatch Range of central Colorado. Liz spent Summer 2010 working as an intern with ExxonMobil, and has since accepted a position as a geologist with ExxonMobil Exploration Company in Houston, Texas.